SAPIENZA

Università di Roma

Facoltà di Scienze Matematiche Fisiche e Naturali

DOTTORATO DI RICERCA
IN GENETICA E BIOLOGIA MOLECOLARE

XXXIII Ciclo

(A.A. 2019/2020)

Characterisation of circRNA molecular functions in rhabdomyosarcoma tumour

Dottoranda
Francesca Rossi

Docente guida
Prof.ssa Irene Bozzoni

Coordinatore
Prof. Fulvio Cruciani

Index

Glossary

***Back-splicing**:* a particular kind of alternative splicing in which a 5' splice site is joined to an upstream 3' splice site, giving rise to a circularised exon(s).

***Cell proliferation**:* the highly regulated set of processes through which a cell grows and divides into two daughter cells.

***circRNA (circular RNA)**:* a covalently closed single-stranded RNA molecule whose 5' and 3' extremities are covalently joined together.

***FACS analysis of cell cycle**:* flow cytometry-based method to calculate the distribution of cells in each cell cycle phase (G1, S, G2-M); it relies on the quantification of the DNA content *via* staining with fluorescent DNA-intercalant dyes.

***G1-S transition**:* the cell cycle stage between the end of G1 phase and the start of S phase; it is regulated by specific checkpoints, e.g. the DNA-damage checkpoints which prevent the cell from replicating damaged DNA.

***Knock-down**:* reduction of the expression of a gene, e.g. through the transfection of siRNAs in the cells.

***Master regulator**:* a protein factor which is an upstream modulator of a particular pathway involved in the regulation of a cellular process, e.g. proliferation.

***miRNAs (microRNAs)**:* small non-coding RNAs involved in the post-transcriptional regulation of gene expression;

miRNAs target complementary sequences on messenger RNAs, inducing their destabilisation and/or translational suppression.

***Microtubules**:* fundamental constituents of the cell cytoskeleton; they are highly dynamical polymers of Tubulin, with a role in cell shape, intracellular transport and mitotic spindle formation.

***Mitosis**:* the last stage of cell cycle, through which a cell divides into two daughter cells having the same number and kind of chromosomes as the mother cell.

***mRNA (messenger RNA)**:* single-stranded RNA molecule which can be translated into a specific protein.

***Myoblasts**:* proliferating myogenic precursors with mesodermal origin.

***PAR-CLIP-sequencing**:* photoactivatable ribonucleoside-enhanced crosslinking and immunoprecipitation; the incorporation of photoreactive ribonucleoside analogues into nascent RNA transcripts allows an efficient 365-nm UV irradiation-induced crosslinking of labelled RNAs to their interacting proteins. Protein immunoprecipitation allows recovering all the RNAs bound to it, which are then identified by RNA-sequencing. The PAR-CLIP protocol allows the identification of the specific protein binding sites on the RNAs with nucleotide-level resolution.

***qRT-PCR**:* the real-time quantitative Reverse Transcription PCR allows an accurate measurement of the PCR product during each amplification cycle; the template for qRT-PCR amplification is copy DNA (cDNA) generated from RNA through a reverse transcription reaction.

***RBP (RNA binding protein)**:* a protein which can bind to single- or double-stranded RNA thanks to its RNA-binding domains, e.g. RNA recognition motif and double-stranded RNA-binding domain.

***RD cells**:* cell line derived from a tumour biopsy of a 7-year-old female child with refractory pelvic embryonal rhabdomyosarcoma (ATCC: CCL-136; Resource Identifiers RRID: CVCL_1649).

***Regulon**:* a group of genes that are regulated altogether by the same transcription factor, or whose differential expression correlates to changes in the activity of a specific protein (even if not a transcription factor).

***RH4 cells**:* cell line derived from a biopsy of an alveolar rhabdomyosarcoma lung metastasis in a 7-year-old female child; these cells are positive for the t(2;13)(q35;q14) translocation (Resource Identifiers RRID: CVCL_5916).

***Rhabdomyosarcoma (RMS)**:* a skeletal muscle-derived paediatric malignancy; the main RMS subtypes are the embryonal (ERMS) and the alveolar (ARMS).

***RIP assay**:* RNA-immunoprecipitation technique used to investigate RNA-protein interactions.

***RNA-pulldown**:* experimental technique which allows the precipitation of a specific RNA molecule usually through biotinylated probes binding to it. It allows the recovery of the specific RNA's interactors, either RNAs or proteins.

***RNA-sequencing**:* a wide class of experimental techniques using Next-Generation Sequencing approaches for the high-throughput identification and quantification of RNA species expressed in a biological sample.

***rRNA (ribosomal RNA)**:* non-coding RNA which associates to ribosomal proteins to form the ribosomal subunits.

***siRNAs (small interfering RNAs)**:* small non-coding RNAs involved in the post-transcriptional silencing of gene expression. They can target a specific RNA through perfect base-pairing, inducing its degradation.

***Splicing**:* the process through which introns are co-transcriptionally removed from a precursor-RNA molecule and exons are joined together. Alternative splicing mechanisms can direct the exclusion or the inclusion of specific exons from the mature mRNA, giving rise to different mRNA isoforms.

***Transfection of cells**:* experimental procedure to introduce foreign DNA or RNA molecules in the cells, in order to modify gene expression.

Western blot: experimental technique allowing detection and quantification of a specific protein expressed in a biological sample.

Summary

Circular RNAs (circRNAs) are covalently closed single-stranded RNA molecules whose important role in regulating gene expression at different levels is recently emerging. Particularly, circRNAs often show a deregulated expression in several pathological processes, including cancer, contributing to the disease's onset and progression.

My PhD work aimed at investigating the molecular role of a specific circRNA, named circZNF609, in regulating cell proliferation in rhabdomyosarcoma, a paediatric skeletal muscle tumour. We found that circZNF609 is overexpressed in rhabdomyosarcoma with respect to primary myoblasts and its depletion slows down cell-cycle progression at the G1-S transition. We also characterised the impact of circZNF609 knock-down on rhabdomyosarcoma cell transcriptome and major pathways involved in proliferation, e.g. Retinoblastoma/E2F1 and PI3K/AKT pathways.

Thanks to the analysis of circZNF609 molecular interactors, we discovered that the circRNA can bind to Ckap5 mRNA, a transcript encoding a microtubule polymerase with a fundamental role in controlling mitotic spindle assembly and chromosome segregation. We found that circZNF609 depletion impairs CKAP5 protein expression possibly through

HUR, an RNA-binding protein promoting mRNA stability and translation.

By reducing Ckap5 mRNA stability and protein levels, circZNF609 knock-down impairs microtubule dynamics and induces defective chromosome segregation. This results in the accumulation of DNA damage that could be responsible for the activation of checkpoints during the following cell cycle, blocking it at the G1-S transition.

Therefore, our research unveiled a novel molecular circuit through which a circRNA regulates cell cycle progression in rhabdomyosarcoma tumour.

In the last part of this work, we identified other circRNAs deregulated between myoblasts and rhabdomyosarcoma cells, and we started to elucidate the role of circHIPK3 in modulating YAP/TAZ activation in tumour cells.

Our long-term aims are to unveil circRNA-dependent circuits which can be responsible for tumour onset and progression, and to investigate potential uses of these circRNAs as rhabdomyosarcoma biomarkers and/or therapeutic targets.

Introduction

Circular RNAs, a novel and intriguing class of RNAs

Circular RNAs (circRNAs) are covalently closed single-stranded RNA molecules, lacking 5' and 3' free ends. They were first observed in eukaryotic cells many decades ago thanks to electron microscopy [1]. In the early 1990s, circular RNA molecules with an inverted exon order with respect to their position in the genome were identified, and were therefore referred to as scrambled exons [2,3].

Although circRNAs are ubiquitously expressed among eukaryotes [4] and also in archaea and viruses [5,6], they have been considered a rare class of transcripts for a long time. It is only in recent years that circRNAs have come to the scene again. The improvement of Next Generation Sequencing techniques and the invention of dedicated bioinformatics scripts for their identification allowed researchers to recognize circRNAs as a large class of transcripts originating from thousands of genes, expressed in different cell types and often conserved among eukaryotes [7].

Biogenesis of circRNAs

In eukaryotic cells, circRNAs are produced by the canonical spliceosome through a particular splicing event called back-splicing. During this process, a 5' splice site is joined to an upstream 3' splice site, giving rise to a circularised exon(s) whose ends are connected through a phosphodiester bond [8]. The back-splicing reaction and the circularisation process account for the fact that circRNA-composing exons appear to be in an inverted order with respect to the reference transcriptome.

The back-splicing junction is the only region distinguishing the circularised exon in the circRNA from the corresponding linear exon included in the mRNA transcribed from the same genomic locus (***Fig. 1***).

There are evidences suggesting that back-splicing occurs co-transcriptionally, like linear splicing. Indeed, hundreds of reads on back-splicing junctions have been found in datasets of chromatin-bound nascent RNA in *D. melanogaster* [9]. Moreover, the linear splicing can compete with the back-splicing, since when the linear splicing is potentiated, the back-splicing is disadvantaged. This was observed in mutant flies expressing a slower RNA Polymerase II: while their linear splicing was more efficient, they produced significantly fewer circRNAs with respect to wild-type flies [9].

Back-splicing can be considered as a kind of alternative splicing and, similarly to linear alternative splicing, it is highly regulated. The factors that modulate circRNA production can act both in *cis* and in *trans* (***Fig. 1***).

The introns flanking circularising exons often harbour repetitive complementary and inverted sequences (e.g. Alu repeats) favouring the pairing across bordering introns, so that the two splice sites can get closer and the back-splicing is favoured [10,11]. It has been observed that in some cases even very short intronic inverted repeats (30 or 40 nucleotide-long) are sufficient to promote back-splicing [11].

Introns flanking circularizing exons also show an enrichment in adenosine-to-inosine (A-I) editing performed by the Adenosine Deaminase RNA Specific (ADAR) enzyme [12]. The A-I transition significantly reduces the pairing capacity of the edited intronic sequences, representing an interesting mechanism to regulate circRNA production by inhibiting back-splicing [13].

Among *cis*-acting elements regulating back-splicing, there is also the length of circularising exons, which is positively related to their circularisation propensity [14]. This could be due to steric reasons, as a minimal distance between the two splice sites could favour the back-splicing reaction.

RNA-binding proteins (RBPs) can promote or inhibit

circRNA biogenesis acting in *trans* on circularizing exons and their flanking introns.

The splicing factors hnRNPs and SR proteins regulate the back-splicing of *D. melanogaster* circRNAs transcribed from the Laccase-2 and Plexin-A genes [15].

The RBP Quakin (QKI) can directly bind intronic sequences flanking the circularising exons. Its dimerization can then bring the splice sites closer, promoting circRNA production during epithelial-mesenchymal transition [16].

Similar to QKI, other RBPs can regulate back-splicing by binding bordering intronic sequences. This is the case of the Mannose-binding Lectin (MBL), which promotes the circularisation of the second exon of its own transcript, giving rise to circMBL, in *D. melanogaster* [9].

Finally, the Fused in Sarcoma protein (FUS) regulates the biogenesis of 132 circRNAs in *in vitro*-derived mouse motor neurons [17].

Recently it has been shown that specific patterns of N6-methyladenosin RNA modification (m^6A) can direct the back-splicing of the m^6A-containing exon in the primary transcript. This could depend on the m^6A reader YTHDC1, as a significant positive correlation has been found between YTHDC1 binding and the ability of methylated exons to circularise [18].

These mechanisms of back-splicing regulation highlight the fact that circRNAs are far from being only splicing by-products and are a class of molecule the biogenesis of which can be regulated at different levels.

Fig. 1

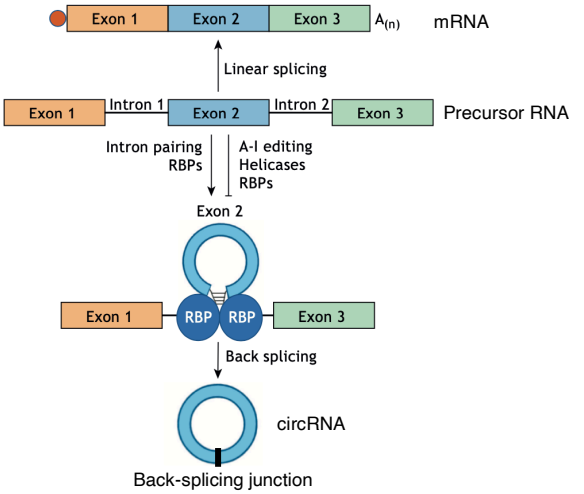

Fig. 1 Schematic representation of linear splicing (top) and back-splicing (bottom). Intron pairings and some RBPs are among the *cis*- and *trans*-acting factors that can enhance back-splicing. By contrast, A-I editing, some helicases and other RBPs can inhibit back-splicing. Adapted from Di Timoteo, Rossi and Bozzoni, 2020.

Molecular functions of circRNAs

CircRNAs are broadly expressed, often conserved among different species, and a large number of them also shows a cell-type specific expression pattern [7,10,19].

CircRNAs are generally expressed at lower levels than their linear mRNA counterpart [20], but there are also cases in which the circular RNA is the most abundant transcription product [19]. This is frequently observed in the mammalian brain. Indeed, many circRNAs are upregulated during neuronal differentiation, and their expression is often regulated differently from their linear mRNA counterpart [13].

These features of circRNA expression suggest that circRNAs could actually be functional molecules, whose expression needs to be modulated during physiological (as well as pathological) processes.

Indeed, many examples of functional circRNAs have been reported so far, with roles in regulating gene expression at different levels (***Fig. 2***).

The first functional circRNA to be described was CDR1as. Its sequence harbours 74 miR-7 seed matches, with most of them conserved in at least one more species [7]. The first hypothesis about its molecular function was that CDR1as could act as a competing endogenous RNA (ceRNA), sponging miR-7 and interfering with its ability to target specific mRNAs [7,21] (***Fig. 2A***).

Few years later, however, an alternative molecular mechanism of action has been proposed for CDR1as, and a deeper insight into the phenotype associated to its loss was gained. The CDR1as knock-out mouse exhibited a dysfunction of excitatory synaptic transmission. At the molecular level, CDR1as depletion was associated with the downregulation of miR-7 and the upregulation of its target mRNAs. Since these observations contrasted with the previously proposed ceRNA activity of CDR1as, it was hypothesised that CDR1as may stabilize miR-7 and translocate it towards neuronal synapses. Here it contributes to the regulation of miR-7-targeted mRNAs encoding factors with a role in synaptic transmission [22].

Another circRNA harbouring a high number of binding sites for the same microRNA is the one coming from SRY gene [23]. SRY circRNA hosts 38 binding sites for miR-138 and acts as a ceRNA for this microRNA [21].

So far, several other circRNAs have been proposed to act as ceRNAs, regulating microRNA activity and impacting on different cellular pathways, particularly related to cell proliferation and differentiation [24,25]. However, the ceRNA activity for circRNAs cannot be generalised.

Besides the miRNA-sponging activity, other molecular functions have been ascribed to circRNAs.

There are examples of circular transcripts working as protein scaffolds or decoys to regulate their activity (***Fig. 2B***).

This is the case of circANRIL sequestering PES1 protein and affecting rRNA processing [26], and circFOXO3 which can bind both p21 and CDK2 proteins favouring the inhibition of CDK2 by p21 and impacting cell cycle progression [27].

A few circRNAs have also been shown to harbour an open reading frame (ORF) and to be translated in a cap-independent manner (***Fig. 2C***) [28–33]. The typical circRNA-specific ORF spans the back-splicing junction, finally encountering a downstream stop-codon. In many cases the circRNA-encoded protein corresponds to a truncated version of the corresponding mRNA-encoded full-length protein, with the addition of a new aminoacidic sequence encoded by the codons downstream the back-splicing junction.

Although the majority of circRNAs is predominantly located in the cytoplasm and acts in this cellular compartment, there are also examples of nuclear functional circRNAs. The Exon-Intron circRNAs (EIciRNAs) retain intronic sequences between circularising exons and show a nuclear localisation. In the nucleus, they can regulate the transcription of their parental gene (***Fig. 2D***). This is the case of EIciRNAs circPAIP2 and circEIF3J regulating RNA Polymerase II activity by base-pairing with U1 small nuclear RNA (snRNA) [34].

Fig. 2

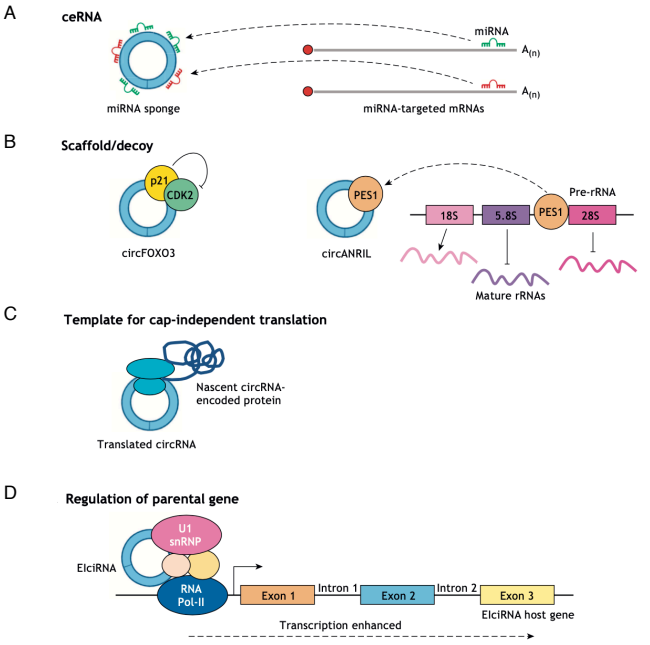

Fig. 2 Schematic representation of circRNA molecular functions. They can act as ceRNAs by sequestering or stabilizing miRNAs (A). CircRNAs can act as scaffolds or decoys for RBPs (B). Some circRNAs can act as a template for cap-independent translation (C). Nuclear circRNAs can regulate the transcription of their parental gene (D). Adapted from Di Timoteo, Rossi and Bozzoni, 2020.

CircRNAs in cancer biology

Since circRNAs have been found to be broadly expressed, regulated in their production and possibly functional, a great interest arose regarding their modulation and roles in pathological processes, particularly cancer.

Thousands circRNAs are differentially expressed among normal and cancer tissues, and many of them can regulate several aspects of cancer biology, e.g. aberrant cell proliferation, metabolic reprogramming, migration and metastasis, angiogenesis, and evasion of immune suppression [35,36].

One of the most studied oncogenic circRNA is circHIPK3, deriving from the circularisation of the second exon of HIPK3 precursor RNA. It is overexpressed in many cancers, including hepatocellular carcinoma [37], epithelial ovarian cancer [38] and lung cancer [39]. CircHIPK3 mainly acts as a promoter of cancer cell proliferation, migration and invasion by sequestering tumour-suppressor microRNAs, such as miR-124 [37,40].

Besides circHIPK3, a large number of circRNAs are deregulated in many cancers with respect to normal tissues, and most of them have been proposed to act as ceRNAs for either oncogenic or tumour-suppressor microRNAs [41,42].

However, alternative molecular mechanisms of actions have been discovered for some cancer-related circRNAs.

For example, CDR1as expression is epigenetically silenced in invasive melanoma cells with respect to the non-invasive stage. When expressed in the non-invasive condition, CDR1as can interact with the RBP IGF2BP3. This is a member of the IGF2BP-family, which are oncofetal proteins regulating target mRNAs at a post-transcriptional level, and have been shown to have an oncogenic role in several cancers. When CDR1as binds to IGF2BP3, it sequesters the protein interfering with its role in sustaining melanoma metastasis. When CDR1as is epigenetically silenced, IGF2BP3 is released and contributes to the increased cancer invasiveness. Therefore, in this case, CDR1as contributes to melanoma cell metastasis by acting as an RBP-sponge, in a miR-7-independent way [43].

In glioblastoma, circSHPRH is downregulated with respect to the healthy brain tissue. This circRNA can be translated into a tumour-suppressive protein, named SHPRH-146aa. SHPRH-146aa protects the SHPRH mRNA-encoded full-length protein from proteasomal degradation. When circSHPRH is overexpressed in glioblastoma cells, the full-length SHPRH protein is stabilised and inhibits cancer cell proliferation by ubiquitinating the Proliferating Cell Nuclear Antigen (PCNA) [44].

A second protein-encoding circRNA has been found to inhibit glioblastoma cell proliferation. CircAKT3 is translated

into a 174aa-long protein (AKT3-174aa). The overexpression of the circAKT3-encoded protein reduces proliferation and *in-vivo* tumorigenicity of glioblastoma cells, by acting as a dominant-negative variant of the full-length AKT3 protein. Indeed, AKT3-174aa competes with AKT3 for the binding to PDK1, resulting in lower PDK1-mediated phosphorylation and consequent lower activation of AKT3 [32].

Interestingly, circRNAs can also originate from tumour-specific chromosomal rearrangements. For example, the chromosomal translocation t(15;17)(q24;q21), giving rise to the PML/RARα fusion gene, characterises acute promyelocytic leukaemia cells. The circRNAs originating from the circularisation of the PML and RARα exons juxtaposed to the breakpoint are called fusion-circRNAs (F-circRNAs). F-circRNAs contribute to sustained proliferation, malignant transformation and resistance to drug treatments in leukaemia cells, both *in-vitro* and *in-vivo* [45].

CircRNAs as cancer biomarkers

In the last years, there has been a growing effort to identify specific circRNAs to be used as novel biomarkers for several pathologies, from diabetes [46] to coronary artery disease [47], from pre-eclampsia [48] to cancer [49].

CircRNAs have the right features to be considered as biomarkers. Most of them are differentially expressed in many

pathological processes and sometimes specifically expressed in one condition compared to another one. Moreover, although there is still much to discover about circRNA turnover, circRNA covalently closed structure makes them resistant to exoribonuclease-initiated RNA decay pathways [50], and their half-life is generally longer than their mRNA counterparts [51].

So far, many circRNAs have been proposed as biomarkers for specific cancers.

Two examples are hsa_circ_0000190, which is downregulated in tumour tissues and plasma of gastric cancer patients as compared to controls, showing better specificity and sensitivity than classic biomarkers for this tumour (e.g. CA19-9 and Carcinoembryonic Antigen) [52], and hsa_circ_100855, which is upregulated in laryngeal squamous cell cancer compared to normal tissues. Its overexpression positively correlates with advanced clinical stages and metastasis [53].

CircRNAs are also present and differentially expressed in extracellular fluids of healthy people and cancer patients, such as saliva and blood [54,55], thus allowing non-invasive approaches to evaluate the presence of the pathology.

CircRNAs are very abundant in human whole blood, sometimes more than their mRNA counterpart [55]. CircRNAs are very stable in the blood also because they are loaded into

cell-secreted exosomal vesicles, being often enriched in exosomes as compared to parental cells [56].

Interestingly, tumour-derived exosomal circRNAs have been identified, such as in the case of KRAS-mutant colon cancer cell-derived vesicles [57], and a significant difference in the circRNA-content of serum exosomes between colon cancer patients and controls has been observed [56].

In conclusion, circRNAs are relevant molecules for cancer progression, and the analysis of their expression in tumour biopsies, as well as in body fluids, could be of significant help for a rapid and non-invasive cancer diagnosis.

Rhabdomyosarcoma, a paediatric soft tissue tumour

Characteristics of rhabdomyosarcoma subtypes

Rhabdomyosarcoma (RMS) is a malignant cancer of muscular origin. It is the most common soft tissue malignancy in children, accounting for about 5% of all paediatric tumours, while it is very rare in adults [58]. Boys develop RMS with a slightly higher incidence than girls, with a male to female rate ratio of 1.37 [59].

The majority of RMS cases occurs sporadically. However, this tumour shows association with some familial diseases, e.g. neurofibromatosis and Li-Fraumeni syndrome [60–62].

RMS is generally classified based on its histology. According to the classical histological classification of this tumour, four main RMS subtypes can be identified: the embryonal (ERMS), the alveolar (ARMS), the pleomorphic and the botryoid [63].

ERMS is the most common subtype, accounting for almost 60% of RMS cases, and generally has a favourable prognosis. It frequently affects young children (from 0 to 10 years old) and preferentially arises from the genitourinary tract and the head/neck district [64]. ERMS cells are small, round or elongated, resembling those of a 6/8-week-old fetal muscle (American Cancer Society), and are embedded in a loose myxoid stroma [64].

Instead, ARMS represents 20% of all RMS cases and is more aggressive than ERMS. It often shows metastasis at diagnosis and is characterised by unfavourable prognosis [65]. ARMS preferentially affects adolescents and young adults, and originates from body extremities, but also from abdomen, genitals and the head/neck district [64]. ARMS cells resemble those of a 10-week-old fetal muscle (American Cancer Society), are round-shaped and arranged in a sort of alveolar structures separated by fibrous septa [64].

Pleomorphic RMS is a very rare and poorly characterised high-grade sarcoma with unfavourable prognosis, generally arising in older adults at their body extremities [66].

Botryoid RMS often occurs in children and adolescents and originates under the mucosa in the genitourinary tract, especially cervix and vagina. It is described as a grape-like lesion with a polypoid aspect [67].

Genetic alterations in ERMS and ARMS subtypes

ERMS and ARMS tumours are characterised by specific genetic alterations.

ERMS commonly show loss of imprinting and frequent loss of heterozygosity on chromosomes 11p, 11q and 16q [68]. Particularly, this affects the 11p15 chromosome [69].

The ARMS subtype is characterised by two non-random chromosomal translocations. The most frequent (70% of ARMS cases) is the t(2;13)(q35;q14), while a rarer translocation is the t(1;13)(p36;q14) [69].

These two genetic alterations affect PAX3 and PAX7 genes respectively, which are members of the Paired Box Transcription Factor family involved in the regulation of embryonic development. Indeed, both PAX3 and PAX7 are expressed in myogenic progenitor cells and participate in skeletal muscle development [70,71]. Upon translocation, PAX3 or PAX7 are fused to FOXO1 gene, which belongs to the Forkhead family of transcription factors and is involved in the regulation of insulin signalling [72]. Particularly, the 5' exons of PAX3 or PAX7 (encoding the DNA-binding domain) are fused with the 3' exons of the FOXO1 gene (encoding the transactivation domain), giving rise to the chimeric transcription factors PAX3-FOXO1 and PAX7-FOXO1, respectively [73].

PAX3-FOXO1 and PAX7-FOXO1 are expressed at higher levels than PAX3 and PAX7 transcription factors, and also have a more potent capacity to activate target gene expression, thus having a primary role in the dysregulation of many pathways related to cell proliferation, apoptosis, myogenesis and migration that contribute to ARMS tumorigenesis [69,73].

RMS cell origin and main altered pathways

RMS derives from the disruption of the skeletal muscle differentiation programme of mesenchymal cells committed to a myogenic lineage. These muscular progenitors express some myogenic markers, but then fail to differentiate properly [68]. Particularly, MyoD and Myogenin are expressed by RMS cells, and they are used in the differential diagnosis of this tumour from other malignancies [74,75].

The alteration of key cellular pathways sustains RMS cells' aberrant proliferation and impossibility to differentiate [76] (***Fig. 3***).

The RAS pathway is often constitutively activated in ERMS, generally due to point mutations in RAS-family genes [68], while the loss of imprinting on the Insulin-like Growth Factor 2 (IGF2) gene and the upregulation of its expression by the PAX3-FOXO1 transcription factor in ARMS have a fundamental role in the activation of the IGF pathway in RMS [77].

The Fibroblast Growth Factor Receptor 4 (FGFR4) is overexpressed in RMS, particularly in ARMS where it is transcriptionally activated by PAX3-FOXO1. FGF ligands are expressed in RMS cells. Therefore, the whole pathway is overactivated, with consequent upregulation of downstream signalling pathways, e.g. PI3K-AKT [77].

Fig. 3

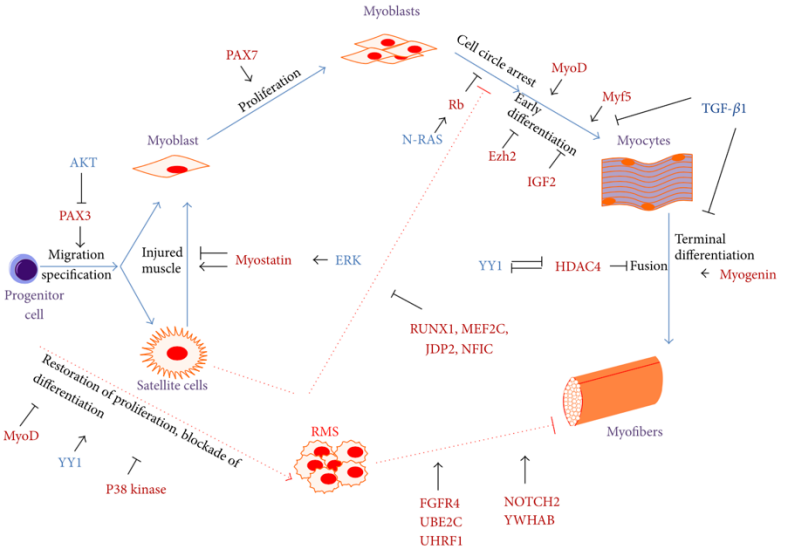

Fig. 3 Schematic representation of cellular origin and altered myogenic pathways in rhabdomyosarcoma tumour. Adapted from Sun *et al*., 2015.

RMS survival rate and current treatments

The 5-year survival rate for RMS is strongly related to the specific risk group assigned to the patient. The risk group is determined based on the location and size of the tumour, the metastasis to nearby lymph nodes and to other body districts, how much of the tumour was removed from initial surgery, the tumour subtype and the presence of the PAX3-FOXO1 translocation for ARMS (*American Cancer Society*).

For the low-risk group, the overall survival is about 70% to 90%. For the intermediate-risk group, it ranges from 50% to 70%, while for the high-risk group the overall survival drops down to 20-30% (*American Cancer Society*).

Standard treatments to fight RMS include surgery, radiotherapy and chemotherapy.

Surgery is the first-line approach to remove resectable tumours completely and is often associated to radiotherapy, especially when there is the involvement of nearby lymph nodes.

Chemotherapy is recommended to all RMS patients and the standard treatment is the VAC regimen, a mix of three drugs: Vincristine, Actinomycin D and Cyclophosphamide [78]. Particularly, Vincristine impairs microtubule polymerisation by sequestering Tubulin monomers [79]. Targeting microtubule dynamics is one of the best anti-tumour strategies identified so far, not only for RMS but also for many

other solid and blood cancers [80]. Indeed, Vincristine-induced microtubule cytoskeleton destabilisation results in the block of chromosome segregation during mitosis, preventing cells from dividing, and leading them to apoptosis [79].

Molecular targets with an aberrant upregulation in RMS can be inhibited by administering specific drugs (targeted therapies), such as the antibody against IGFR1 (Cixutumumab). There are preclinical and clinical trials investigating the benefits of combined targeted therapies, also administered in combination to chemotherapy, in order to bypass resistance to standard treatments. For example, the combination of Cixutumumab with standard chemotherapy shows promising results, as it increased the percentage of patients with an 18-month event-free survival [81].

Despite these encouraging results, there are still poor chances to cure high-risk RMS patients. Moreover, many of the standard treatments can have important side-effects in children (such as radiotherapy and high doses of chemotherapeutics). Therefore, there is the need to expand our knowledge about the molecular pathways involved in the progression of this cancer, to study more efficient treatments and ameliorate children survival rate.

Aim of the thesis

The work I carried out during my PhD aimed at elucidating the molecular role of circRNAs in regulating RMS tumorigenesis.

The main part of my research focused on understanding the role of a circRNA, circZNF609, in regulating cell cycle progression in this tumour.

As circRNA functions in RMS have not been elucidated yet, another part of my PhD work aimed to explore more generally the circRNA deregulation in RMS cells compared to wild-type myoblasts, in order to investigate their roles in tumorigenesis and their possible use as biomarkers for RMS diagnosis.

Studying circZNF609 role in regulating RMS cell proliferation

Myogenesis is a highly regulated process by which skeletal muscle is generated.

In the laboratory where I carried out my PhD research we previously identified a subset of circRNAs expressed and modulated during myogenesis [28]. Thanks to an siRNA-based phenotypic screening, we studied the effects of the knock-down of some circRNAs on human myogenesis. Indeed, we were interested in finding new regulatory circRNAs controlling proliferation in myoblasts (i.e.

proliferating myogenic precursors), and myoblast differentiation into myotubes (i.e. non-proliferating multinucleated muscle cells originating muscle fibres). Among the candidates tested, we focused our attention on circZNF609.

CircZNF609 derives from the circularisation of the second exon of ZNF609 primary transcript (***Fig. 4***). The full-length linear ZNF609 mRNA encodes for a poorly studied zinc-finger protein, involved in thymocyte maturation [82] and in neuron migration in the developing mouse brain [83].

ZNF609 second exon contains the last part of the 5'UTR of the gene and the start of its ORF, with two in-frame start codons (ATGs).

Upon circularisation of the second exon, the two ATGs are in frame with a stop codon which is downstream circZNF609 back-splicing junction (***Fig. 4***). Therefore, circZNF609 harbours a circRNA-specific ORF and can be translated into two proteins [28]. This was the first example of a translated circRNA in mammalian cells.

CircZNF609 also harbours m^6A modifications, with specific m^6A residues having a fundamental role in regulating its biogenesis and translation [18].

In human primary myoblasts, circZNF609 knock-down by an siRNA targeting its back-splicing junction (si-Circ) inhibits cell proliferation [28] (***Fig. 5***).

In order to understand how circZNF609 regulates myoblasts proliferation, during my Master's Degree I analysed the effects of circZNF609 depletion on the transcriptome of human primary myoblasts. Thanks to a differential expression analysis, we found 204 genes to be downregulated and 116 genes to be upregulated upon circZNF609 depletion [84].

We then performed a Gene Ontology (GO) term enrichment analysis on differentially expressed genes and found that the GO Biological Process terms enriched among downregulated genes were mainly related to cell cycle progression (***Fig. 6***). This was consistent with the impairment of myoblasts proliferation observed upon circZNF609 depletion [84].

To better investigate circZNF609 role in regulating cell proliferation, we decided to move to a system where cell cycle progression is altered, such as cancer. Therefore, we investigated circZNF609 expression and function in RMS, a skeletal muscle-related tumour.

My PhD thesis continues the work I started during my Master's Degree in Prof. Irene Bozzoni's lab. It aims to elucidate circZNF609 molecular mechanism of action in regulating cell cycle progression in two RMS subtypes, ERMS and ARMS.

Having found that circZNF609 is upregulated in ERMS and ARMS with respect to primary myoblasts, we

analysed the effects of circZNF609 knock-down on RMS cell cycle progression. We observed that circZNF609 depletion induced a slow-down of the G1-S phase transition in ERMS cells.

The analysis of known protein factors regulating cell proliferation, and particularly G1-S transition, revealed that circZNF609 depletion impairs both AKT and Retinoblastoma pathways. In this work, we aimed at distinguishing between the direct and indirect effects of circZNF609 knock-down on cell cycle regulators, to understand whether circZNF609 could affect AKT and Retinoblastoma directly or this is just an effect of a general cell cycle alteration induced by the circRNA modulation.

Since we found that circZNF609 depletion has different effects on ERMS and ARMS cell cycle progression, we compared circZNF609-induced transcriptomic changes and pathway alterations in the two RMS subtypes.

To understand circZNF609 molecular mechanism of action in regulating cell proliferation and highlight its direct effects on cell cycle progression, we investigated its molecular partners starting from its mRNA interactors. Therefore, we pulled down circZNF609 and sequenced the recovered RNA fraction. From this analysis we found Ckap5 transcript to directly interact with circZNF609.

As circZNF609 knock-down reduced Ckap5 mRNA stability and negatively affected its protein levels, we investigated whether and how circZNF609-Ckap5 interaction could regulate Ckap5 transcript stability and translation.

CKAP5 protein is a fundamental regulator of microtubule polymerisation and mitotic spindle assembly. Therefore, we analysed whether circZNF609 could directly regulate microtubule cytoskeleton and mitotic progression through the regulation of CKAP5 protein, obtaining encouraging results.

Since we found circZNF609 knock-down to impair a correct chromosome segregation and mitotic progression, we investigated whether this could lead to an accumulation of DNA damage in circZNF609-depleted RMS cells.

We actually found an accumulation of DNA damage and hypothesised this could lead to defects in cell cycle progression, such as the impaired G1-S progression previously observed.

Fig. 4

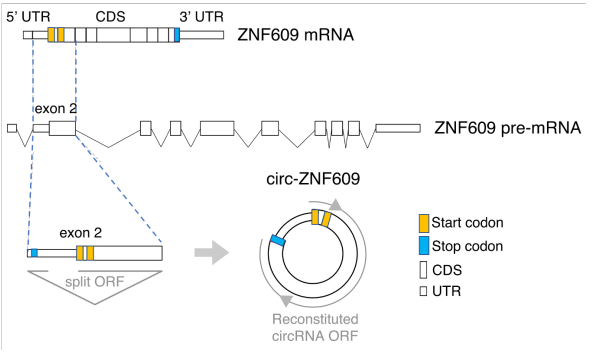

Fig. 4 Schematic representation of ZNF609 pre-mRNA and mRNA (top), and the circularisation process originating circZNF609 (bottom). ZNF609 exon 2 also harbours a split ORF which is then reconstituted upon circularisation. Adapted from Legnini *et al*., 2017.

Fig. 5

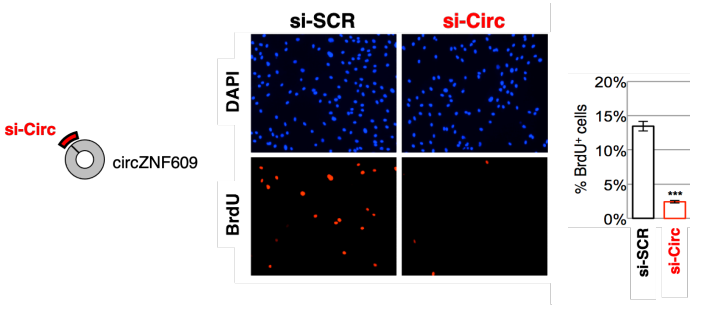

Fig. 5 Schematic representation of circZNF609-targeting siRNA (si-Circ) (left). BrdU assay in human primary myoblasts in control condition (si-SCR) and upon circZNF609 knock-down (si-Circ), and corresponding quantification of proliferant BrdU+ cells (right). Adapted from Legnini *et al.*, 2017.

Fig. 6

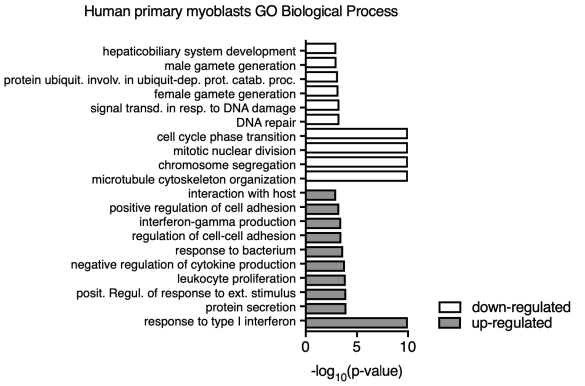

Fig. 6 Gene Ontology (GO) Biological Process term enrichment analysis on genes downregulated (white) and upregulated (grey) upon circZNF609 knock-down in human primary myoblasts.

Exploring circRNAs deregulated in RMS

We were interested in identifying other circRNAs differentially expressed between RMS cells and myoblasts, to explore whether they have a role in RMS tumorigenesis.

To this aim, we performed a circRNA differential expression analysis, starting from our total RNA-sequencing data from myoblasts, ERMS and ARMS cells [84].

We then selected a subset of differentially expressed circRNAs for further analyses.

Particularly, we decided to study the effects of circAFF1, circVAMP3 and circHIPK3 knock-down on ARMS cell transcriptome. Therefore, we performed an RNA-sequencing analysis in ARMS cells upon their depletion.

While the role of circAFF1 and circVAMP3 are currently being investigated by another PhD student in the lab, I am focusing on circHIPK3 and on its modulation of the YAP/TAZ pathway through specific miRNAs in ARMS cells. This part of my research is still at its beginning, and here I will present some preliminary results about circHIPK3 and its function in ARMS.

Results

CircZNF609 regulates RMS cell proliferation

CircZNF609 is upregulated in RMS and localises in specific cytoplasmic spots

The finding that circZNF609 regulates cell proliferation in human primary myoblasts [28], inspired us to investigate circZNF609 expression and function in a skeletal muscle related tumour, which is RMS.

We analysed circZNF609 expression levels in primary myoblasts and in ERMS and ARMS cell lines (RD and RH4, respectively). We found the circRNA to be significantly upregulated in both the RMS cell lines compared to myoblasts (***Fig. 7A***). The linear ZNF609 mRNA followed the same trend (***Fig. 7B***), suggesting that the ZNF609 locus may be activated at a transcriptional level in RMS.

We also analysed circZNF609 and ZNF609 mRNA expression in primary RMS biopsies from 6 ERMS and 5 ARMS paediatric patients, and in skeletal muscle biopsies from 3 age-matched donors who underwent surgery for non-oncological reasons. We found that both the circRNA and the mRNA were significantly upregulated in RMS biopsies compared to controls (***Fig. 7C-D***).

The upregulation of circZNF609 in RMS cell lines and biopsies is coherent with its function in promoting cell proliferation.

We previously observed that circZNF609 has a cytoplasmic localisation in myoblasts [28]. We then investigated its subcellular localisation in RMS cells by fluorescent in situ hybridization (FISH) using a probe targeting its back-splicing junction.

When looking at circZNF609 subcellular distribution in RD and RH4 cells, we observed that it showed a spotted cytoplasmic localisation (***Fig. 8A***). The signal was specific for the circRNA, as it disappeared upon its knock-down (***Fig. 8B***).

ZNF609 mRNA localisation was also checked and appeared to be cytoplasmic and spotted as well, but with a higher number of cytoplasmic spots than the circRNA (***Fig. 8C, left***). As a negative control for the FISH experiment, a probe targeting a bacterial mRNA was used, providing no signal (***Fig. 8C, right***).

Although the FISH protocol we used has a single-molecule sensitivity, we hypothesized that circZNF609 spots could contain more than one circZNF609 molecule, as they often showed different diameters (***Fig. 8D, asterisks***). Moreover, RD and RH4 cells showed very few circZNF609 spots (usually 1 or 2 spots per cell). Based on the circRNA expression level, it is unlikely that there could be so few circZNF609 molecules per cell, therefore we believe that the circRNA could aggregate in particular cytoplasmic sub-compartments. However, due to the signal amplification

obtained with the FISH protocol and to the limitations of optical microscope resolution, we were not able to establish the number of circZNF609 molecules in each aggregate.

Subsequently, we coupled circZNF609 FISH with immunofluorescence (IF) for either KDEL peptide (i.e. endoplasmic reticulum marker), or GM-130 (i.e. *cis*-Golgi marker), or pericentrin (i.e. centrosome marker), but observed no colocalisation of the circRNA with these organelles (***Fig. 9A-B-C***). Therefore, further investigation is needed to understand the specific cytoplasmic sub-compartment hosting circZNF609 aggregates.

Fig. 7

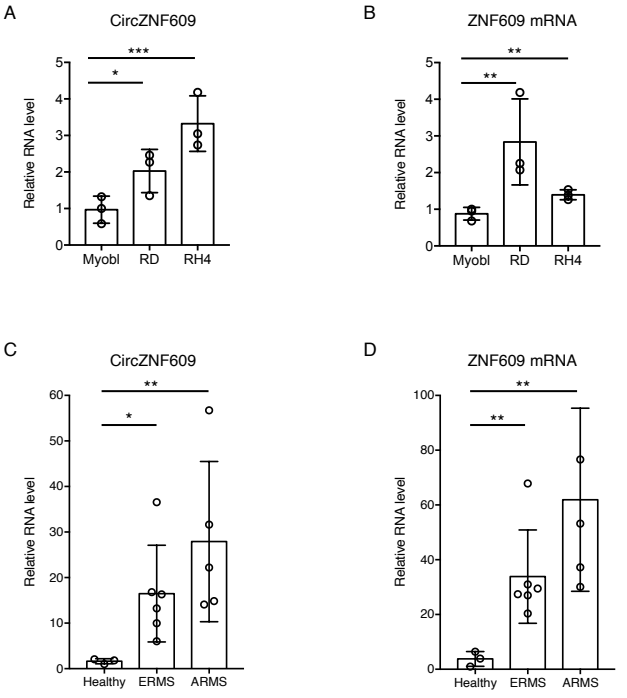

Fig. 7 CircZNF609 (A) and linear ZNF609 (B) RNA levels measured by qRT-PCR in human primary myoblasts (Myobl), RD and RH4 cells; N=3. CircZNF609 (C) and linear ZNF609 (D) RNA levels measured by qRT-PCR in 3 healthy skeletal muscle biopsies, 6 ERMS and 5 ARMS tumour biopsies.

In all panels relative RNA levels are represented as mean of the Fold Changes ± standard deviation of biological replicates, and dots represent individual data points. The ratio of each sample *versus* its experimental control was tested by two-tailed unpaired Student's t test. *: p-value < 0.1, **: p-value < 0.05, ***: p-value < 0.01.

Fig. 8

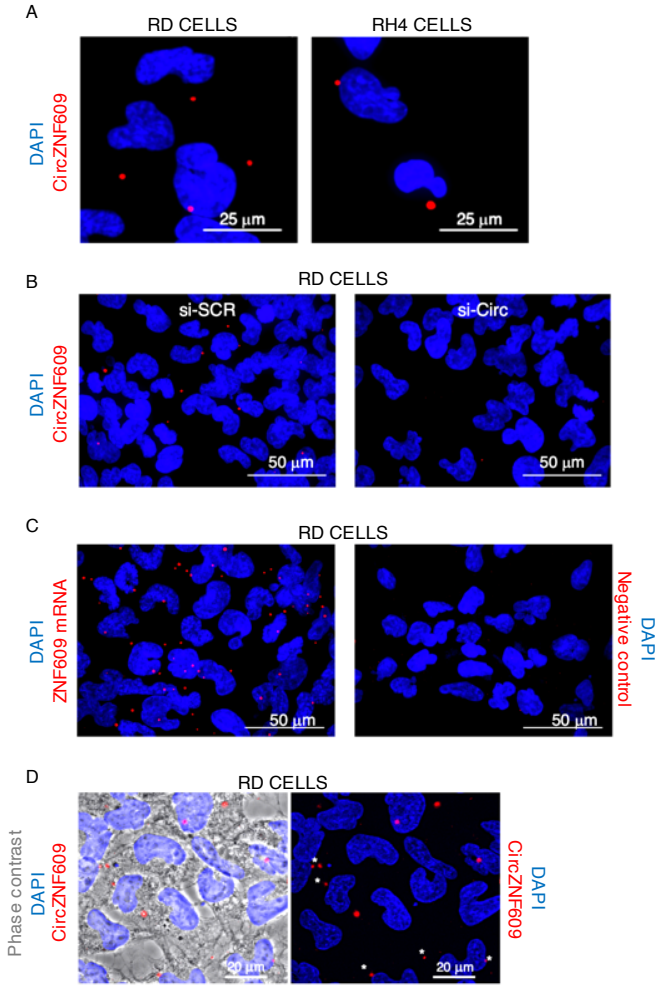

Fig. 8 FISH in RD and RH4 cells using a circZNF609-specific probe (A). FISH in RD cells using a circZNF609-specific probe in control condition (si-SCR) and upon circZNF609 knock-down (si-Circ) (B). FISH in RD cells using a ZNF609-specific probe or a bacterial mRNA-specific probe (negative control) (C). FISH in RD cells using a circZNF609-specific probe, merged with DAPI staining and phase contrast to highlight cell borders (left); white asterisks indicate smaller circZNF609 spots (right).

Fig. 9

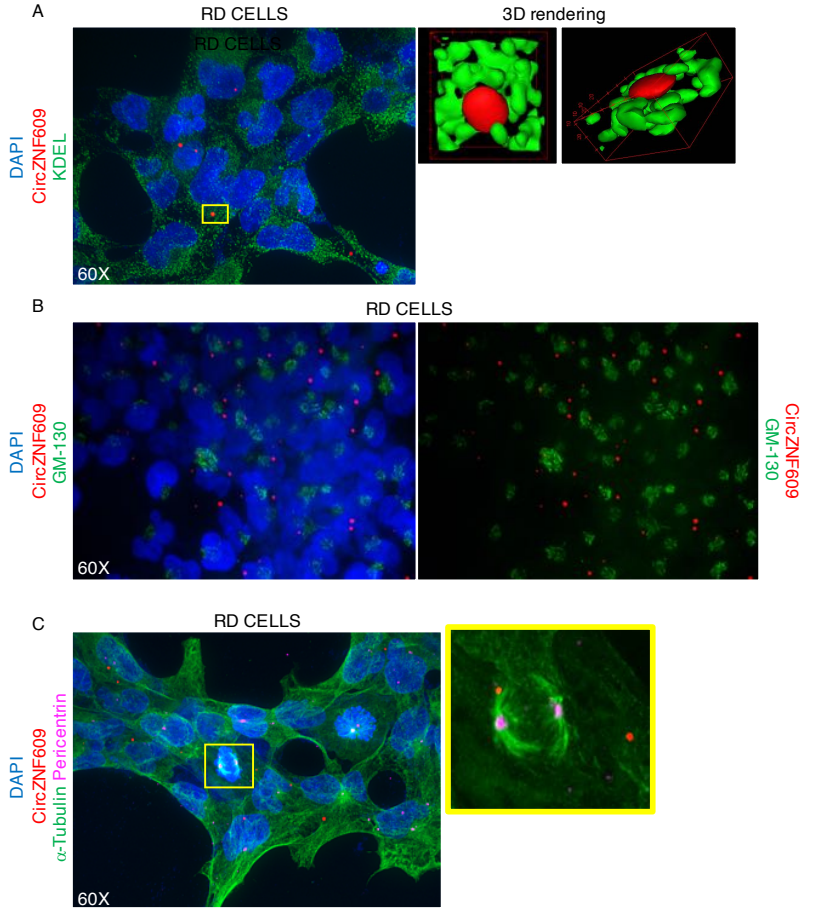

Fig. 9 FISH in RD cells using a circZNF609-specific probe combined with an immunofluorescence for KDEL peptide; 3D rendering of the spatial localisation of the circZNF609-spot and KDEL signal in the yellow rectangle is shown on the right, revealing no colocalisation (A). FISH in RD cells using a circZNF609-specific probe combined with an immunofluorescence for GM-130 protein (B). FISH in RD cells using a circZNF609-specific probe combined with an immunofluorescence for α-Tubulin and Pericentrin; a magnification of the area defined by the yellow rectangle is shown on the right (C).

CircZNF609 knock-down impairs G1-S transition in ERMS

To evaluate the effects of circZNF609 depletion on ERMS and ARMS cell cycle progression, we knocked down circZNF609 using an siRNA targeting its back-splicing junction (si-Circ) in RD and RH4 cell lines (***Fig. 10A***). We then performed a FACS cell-cycle analysis and found that circZNF609 knock-down induced a reproducible slow-down of cell cycle progression at the G1-S transition, with an increase of cells in G1 phase and a decrease of cells in S phase. Interestingly, this occurred only in RD cells (***Fig. 10B***) and not in RH4 cells (***Fig. 10C***).

We also performed the same analysis after the transfection of either an siRNA targeting both circZNF609 and ZNF609 mRNA (si-Circ+Lin) or an siRNA targeting only ZNF609 mRNA (si-Lin) (***Fig. 10D***). While si-Circ+Lin induced a G1-S transition slow-down in RD cells, si-Lin had no effects (***Fig. 10E***), confirming the specific role of circZNF609 (but not of its linear counterpart) in regulating ERMS cell cycle progression.

Since we observed a defect at the G1-S transition, we investigated some of the protein factors regulating G1-S checkpoint and cell proliferation, i.e. Retinoblastoma (RB) and Protein Kinase B (AKT).

RB is a fundamental regulator of G1-S transition, controlling the expression of E2F1-dependent S-phase genes. When hypo-phosphorylated, RB binds to E2F1 transcription factor, blocking its activity and consequently the expression of S-phase genes. When hyper-phosphorylated, RB cannot bind E2F1 protein anymore, therefore S-phase genes are transcribed [85].

Upon circZNF609 depletion in RD cells, the total RB protein level decreased. Interestingly, Rb mRNA levels were unchanged (***Fig. 11A***).

The levels of the phosphorylated form of RB (p-RB) strongly decreased as well. We measured the relative quantity of p-RB over total RB and found that circZNF609 depletion reduced the p-RB/RB ratio down to approximately 50% compared to the control condition in RD cells (***Fig. 11A***). This suggests that the RB/E2F1 pathway controlling G1-S transition is impaired upon circZNF609 knock-down.

Indeed, a transcriptomic analysis performed in circZNF609-depleted RD cells (discussed in the next paragraph) revealed that many E2F1-targets were downregulated, such as Cdk1, Cyclin A2, Cyclin B1, Cyclin B2, Pcna and some DNA polymerase subunits.

In RH4 cells, we observed a downregulation of both total RB and p-RB protein levels, but the p-RB/RB ratio did not decrease reproducibly (***Fig. 11B***), suggesting that these

cells could be more resistant to the RB/E2F1 pathway modulation following circZNF609 knock-down.

AKT protein is a fundamental modulator of cell growth and proliferation, standing at the crossroad of the regulation of cell cycle progression, glucose metabolism and protein translation [86,87]. Total AKT protein levels showed no changes, while the phosphorylated and active form of AKT (p-AKT) decreased upon circZNF609 depletion in both RD and RH4 cells (***Fig. 11A-B***).

This suggests that even if the circRNA knock-down does not affect RH4 cell proliferation, circZNF609 specificity of action on RB and AKT pathways is maintained also in RH4 cells.

To elucidate whether the decrease in total RB and p-AKT protein levels upon circZNF609 depletion was due to an increased degradation by the proteasome, we treated control and circZNF609-depleted RD cells with MG132, a proteasome inhibitor. To check whether the proteasome was correctly inhibited, we used $p27^{Kip1}$ protein as a positive control [88].

Following proteasome inhibition, RB protein levels showed no recovery (**Fig. 11C**). This suggests that the RB decrease upon circZNF609 knock-down could be due either to an inhibited translation of its mRNA or to a proteasome-independent protein degradation. So far, our preliminary data do not support an impaired translation of Rb mRNA (data not

shown). Therefore, we are still investigating whether a proteasome-independent protein degradation could be involved in RB downregulation upon circZNF609 depletion.

On the other hand, p-AKT protein levels were partially rescued in circZNF609-depleted cells upon MG132 treatment (***Fig. 11C***), suggesting that circZNF609 could contrast p-AKT proteasome-mediated degradation.

These effects on RB and AKT pathways indicate that the circRNA knock-down can affect key regulators of cell proliferation and that it maintains its specificity of action on common pathways in both RD and RH4 cells. However, further investigation is needed in order to discriminate whether these are direct effects or indirect effects due to a general alteration of cell proliferation following circZNF609 knock-down. In the following paragraphs, however, we will discuss a more direct effect of circZNF609 on a specific cell cycle-related pathway which could explain how circZNF609 can ultimately affect G1-S transition.

Fig. 10

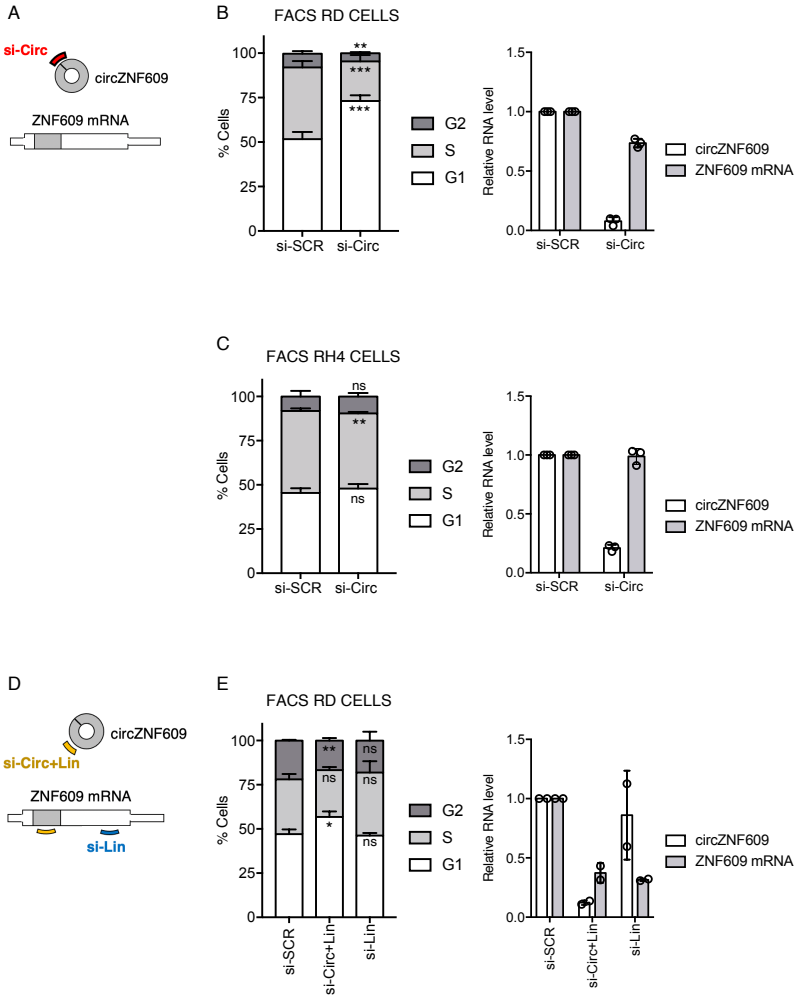
A
si-Circ
circZNF609
ZNF609 mRNA
B
FACS RD CELLS
% Cells
G2
S
G1
si-SCR
si-Circ
Relative RNA level
circZNF609
ZNF609 mRNA
C
FACS RH4 CELLS
ns
D
si-Circ+Lin
si-Lin
E
si-Circ+Lin

Fig. 10 Schematic representation of the siRNA used against circZNF609 (si-Circ) (A). Cell cycle analysis by FACS of RD cells upon control treatment (si-SCR) or circZNF609 knock-down (si-Circ), and corresponding relative RNA levels; N=3 (B). Cell cycle analysis by FACS of RH4 cells upon control treatment (si-SCR) or circZNF609 knock-down (si-Circ), and corresponding relative RNA levels; N=3 (C). Schematic representation of the siRNAs used against either both circZNF609 and ZNF609 mRNA (si-Circ+Lin) or against ZNF609 mRNA (si-Lin) (D). Cell cycle analysis by FACS of RD cells upon control treatment (si-SCR), circZNF609+ZNF609 knock-down (si-Circ+Lin) or ZNF609 knock-down (si-Lin), and corresponding relative RNA levels; N=2 (E).

In all panels FACS data are shown as mean of the percentage of cells in each cell-cycle phase + standard deviation of biological replicates; relative RNA levels are represented as mean of the Fold Changes ± standard deviation of biological replicates, and dots represent individual data points. Where statistical analysis was performed, the ratio of each sample *versus* its experimental control was tested by two-tailed unpaired Student's t test. *: p-value < 0.1, **: p-value < 0.05, ***: p-value < 0.01.

Fig. 11

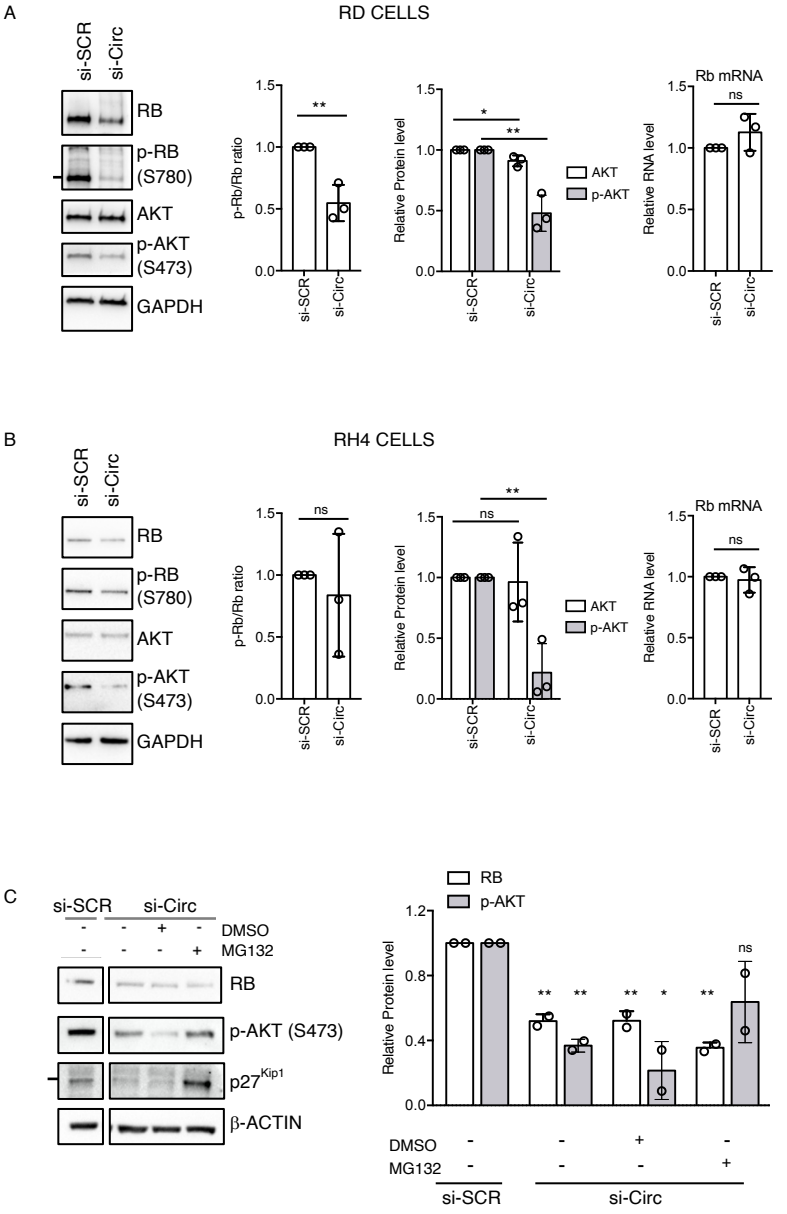
A
RD CELLS
si-SCR
si-Circ
RB
p-RB (S780)
AKT
p-AKT (S473)
GAPDH
p-Rb/Rb ratio
Relative Protein level
AKT
p-AKT
Rb mRNA
Relative RNA level
ns
B
RH4 CELLS
C
DMSO
MG132
p27Kip1
β-ACTIN

Fig. 11 Representative Western blot of RD cells in control conditions (si-SCR) and upon circZNF609 knock-down (si-Circ) with GAPDH hybridization used as loading control; ratio of pRB/RB protein levels, AKT and p-AKT protein levels (relative to GAPDH), and Rb mRNA levels (relative to Gapdh); N=3 (A). Representative Western blot of RH4 cells in control conditions (si-SCR) and upon circZNF609 knock-down (si-Circ) with GAPDH hybridization used as loading control; ratio of pRB/RB protein levels, AKT and p-AKT protein levels (relative to GAPDH), and Rb mRNA levels (relative to Gapdh); N=3 (B). Representative proteasome inhibition experiment in RD cells in control conditions (si-SCR) and upon circZNF609 knock-down (si-Circ) with $p27^{Kip1}$ hybridization used as positive control and β-ACTIN hybridization used as loading control; correspondent RB and p-AKT protein quantifications relative to β-ACTIN; N=2 (C).

All the graphs referred to proteins show the mean of protein quantification relative to the loading control ± standard deviation of biological replicates, with dots representing individual data points. Relative RNA levels are represented as mean of the Fold Changes ± standard deviation of biological replicates, and dots represent individual data points. The ratio of each sample *versus* its experimental control was tested by two-tailed unpaired Student's t test. In panel C, all the statistical confrontations were referred to the si-SCR sample. p-value: *: p-value < 0.05, **: p-value < 0.01, ***: p-value < 0.001, ****: p-value < 0.0001.

CircZNF609 knock-down affects different pathways in ERMS and ARMS cells

Since circZNF609 knock-down had different effects on ERMS and ARMS cell proliferation, we compared the transcriptomic responses of RD and RH4 cells upon circZNF609 depletion, to identify divergences in the pathways altered in the two cell lines.

Therefore, an RNA-sequencing analysis was performed on two biological replicates of circZNF609 knock-down in RD and RH4 cells, respectively.

With the support of the bioinformaticians in our laboratory, we performed a differential expression analysis, and then a GO term enrichment analysis on downregulated and upregulated genes in RD and RH4 cells, obtaining different results in the two RMS subtypes.

In RD cells, the Biological Process (BP) GO terms enriched among the downregulated genes were related to cell proliferation, consistently with the phenotype observed in these cells upon circZNF609 depletion. Among the most significant terms, there were “DNA replication”, “chromosome segregation”, “mitotic nuclear division” and “cell cycle phase transition” (***Fig. 12A***).

These results highlight a profound effect of circZNF609 knock-down on cell cycle-related genes. As circZNF609 depletion affects Retinoblastoma/E2F1 pathway,

it is likely that the downregulation of the majority of the genes related to DNA replication and S-phase entry are indirectly regulated by circZNF609 through RB/E2F1.

Interestingly, the categories enriched among the downregulated genes were related to different phases of the cell cycle, also including mitosis.

In contrast, the GO BP term enrichment analysis on the downregulated genes in RH4 cells did not reveal any cell proliferation-related category. Indeed, RH4 cells did not show any significant alteration of the RB/E2F1 pathway, and this could explain the lack of deregulation of E2F1-dependent S-phase entry genes.

Instead, some of the enriched terms were related to cell locomotion (e.g. “actin filament organisation”, “positive regulation of locomotion”). Finally, no GO term enrichment was found among the upregulated genes in RH4 cells (***Fig. 12B***).

We then explored and compared the pathways deregulated upon circZNF609 knock-down in RD and RH4 cells. To do this, we performed a Gene Graph Enrichment Analysis (GGEA) [89], which allows to compute consistency of the differentially expressed genes with the regulatory interactions existing among them according to KEGG pathways [90].

GGEA outputs are graphs representing sets of genes involved in the same pathway. Genes are represented as nodes, coloured either in red (if downregulated) or in green (if upregulated). The activating/inhibitory interaction between two genes is represented as an edge, coloured according to consistency (***Fig. 12C-D***).

In circZNF609-depleted RD cells, GGEA revealed "DNA replication", "cell cycle" and "PI3K-AKT signalling pathway" among the most significantly and consistently deregulated pathways (***Fig. 12C, Table 1***).

Instead, in RH4 cells we obtained less significant results, with almost no enrichment of cell proliferation-related pathways (***Table 1***). However, the "PI3K-AKT signalling pathway" was found to be altered (***Fig. 12D***), in line with the previously shown data indicating that circZNF609 depletion downregulated p-AKT protein levels also in RH4 cells.

In conclusion, the GO term enrichment analysis and GGEA revealed that circZNF609 knock-down induces a downregulation of cell cycle-related genes in RD cells, affecting different proliferation-related pathways.

These analyses also confirmed that circZNF609 depletion does not affect the proliferative capacity of RH4 cells. In fact, no significant alteration of cell proliferation-related pathways was observed in this cell line.

Subsequently, we performed a msVIPER (Virtual Inference of Protein-activity by Enriched Regulon) analysis to identify the upstream regulators of the transcriptomic responses induced by circZNF609 knock-down in RD and RH4 cells.

msVIPER allows to predict changes in protein activity, based on the differential expression of the genes which are part of the protein's regulon [91]. Since the relationship between the protein and its regulon depends on the specific tumour context, we based our analysis on human sarcoma regulons [92].

In ***Fig. 13A-B*** the typical msVIPER output is shown. The "Set" column contains the names of proteins whose activity status is predicted. Red colours in the "Act" column indicate a predicted protein activation, while blue colours stand for a predicted de-activation. Protein expression is described in the "Exp" column, with white meaning that the protein is expressed and grey that it is not expressed in RD or RH4 cells. Rows represent the gene regulon associated with each protein. Red and blue vertical bars in the rows represent genes in the regulon; particularly red bars are genes generally observed to be upregulated if the protein is active, while blue bars are genes downregulated if the protein is active. The more the genes are packed to the right and left extremities of the row, the more they are upregulated or downregulated upon

circZNF609 knock-down, respectively. Therefore, in the case of a predicted protein activation, the more the red genes are packed to the right and the blue genes are packed to the left, the more their deregulation upon circZNF609 depletion is consistent with the activation of a particular protein (p-values indicating the significance of the prediction are listed at the left of the table). On the other hand, in the case of a predicted protein de-activation, the more the red genes are packed to the left and the blue genes are packed to the right, the more their deregulation is consistent with the protein de-activation.

According to msVIPER analysis, circZNF609 depletion in RD cells induced the de-activation of TCF19, CENPU, MCM7 and ZWINT (***Fig. 13A, asterisks***). These factors are known master regulators of cell cycle progression, promoting not only G1-S transition but also chromosome segregation, as in the case of CENPU and ZWINT [93–100]. This suggests that circZNF609 knock-down could have an impact on mitotic progression as well.

We then analysed the relative RNA levels of these master regulators upon circZNF609 knock-down in RD cells, and we found all of them to be actually downregulated (***Fig. 13C***).

In RH4 cells, among the proteins predicted to be de-activated upon circZNF609 knock-down there were not known master regulators of cell cycle progression, except for Cyclin

E1 and MCM7, which however had higher p-values than those observed in RD cells (***Fig. 13B, asterisks***). This was again coherent with the fact that circZNF609 depletion does not alter cell cycle progression in RH4 cells.

We also checked whether Tcf19, Cenpu, Mcm7 and Zwint were downregulated at their RNA level in RH4 cells upon circZNF609 depletion, but they were not affected (***Fig. 13D***).

Interestingly, by comparing RD and RH4 transcriptomes in control conditions, we noticed that Mcm7, Cenpu and Zwint were expressed at lower levels in RH4 with respect to RD cells (***Fig. 13E***).

We also observed that in RH4 many cell-cycle related genes were expressed at higher levels than in RD cells, but their expression was stable upon circZNF609 knock-down (***Fig. 13E, asterisk***). Among these genes, there was a significant enrichment of p53 targets (i.e. Cdk2, Cdkn1b, E2f7, E2f1, Znf385a, Pcbp4, Ccna2, Ccna1, Ccne1, Ccne2, enriched in the Reactome pathway "TP53 regulates transcription of genes involved in G1 cell cycle arrest"; FDR = $4.02e^{-02}$).

We checked for p53 expression in RD and RH4 cells in control condition, and we found it to be strongly downregulated in RH4 cells (log_2 Fold Change = -3.7; FDR = 0). It has also been reported in literature that p53 gene carries a gain-of-function mutation in RD (R248W homozygous

mutation), while it shows a loss-of-function mutation in RH4 cells (frameshift deletion of nucleotides 1001–1013) [101–103].

Therefore, we hypothesised that p53 lower expression in RH4 than in RD cells contributed to the upregulation of many p53-target cell cycle-related genes in RH4.

This could account for a more complex dysregulation of proliferation-related pathways in RH4 cells, which cannot be counteracted by the knock-down of circZNF609 alone. In this way we could explain the lack of effects of circZNF609 depletion on RH4 cell cycle progression.

Fig. 12

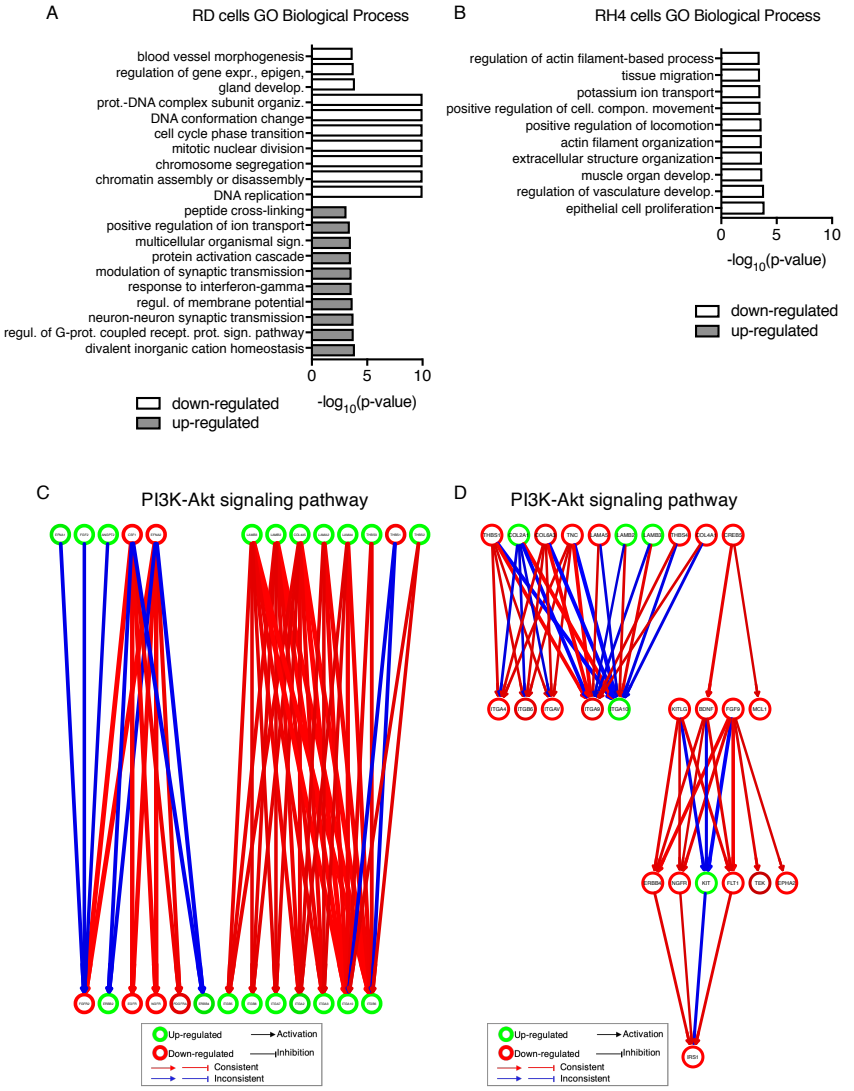

Fig. 12 Gene Ontology (GO) term enrichment analysis (Biological Process) performed on genes downregulated (white) and upregulated (grey) upon circZNF609 depletion in RD cells (A) and RH4 cells (B). One of the most significant GGEA results upon circZNF609 knock-down in RD cells (C) and RH4 cells (D); the clearer the node/edge colour appears in the graph, the more significant it is.

Fig. 13

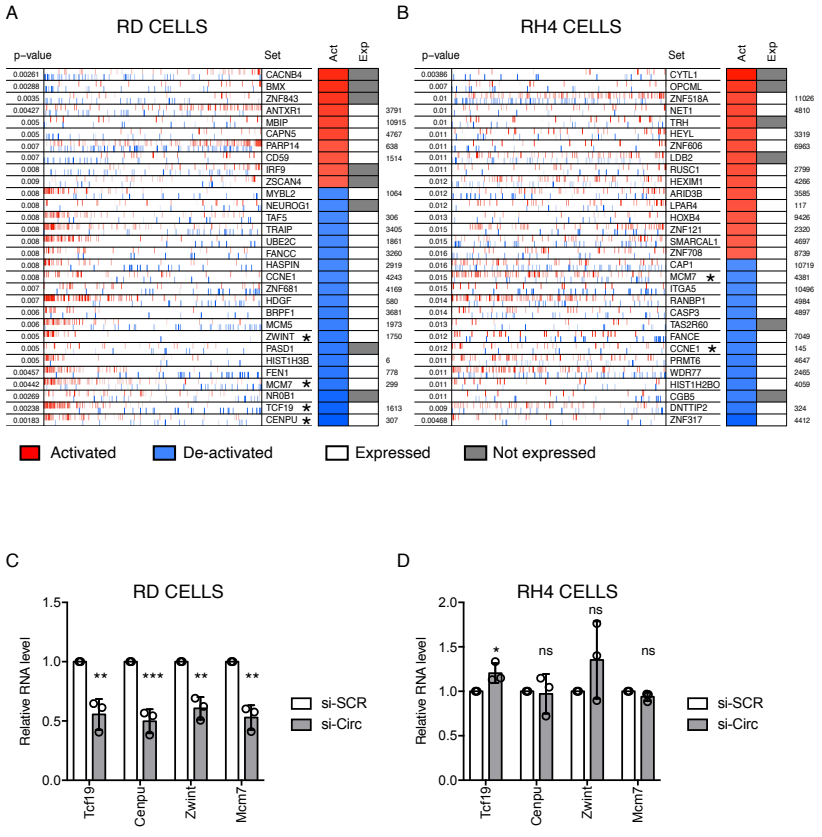
A
RD CELLS
p−value
Set
Act
Exp
CACNB4
BMX
ZNF843
ANTXR1
MBIP
CAPN5
PARP14
CD59
IRF9
ZSCAN4
MYBL2
NEUROG1
TAF5
TRAIP
UBE2C
FANCC
HASPIN
CCNE1
ZNF681
HDGF
BRPF1
MCM5
ZWINT
PSD1
HIST1H3B
FEN1
MCM7
NR0B1
TCF19
CENPU
B
RH4 CELLS
CYTL1
OPCML
ZNF518A
NET1
TRH
HEYL
ZNF606
LDB2
RUSC1
HEXIM1
ARID3B
LPAR4
HOXB4
ZNF121
SMARCAL1
ZNF708
CAP1
MCM7
ITGA5
RANBP1
CASP3
TAS2R60
FANCE
CCNE1
PRMT6
WDR77
HIST1H2BO
CGB5
DNTTIP2
ZNF317
Activated
De-activated
Expressed
Not expressed
C
RD CELLS
Relative RNA level
si-SCR
si-Circ
Tcf19
Cenpu
Zwint
Mcm7
D
RH4 CELLS
ns

E

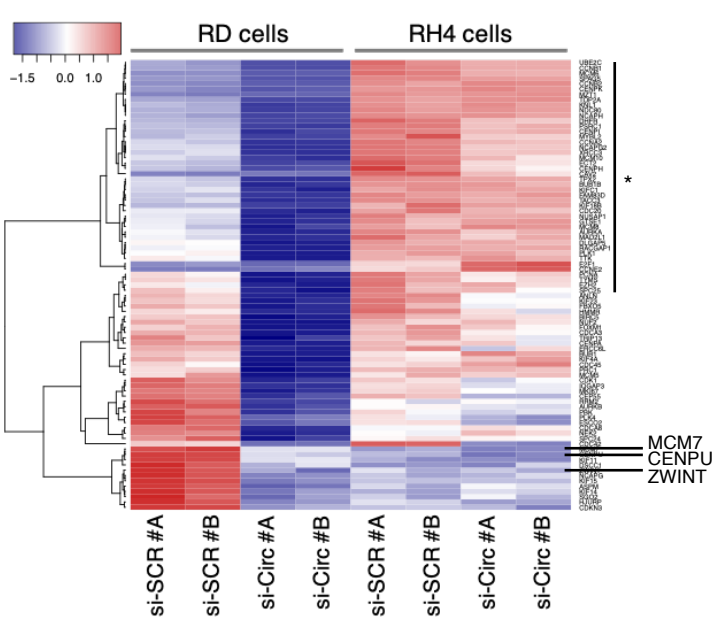
RD cells
RH4 cells
−1.5
0.0
1.0
*
MCM7
CENPU
ZWINT
si-SCR #A
si-SCR #B
si-Circ #A
si-Circ #B
si-SCR #A
si-SCR #B
si-Circ #A
si-Circ #B

Fig. 13 msVIPER plot for RD (A) and RH4 cells (B) showing the transcriptional status (blue=repressed, red=activated) of the target genes (bars in each row) for each differentially active transcriptional regulator; the inferred differential activity is shown in the first column (red=activated, blue=de-activated), and the expression is shown in the second column (grey=not expressed, white=expressed); the numbers at the right side of the plot indicate the rank of the displayed genes in the VIPER inferred gene expression signature; p-values refer to the differential activity of the factor calculated by msVIPER. Relative RNA levels of some master regulators identified though msVIPER analysis in control condition (si-SCR) and upon circZNF609 knock-down (si-Circ), in RD (C) and RH4 cells (D); N=3. Heatmap representing differential expression of some cell-cycle related genes in RD and RH4 cells in control condition (si-SCR) and upon circZNF609 knock-down (si-Circ), in two replicates (#A and #B) analysed by RNA-sequencing; expression values are plotted as colour-coded mean-centred $\log_2$-transformed RPKM values (E).

Relative RNA levels are represented as mean of the Fold Changes ± standard deviation of biological replicates, and dots represent individual data points. The ratio of each sample *versus* its experimental control was tested by two-tailed unpaired Student's t test. p-value: *: p-value < 0.05, **: p-value < 0.01, ***: p-value < 0.001, ****: p-value < 0.0001.

Identifying circZNF609 molecular interactors to understand its mechanism of action

Once we elucidated the effects of circZNF609 knock-down on RMS cell proliferation and transcriptome, we were interested in deepening our knowledge about circZNF609 molecular mechanism of action. Therefore, we decided to focus on its molecular interactors, starting from the analysis of circRNA-mRNA interactions.

A pulldown of the endogenous circZNF609 was performed in RD cells after 4'-aminomethyl-4,5',8-trimethylpsoralen (AMT) crosslinking, according to an established protocol [104].

We opted for a crosslinked RNA-pulldown because we were interested only in direct interactions between circZNF609 and mRNAs, and we chose the psoralen-mediated crosslinking as it is specific for RNA-RNA interactions. Indeed, AMT can intercalate into double-stranded RNA and form covalent bonds between pyrimidines on adjacent RNA molecules, upon a 365-nm UV irradiation. The crosslinking can then be reverted by irradiating RNA with 254-nm UV light.

To pull down circZNF609, we used two sets of biotinylated probes (named *odd* and *even*) targeting ZNF609 exon 2. All the probes can pair both on the circularized exon 2 (circZNF609) and on the exon 2 included in ZNF609 mRNA,

since it was not possible to design a back-splicing junction-specific probe.

We checked for circZNF609 and ZNF609 mRNA enrichment in two biological replicates of the pulldown experiment (***Fig. 14A***). We then performed an RNA-sequencing analysis on the second replicate, in which no enrichment of the linear mRNA was detected, even if circZNF609 enrichment was about 10-fold lower compared to the first replicate. Indeed, we aimed to limit the pulldown of mRNAs interacting also with ZNF609 linear transcript.

The analysis of the RNA-sequencing data was complicated by the fact that only a small percentage of the total number of reads could be aligned to the reference transcriptome, as the majority of them was too degenerated. Particularly, the uniquely mapping reads were 17.02% for the *even* pulldown, 13.35% for the *odd* pulldown, 9.63% for the Input and 3.68% for the LacZ pulldown (the negative control). We think that this could be due to either the AMT-crosslinking or the reverse-crosslinking procedure, as the protocol we used was not optimised for a subsequent RNA-sequencing analysis and may require adaptations.

However, with the help of the bioinformaticians of our group, we could identify some mRNAs enriched in the *odd* and *even* circZNF609 pulldown samples compared to the pulldown

of the bacterial LacZ mRNA. These candidate mRNAs interacting with circZNF609 are listed in ***Table 2***.

Among the interactors of circZNF609, we furthered our investigations on Ckap5, Ddx27 and Pes1 mRNAs.

Their interaction with the circRNA was validated by qRT-PCR on two native (i.e. not crosslinked) circZNF609 pulldown experiments performed by mixing *odd* and *even* probes together (***Fig. 14B-C***). These interactions were also validated in the non-sequenced replicate of the psoralen-crosslinked pulldown with *odd* and *even* probes used separately (***Fig. 14D***). In this experiment, the enrichment of Ckap5 and Ddx27 mRNAs over the Input was higher in the *even* pulldown (***Fig. 14D***), which also showed the higher enrichment of circZNF609 if compared to the *odd* pulldown (***Fig. 14A, left***). However, in this experiment Pes1 mRNA could not be amplified properly (***Fig. 14D***).

Ckap5 (also known as ch-TOG) mRNA encodes for a highly conserved cytoskeleton-associated protein. CKAP5 is a member of the XMAP215 family regulating microtubule dynamics. It binds to the *plus* end of microtubules and promotes their nucleation and elongation. It also regulates mitotic spindle formation and chromosome segregation by stabilising kinetochore fibres, thus having an important role in mitotic progression [105–108].

Pes1 and Ddx27 mRNAs encode for proteins involved in rRNA processing. PES1 is a component of the PeBoW complex, together with BOP1 and WDR12 proteins, while DDX27 is an associated factor of this complex. The PeBoW complex and DDX27 regulate pre-rRNA processing and 60S ribosomal subunit maturation. Therefore, they can be involved in cell growth and proliferation by controlling ribosome biogenesis [109,110].

To investigate whether circZNF609 depletion could have an effect on the stability and/or translation of the interacting mRNAs, we analysed RNA and protein levels of CKAP5, PES1 and DDX27 upon circZNF609 knock-down.

While circZNF609 depletion has no effects on PES1 and DDX27, either at the RNA or at the protein level (***Fig. 15A-B***), a decrease in CKAP5 protein was observed (***Fig. 15C***). On the other hand, Ckap5 mRNA showed a slight downregulation trend upon circZNF609 depletion (***Fig. 15C*** and ***Fig. 20A***), although this trend was not always significant (as in ***Fig. 15C***)

However, to investigate whether the downregulation trend of Ckap5 mRNA upon circZNF609 knock-down could be due to a slightly reduced transcript stability, we treated control and circZNF609-depleted cells with Actinomycin D to inhibit transcription. We found a small but significant decrease in Ckap5 mRNA stability after 2.5 hours and 5 hours of

Actinomycin D treatment (***Fig. 15D***). As controls, we tested the half-life of an mRNA whose levels are stable upon circZNF609 depletion (Gapdh) and of a transcript which is downregulated upon circZNF609 knock-down (AurkA). Both the mRNAs showed a non-significant variation in their half-life in response to circZNF609 depletion (***Fig. 15D***).

These data suggest that the interaction between circZNF609 and Ckap5 mRNA could be functional to the regulation of Ckap5 transcript stability and protein levels. On the other hand, we are still investigating which could be the biological function of the circZNF609 interaction with Ddx27 and Pes1 mRNAs.

Fig. 14

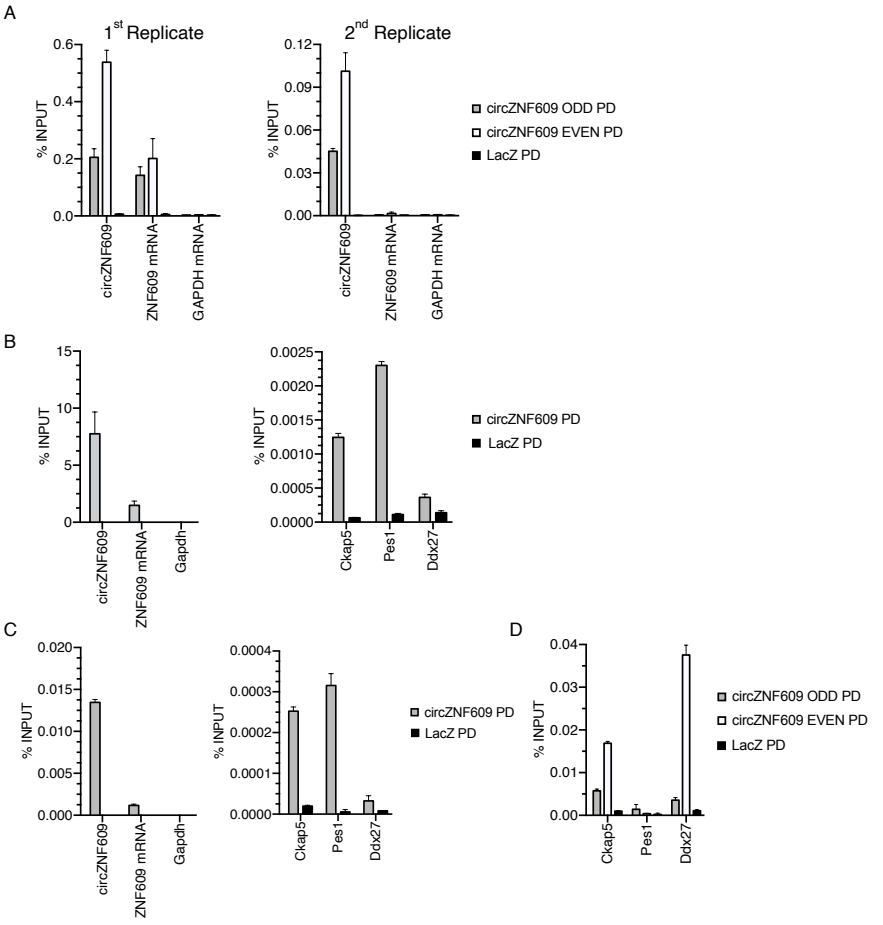

Fig. 14 qRT-PCR experiments showing the enrichment of circZNF609, ZNF609 mRNA and Gapdh mRNA (negative control) with respect to Input in two replicates of the psoralen-crosslinked circZNF609-pulldown in RD cells (A). qRT-PCR experiments showing the enrichment of circZNF609, ZNF609 mRNA, Gapdh mRNA (negative control) and candidate circZNF609 interactors with respect to Input, in two native circZNF609-pulldowns in RD cells (B-C). qRT-PCR experiments showing the enrichment of candidate circZNF609 interactors with respect to Input in the first replicate of the psoralen-crosslinked circZNF609-pulldown shown in *Fig. 14A* (D). Data are shown as mean of Fold Changes ± standard error of technical triplicates.

Fig. 15

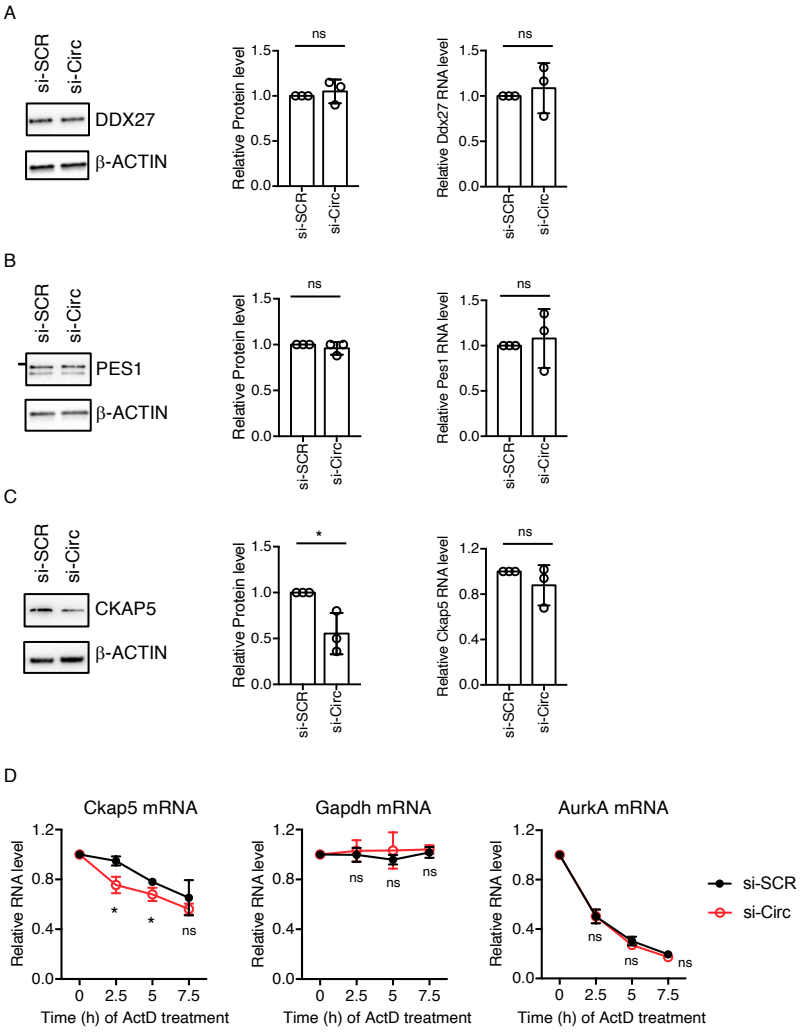
A
si-SCR
si-Circ
DDX27
β-ACTIN
Relative Protein level
Relative Ddx27 RNA level
ns
B
PES1
Relative Pes1 RNA level
C
CKAP5
Relative Ckap5 RNA level
*
D
Ckap5 mRNA
Gapdh mRNA
AurkA mRNA
Relative RNA level
Time (h) of ActD treatment
si-SCR
si-Circ

Fig. 15 Representative Western blot of RD cells in control conditions (si-SCR) and upon circZNF609 knock-down (si-Circ) with β-ACTIN hybridization used as loading control; protein quantifications (relative to β-ACTIN) and corresponding RNA levels of DDX27 (A), PES1 (B) and CKAP5 (C) in RD cells in control conditions (si-SCR) and upon circZNF609 knock-down (si-Circ); N=3. qRT-PCR experiments showing Ckap5, Gapdh and AurkA mRNA half-life upon Actinomycin D treatment in RD cells, in control conditions (si-SCR) and upon circZNF609 knock-down (si-Circ); N=3 (D).

All the graphs referred to proteins show the mean of protein quantification relative to β-ACTIN ± standard deviation of biological replicates, with dots representing individual data points. Relative RNA levels are represented as mean of the Fold Changes ± standard deviation of biological replicates, and dots represent individual data points. The ratio of each sample *versus* its experimental control was tested by two-tailed unpaired Student's t test. p-value: *: p-value < 0.05, **: p-value < 0.01, ***: p-value < 0.001, ****: p-value < 0.0001.

HUR protein can bind Ckap5 mRNA in the circZNF609-interaction site

Using IntaRNA, a software for calculating RNA-RNA interactions [111], we predicted the interacting sequences between circZNF609 and Ckap5 mRNA.

The best predicted interaction involved the 3'UTR of Ckap5 (nucleotides 6443-6451 of the ENST00000529230 isoform) and the coding sequence of circZNF609 (nucleotides 600-671). The calculated Free Energy of the predicted interaction is -31.83 kcal/mol (***Fig. 16A***).

Since the 3'UTR region of mRNAs is known to contain many regulatory sequence elements such as RNA binding protein (RBP) target sites, we analysed the sequence of Ckap5 3'UTR interacting with circZNF609 looking for RBP consensus motifs. There, we found three tandem binding sites for HUR RBP (***Fig. 16A, underlined***).

HUR (also known as ELAVL1) is a member of the ELAV-like RBP family. It generally binds to AU-rich elements (AREs) in the 3'UTR of mRNAs, often stabilising them [112,113] and enhancing their translation [114–116].

Non-ARE motifs for HUR binding have also been described in the literature, e.g. CU_nC and $(CUUU)_{11}(U)_8$ [117,118].

The HUR-binding sites we found in the Ckap5-circZNF609 interacting region belong to the CU_nC type (i.e. $[CU_4]_3$).

Data mining analysis performed using published PAR-CLIP-sequencing data confirmed that Ckap5 3'UTR is bound by HUR in HeLa [119] and HEK293 cells [120], and that the binding occurs in the circZNF609-interacting region in both the cell types (***Fig. 16B***).

We then checked whether HUR could bind Ckap5 mRNA in RD cells and whether this interaction could be affected by circZNF609 depletion. By performing an HUR RIP assay, we found that both circZNF609 and Ckap5 mRNA can be immunoprecipitated with HUR. Interestingly, the interaction between HUR and Ckap5 mRNA is reduced upon circZNF609 knock-down (***Fig. 16C***).

CircZNF609 itself has been reported to have eight binding sites for HUR according to CircInteractome database [121]. These sites were identified on ZNF609 exon 2 in a PAR-CLIP experiment in conjunction with MNase treatment in HEK293 cells [120] (***Fig. 16D***).

We also observed that circZNF609-depletion has no effects on HUR protein levels (***Fig. 16E***).

Subsequently, we checked whether the downregulation of CKAP5 protein, observed upon circZNF609 depletion, could be reproduced by HUR knock-down, in order to

understand whether circZNF609 could modulate CKAP5 levels *via* HUR. A preliminary experiment showed that CKAP5 protein was downregulated compared to control condition upon both circZNF609 knock-down and HUR knock-down (***Fig. 16F***).

In conclusion, we found that circZNF609 could interact with a region in Ckap5 3'UTR hosting three HUR binding sites. HUR actually binds both Ckap5 mRNA and circZNF609, and HUR-Ckap5 interaction decreases when the circRNA is downregulated. We checked whether circZNF609 depletion influences HUR protein levels, but it has no effects. Finally, upon HUR knock-down, CKAP5 protein level decreases, suggesting it can be regulated by HUR.

Altogether these findings indicate that circZNF609 could promote HUR-Ckap5 interaction. Indeed, circZNF609 can bind both HUR and Ckap5 mRNA. We hypothesise that the interaction between the circRNA and the mRNA could bring HUR in the proximity of Ckap5 3'UTR, facilitating its loading onto the mRNA. Therefore, circZNF609 might stabilise Ckap5 mRNA and promote its translation *via* HUR (***Fig. 16G***).

Fig. 16

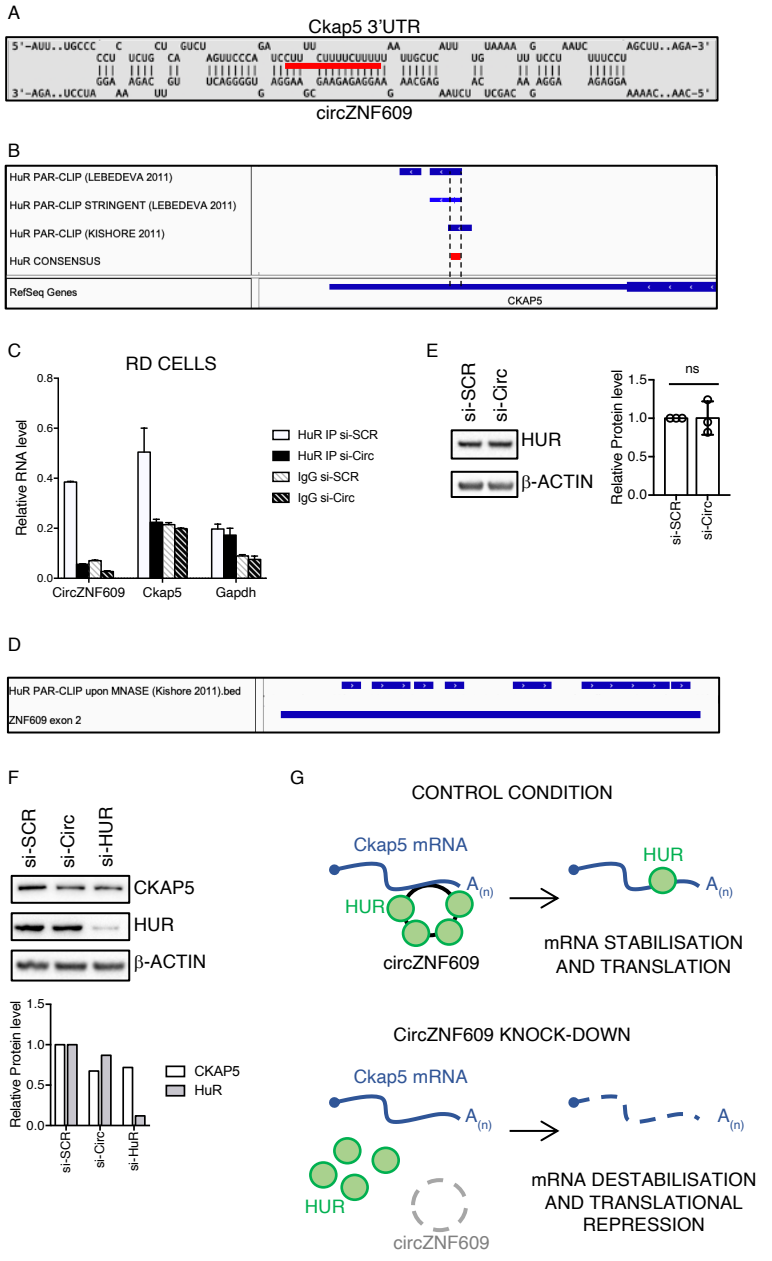
A
Ckap5 3'UTR
circZNF609
B
HuR PAR-CLIP (LEBEDEVA 2011)
HuR PAR-CLIP STRINGENT (LEBEDEVA 2011)
HuR PAR-CLIP (KISHORE 2011)
HuR CONSENSUS
RefSeq Genes
CKAP5
C
RD CELLS
Relative RNA level
HuR IP si-SCR
HuR IP si-Circ
IgG si-SCR
IgG si-Circ
CircZNF609
Ckap5
Gapdh
E
si-SCR
si-Circ
HUR
β-ACTIN
Relative Protein level
ns
D
HuR PAR-CLIP upon MNASE (Kishore 2011).bed
ZNF609 exon 2
F
si-SCR
si-Circ
si-HUR
CKAP5
HUR
β-ACTIN
Relative Protein level
CKAP5
HuR
G
CONTROL CONDITION
Ckap5 mRNA
HUR
circZNF609
mRNA STABILISATION
AND TRANSLATION
CircZNF609 KNOCK-DOWN
mRNA DESTABILISATION
AND TRANSLATIONAL
REPRESSION

Fig. 16 Interaction between Ckap5 mRNA 3'UTR (top) and circZNF609 (bottom) according to IntaRNA prediction; the red bar highlights the HUR binding site on Ckap5 3'UTR (A). HUR binding sites within the 3'UTR of Ckap5 (reverse strand) identified by published PAR-CLIP data; the red track indicates the HUR consensus motif in the 3'UTR of Ckap5 (B). qRT-PCR showing the enrichment of circZNF609, Ckap5 and Gapdh (negative control) mRNAs with respect to Input, in a representative HUR RIP experiment in RD cells; N=3 (C). HUR binding sites within ZNF609 exon 2 identified by published PAR-CLIP data (D). Representative Western blot showing HUR protein levels in RD cells in control conditions (si-SCR) and upon circZNF609 knock-down (si-Circ) with β-ACTIN hybridization used as loading control; HUR protein quantifications (relative to β-ACTIN) in RD cells in control conditions (si-SCR) and upon circZNF609 knock-down (si-Circ); N=3 (E). Western blot showing CKAP5 and HUR protein levels in RD cells in control conditions (si-SCR), upon circZNF609 knock-down (si-Circ) and upon HUR knock-down (si-HUR) with β-ACTIN hybridization used as loading control, and corresponding protein quantifications (relative to β-ACTIN); N=1 (F). Schematic representation of the proposed molecular mechanism through which circZNF609 stabilises Ckap5 transcript and promotes its translation *via* HUR protein.

In panel C, data referred to RNA are shown as mean of Fold Changes ± standard error of technical triplicates. In panel E, data referred to proteins are shown as means of protein quantification relative to β-ACTIN ± standard deviation of biological replicates, and dots represent individual data points. Where statistical analysis was performed, the ratio of each sample *versus* its experimental control was tested by two-tailed unpaired Student's t test. p-value: *: p-value < 0.05, **: p-value < 0.01, ***: p-value < 0.001, ****: p-value < 0.0001.

CircZNF609 could regulate microtubule dynamics and cell cycle progression through CKAP5

CKAP5 is a fundamental regulator of microtubule (MT) dynamics and mitotic spindle stability.

Interestingly, we found GO BP terms related to MT cytoskeleton, mitosis and chromosome segregation to be enriched among downregulated genes upon circZNF609 knock-down, in primary myoblasts and in RD cells (***Fig. 17A***). Moreover, among the msVIPER results in RD cells, we found master regulators of chromosome segregation (e.g. CENPU and ZWINT) to be de-activated and downregulated at the RNA level upon circZNF609 depletion. This suggests that microtubule-dependent chromosome segregation and mitotic progression are impaired, and we hypothesised this is due to the circZNF609-dependent downregulation of CKAP5.

Therefore, we decided to explore MT dynamics upon circZNF609 knock-down, and performed a cold-induced MT depolymerisation and re-polymerisation assay (***Fig. 17B***) in RD cells, in collaboration with Dr Patrizia Lavia's lab.

Preliminary experiments revealed that after 20 minutes of cold-induced MT depolymerisation, circZNF609-depleted cells showed a significant MT destabilisation. Compared to control condition, in fact, there is a lower proportion of cells with partially depolymerised MT and a higher proportion of

cells showing a more advanced MT destabilisation, i.e. only residual MT fibres (***Fig. 17C***).

We checked MT depolymerisation in CKAP5-depleted cells as a positive control, since CKAP5 has a fundamental role in regulating MT elongation. These cells exhibited a more dramatic phenotype, as expected. Indeed, only residual MT fibres or fully depolymerised MT were observed (***Fig. 17C***). No fully polymerised MT were observed in any condition, as we analysed an extensive depolymerisation time point (***Fig. 17C***).

After extensive cold-induced depolymerisation, a MT re-polymerisation assay was performed by shifting cells at 37°C (***Fig. 17B, right***). After 4 minutes at 37°C, in circZNF609 knock-down condition there was a higher percentage of cells in a precocious stage of MT re-polymerisation (i.e. only MT regrowing from asters) and a lower percentage of cells with a partial MT re-polymerisation, compared to control (***Fig. 17D***).

CKAP5-depleted cells displayed an even more delayed regrowth kinetics, with a higher percentage of cells with only MT regrowing from asters and a few cells presenting partially regrown MT (***Fig. 17D***). No fully depolymerised MT and no K-fibres were observed in any condition, as we analysed an extensive re-polymerisation time point.

These preliminary data suggest that circZNF609 knock-down can induce a significant MT destabilisation and an impaired MT polymerisation in RD cells. CircZNF609-depleted cells showed intermediate MT-related phenotypes between control and CKAP5-depleted cells. These results could then support the hypothesis that the defective MT polymerisation in circZNF609-depleted cells could be due to the downregulation of CKAP5 protein observed upon circZNF609 knock-down.

Subsequently, as CKAP5 also regulates mitotic spindle stabilisation and therefore chromosome segregation, we investigated the effects of circZNF609 depletion on mitotic progression.

In collaboration with Dr Lavia's lab, we analysed the proportion of cells in mitosis (mitotic index) and the proportion of cells in each mitotic phase (mitotic progression) in control conditions, upon circZNF609 knock-down, and upon CKAP5 knock-down (positive control).

CircZNF609 depletion induced a decrease in the percentage of mitotic cells, identified by DAPI staining and Tubulin immunofluorescence (***Fig. 18A***), with a smaller proportion of cells in late pro-metaphase/metaphase (LPM/M) and a higher proportion of cells in anaphase/telophase (A/T) (***Fig. 18B***).

In CKAP5-depleted cells, a higher proportion of cells in mitosis was counted (***Fig. 18A***), in pro-metaphase (PM) particularly (***Fig. 18B***), suggesting that upon CKAP5 knock-down cells are stuck in PM and cannot complete mitosis.

When we analysed mitotic abnormalities by DAPI staining and Tubulin immunofluorescence (***Fig. 18C***), we found that circZNF609 depletion increased the proportion of cells displaying mis-segregating chromosomes, while CKAP5 knock-down increased multipolar spindles and misaligned chromosomes (***Fig. 18D***).

In conclusion, CKAP5 knock-down induced a dramatic effect on MT organisation and mitotic progression, while circZNF609 depletion produced a more moderate but still significant effect.

Indeed, CKAP5-depleted cells displayed important defects in assembling the mitotic spindle. Therefore, they could not complete mitosis, they were blocked in pro-metaphase, and showed a low frequency of chromosome mis-segregation in anaphase and telophase since they could not reach these stages.

On the other hand, although circZNF609-depleted cells displayed some defects in microtubule organisation, they could nucleate functional mitotic spindles, could get over metaphase and conclude mitosis. However, they showed abnormalities such as mis-segregating chromosomes in

anaphase and telophase, and we think this is due to the circZNF609-mediated downregulation of CKAP5 protein levels, and we are now working to verify this hypothesis.

In circZNF609-depleted cells, CKAP5 protein levels drop down to approximately 50% (***Fig. 15C***), while in CKAP5-depleted cells the reduction of CKAP5 protein levels is much more dramatic (e.g. ***Fig. 20B***). This could explain why circZNF609 depletion-induced defects in MT dynamics and mitotic progression are milder that those caused by CKAP5 knock-down.

Fig. 17

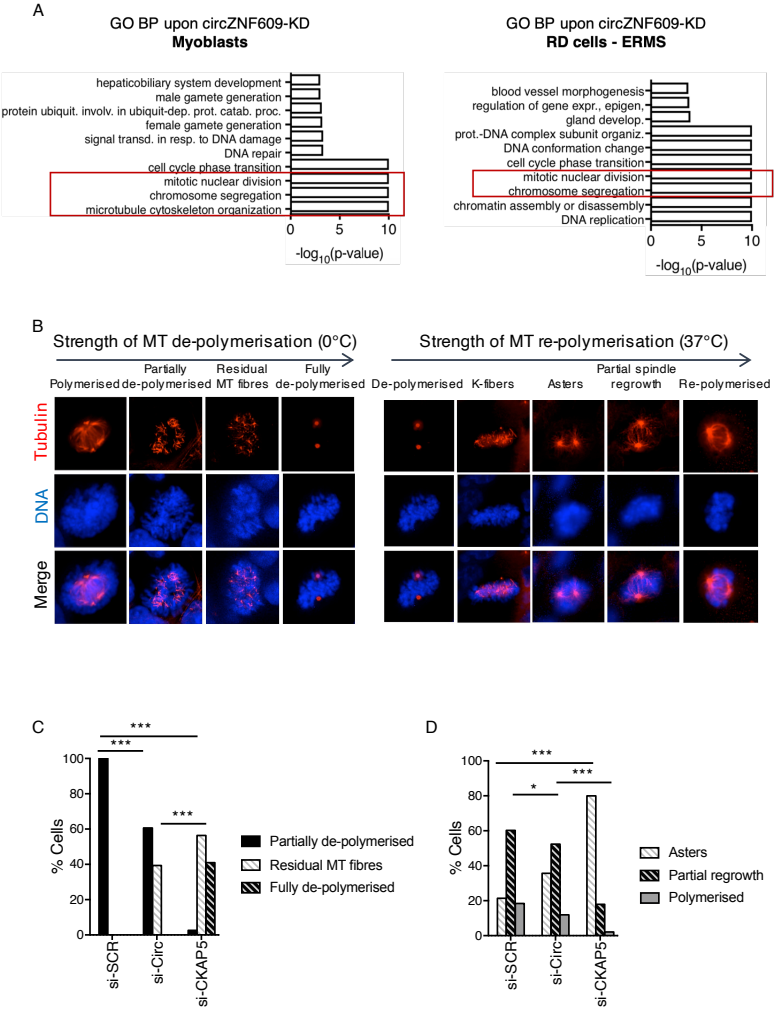
A
GO BP upon circZNF609-KD
Myoblasts
hepaticobiliary system development
male gamete generation
protein ubiquit. involv. in ubiquit-dep. prot. catab. proc.
female gamete generation
signal transd. in resp. to DNA damage
DNA repair
cell cycle phase transition
mitotic nuclear division
chromosome segregation
microtubule cytoskeleton organization
0 5 10
-log10(p-value)
GO BP upon circZNF609-KD
RD cells - ERMS
blood vessel morphogenesis
regulation of gene expr., epigen.
gland develop.
prot.-DNA complex subunit organiz.
DNA conformation change
cell cycle phase transition
mitotic nuclear division
chromosome segregation
chromatin assembly or disassembly
DNA replication
0 5 10
-log10(p-value)
B
Strength of MT de-polymerisation (0°C)
Strength of MT re-polymerisation (37°C)
Polymerised
Partially de-polymerised
Residual MT fibres
Fully de-polymerised
De-polymerised
K-fibers
Asters
Partial spindle regrowth
Re-polymerised
Tubulin
DNA
Merge
C
% Cells
100
80
60
40
20
0
***
***
***
si-SCR
si-Circ
si-CKAP5
Partially de-polymerised
Residual MT fibres
Fully de-polymerised
D
% Cells
100
80
60
40
20
0
***
*
***
si-SCR
si-Circ
si-CKAP5
Asters
Partial regrowth
Polymerised

Fig. 17 Gene Ontology (GO) term enrichment analysis (Biological Process) performed on genes downregulated upon circZNF609 depletion in myoblasts and RD cells; terms related to microtubules and mitosis are highlighted by a red rectangle (A). Stages of progressive microtubule (MT) depolymerisation (left) and re-polymerisation (right) identified by immunofluorescence for Tubulin protein and DAPI DNA-staining, in control RD cells (B). Percentage of RD cells in each stage of microtubule depolymerisation process, in control condition (si-SCR), upon circZNF609 knock-down (si-Circ) and upon CKAP5 knock-down (si-CKAP5); no fully polymerised MT were observed in any condition; N=1; total number of cells counted in si-SCR=90, total number of cells counted in si-Circ=71, total number of cells counted in si-CKAP5=78 (C). Percentage of RD cells in each stage of microtubule re-polymerisation process, in control condition (si-SCR), upon circZNF609 knock-down (si-Circ) and upon CKAP5 knock-down (si-CKAP5); no fully depolymerised MT and no K-fibres were observed in any condition; N=1; total number of cells counted in si-SCR=103, total number of cells counted in si-Circ=84, total number of cells counted in si-CKAP5=95 (D).

The ratio of each sample *versus* its experimental control was tested by χ^2 test. p-value: *: p-value < 0.05, **: p-value < 0.005, ***: p-value < 0.0001.

Fig. 18

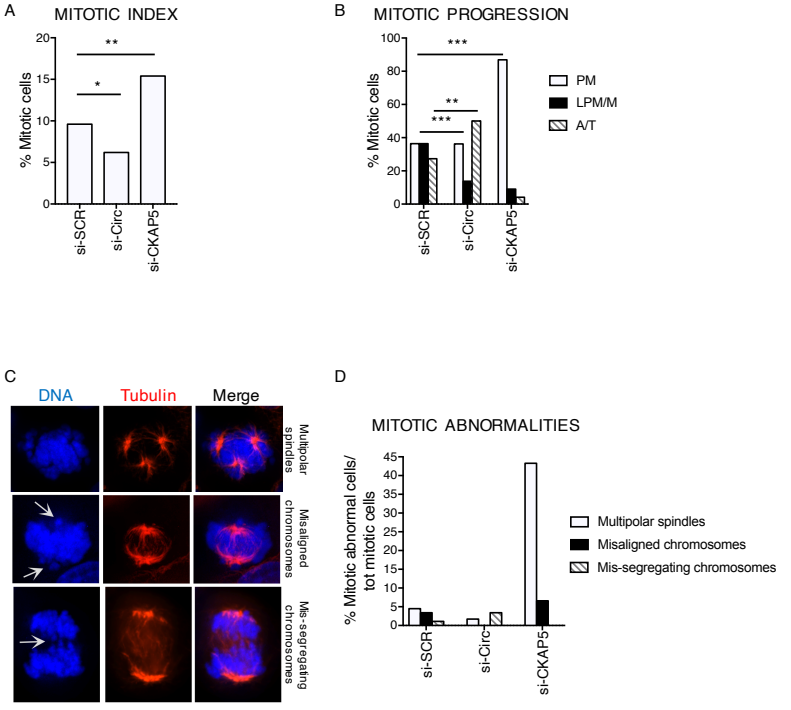
A
MITOTIC INDEX
% Mitotic cells
si-SCR
si-Circ
si-CKAP5
B
MITOTIC PROGRESSION
% Mitotic cells
PM
LPM/M
A/T
C
DNA
Tubulin
Merge
Multipolar spindles
Misaligned chromosomes
Mis-segregating chromosomes
D
MITOTIC ABNORMALITIES
% Mitotic abnormal cells/ tot mitotic cells
Multipolar spindles
Misaligned chromosomes
Mis-segregating chromosomes

Fig. 18 Percentage of mitotic RD cells over the total number of cells in control condition (si-SCR), upon circZNF609 knock-down (si-Circ) and upon CKAP5 knock-down (si-CKAP5); N=1; total number of cells counted in si-SCR=1008, total number of cells counted in si-Circ=996, total number of cells counted in si-CKAP5=914 (A). Percentage of mitotic RD cells in PM=pro-metaphase, in LPM/M=late pro-metaphase/metaphase and in A/T=anaphase/telophase, in control condition (si-SCR), upon circZNF609 knock-down (si-Circ) and upon CKAP5 knock-down (si-CKAP5); N=1; total number of cells counted in si-SCR=1008, total number of cells counted in si-Circ=996, total number of cells counted in si-CKAP5=914 (B). Representative images of mitotic abnormalities identified by immunofluorescence for Tubulin protein and DAPI DNA-staining (C). Percentage of mitotic RD cells showing different kinds of mitotic abnormalities in control condition (si-SCR), upon circZNF609 knock-down (si-Circ) and upon CKAP5 knock-down (si-CKAP5); N=1; total number of cells counted in si-SCR=88, total number of cells counted in si-Circ=58, total number of cells counted in si-CKAP5=122 (D).

The ratio of each sample *versus* its experimental control was tested by χ^2 test. p-value: *: p-value < 0.05, **: p-value < 0.005, ***: p-value < 0.0001.

CircZNF609 depletion induces accumulation of DNA damage

It is known that the accumulation of DNA damage can impair a correct mitotic progression. Reciprocally, mitotic abnormalities could lead to the accumulation of DNA damage [122].

Aneuploidy due to aberrant chromosome segregation could cause altered gene dosage, affecting fundamental processes such as DNA replication and DNA repair, with subsequent accumulation of DNA damage [123,124].

Since in circZNF609-depleted cells we observed a higher frequency of mis-segregating chromosomes, we asked whether this could lead to an accumulation of DNA damage.

Therefore, we performed a COMET assay which allows to quantify DNA damage in individual cells by analysing the pattern of DNA migration by electrophoresis (***Fig. 19A***). This experiment revealed that RD cells accumulate DNA damage upon circZNF609 knock-down (***Fig. 19B***).

This was further confirmed by the analysis of a marker of damaged DNA, the phosphorylated form of H2AX histone (γH2AX). Western blot analysis on three independent biological replicates of circZNF609 knock-down revealed the upregulation of γH2AX upon circZNF609 depletion (***Fig. 19C***). Preliminary data obtained by performing an immunofluorescence for γH2AX also showed an increase in

γH2AX spots in the nuclei of circZNF609-depleted RD cells (***Fig. 19D***).

The presence of damaged DNA induces the cell to arrest at a specific checkpoint to prevent the further spread of damage. The first checkpoints in the cell cycle are found at the G1-S transition [125]. A cell which accumulated damaged DNA during the previous mitosis will delay the S-phase entrance to avoid the replication of damaged DNA.

Therefore, we hypothesised that the cell cycle slow-down at the G1-S transition previously observed upon circZNF609 depletion could be due to the accumulation of damaged DNA, as a consequence of CKAP5-dependent mitotic alterations.

So, we investigated whether CKAP5 downregulation could reproduce the effects of circZNF609 knock-down on known markers controlling G1-S transition.

We analysed the relative RNA levels of factors regulating cell cycle progression and particularly S-phase entrance (E2f1, Cdk1, Cyclins A2 B1 and B2), as well as master regulators of G1-S transition and chromosome segregation (Tcf19, Cenpu, Mcm7). These mRNAs were significantly downregulated upon CKAP5 depletion as much as upon circZNF609 knock-down, with the exception of cyclins (***Fig. 20A***).

We also analysed p-RB and p-AKT protein levels. While p-RB decreased upon circZNF609 as well as CKAP5 depletion, p-AKT showed a negligible change following CKAP5 knock-down (***Fig. 20B***).

Interestingly, upon CKAP5 knock-down we noticed the presence of an additional higher band in the anti-p-RB hybridisation (***Fig. 20B***). This band could represent an increased hyper-phosphorylated RB protein level, that could be the result of a general alteration of the cell cycle in CKAP5-depleted cells.

Fig. 19

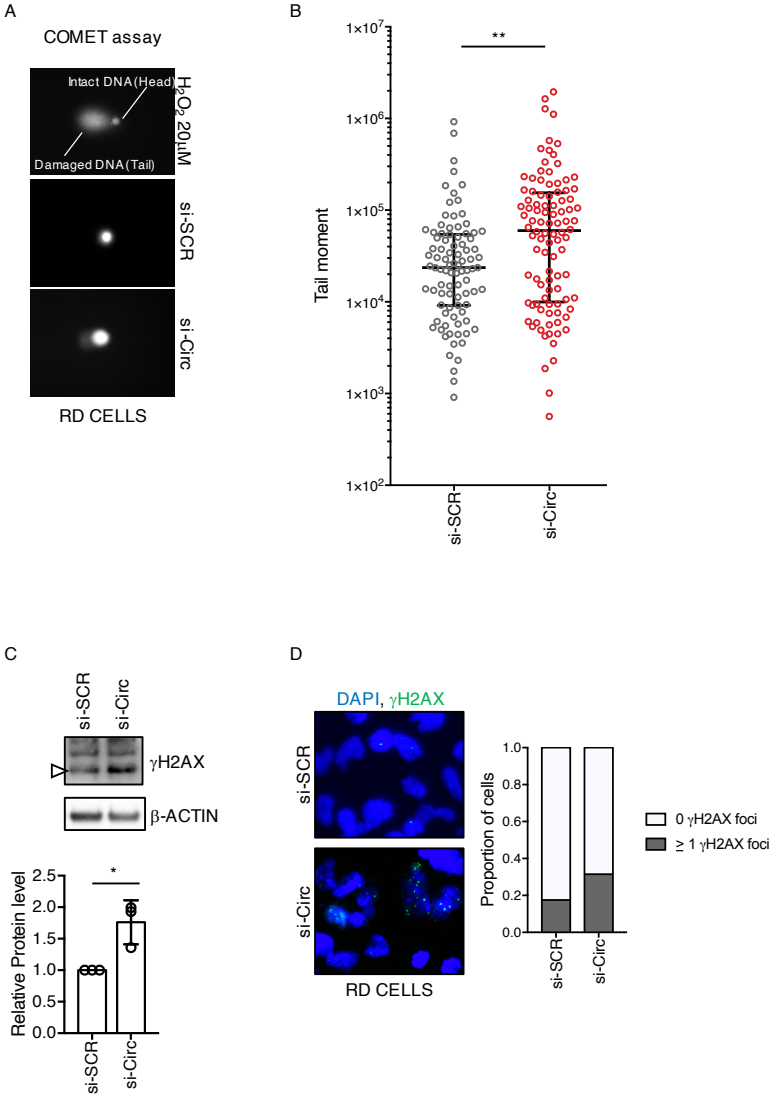
A
COMET assay
Intact DNA (Head)
Damaged DNA (Tail)
H2O2 20µM
si-SCR
si-Circ
RD CELLS
B
Tail moment
1x10^7
1x10^6
1x10^5
1x10^4
1x10^3
1x10^2
**
si-SCR
si-Circ
C
si-SCR
si-Circ
γH2AX
β-ACTIN
Relative Protein level
2.5
2.0
1.5
1.0
0.5
0.0
*
si-SCR
si-Circ
D
DAPI, γH2AX
si-SCR
si-Circ
RD CELLS
Proportion of cells
1.0
0.8
0.6
0.4
0.2
0.0
si-SCR
si-Circ
0 γH2AX foci
≥ 1 γH2AX foci

Fig. 19 COMET assay: representative fluorescence microscopy images showing single nucleoids which underwent electrophoresis from H_2O_2-treated RD cells (positive control for DNA damage induction), RD cells in control condition (si-SCR) and circZNF609-depleted RD cells (si-Circ) (A). COMET assay results: tail moment measurements in RD cells in control conditions (si-SCR) and upon circZNF609 knock-down (si-Circ); $\log_{10}$ scale on the y axis; dots represent individual tail moment values from 3 independent experiments, while horizontal lines represent their median with interquartile range; N=3; total number of nucleoids counted in si-SCR=91, total number of nucleoids counted in si-Circ=100 (B). Representative Western blot showing γH2AX protein levels in RD cells in control conditions (si-SCR) and upon circZNF609 knock-down (si-Circ) with β-ACTIN hybridization used as loading control; γH2AX protein quantifications (relative to β-ACTIN) in RD cells in control conditions (si-SCR) and upon circZNF609 knock-down (si-Circ); N=3 (C). Immunofluorescence for γH2AX merged with DAPI staining in RD cells, in control conditions (si-SCR) and upon circZNF609 knock-down (si-Circ), and proportion of cells showing 0 and ⩾1 γH2AX foci in their nucleus; N=1; total number of nuclei analysed in si-SCR=702, total number of nuclei analysed in si-Circ=537 (D).

Where statistical analysis was performed, the ratio of each sample *versus* its experimental control was tested by two-tailed unpaired Student's t test. p-value: *: p-value < 0.05, **: p-value < 0.01, ***: p-value < 0.001, ****: p-value < 0.0001.

Fig. 20

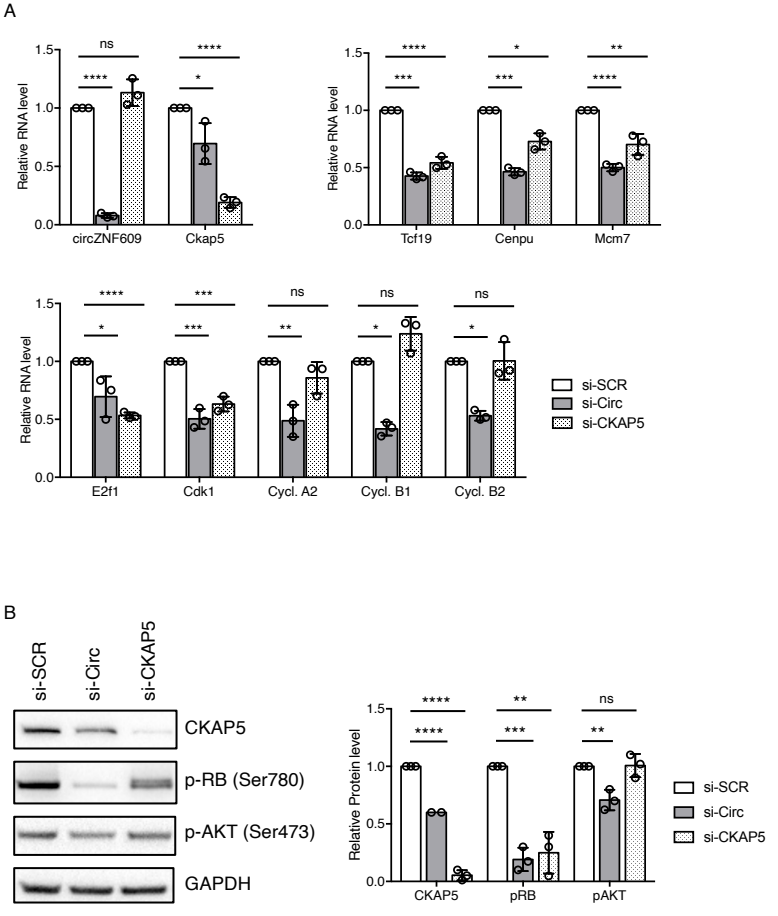
A
Relative RNA level
circZNF609
Ckap5
Tcf19
Cenpu
Mcm7
E2f1
Cdk1
Cycl. A2
Cycl. B1
Cycl. B2
si-SCR
si-Circ
si-CKAP5
B
si-SCR
si-Circ
si-CKAP5
CKAP5
p-RB (Ser780)
p-AKT (Ser473)
GAPDH
Relative Protein level
CKAP5
pRB
pAKT

Fig. 20 qRT-PCR experiments showing relative RNA levels of circZNF609, Ckap5 mRNA and some transcripts encoding proliferation-related factors, in RD cells in control condition (si-SCR), upon circZNF609 knock-down (si-Circ) and upon CKAP5 knock-down (si-CKAP5); N=3 (A). Representative Western blot in RD cells in control condition (si-SCR), upon circZNF609 knock-down (si-Circ) and upon CKAP5 knock-down (si-CKAP5) with GAPDH hybridization used as loading control; protein quantifications (relative to GAPDH) in RD cells in control condition (si-SCR), upon circZNF609 knock-down (si-Circ) and upon CKAP5 knock-down (si-CKAP5); N=3; 1 outlier in CKAP5 hybridisation upon circZNF609 depletion was removed while calculating relative CKAP5 protein level (B).

Relative RNA levels are represented as mean of the Fold Changes ± standard deviation of biological replicates, and dots represent individual data points. Graphs referred to proteins show the mean of protein quantification relative to GAPDH ± standard deviation of biological replicates, with dots representing individual data points. The ratio of each sample *versus* its experimental control was tested by two-tailed unpaired Student's t test. p-value: *: p-value < 0.05, **: p-value < 0.01, ***: p-value < 0.001, ****: p-value < 0.0001.

Analysis of circRNA deregulation in RMS

Identification of differentially expressed circRNAs among myoblasts and RMS subtypes

To identify new circRNAs with a possible role in regulating RMS tumorigenesis, we started from the analysis of differentially expressed circRNAs among human primary myoblasts, ERMS (RD) and ARMS (RH4) cells.

Since we already had total RNA-sequencing data from control and circZNF609-depleted myoblasts, RD and RH4 cells, we applied a dedicated bioinformatic pipeline for identifying circRNAs only to control samples, and then we evaluated circRNA differential expression among the three cell lines. In parallel, we analysed linear mRNA differential expression among samples.

We considered as "concordant" a circRNA and its cognate linear mRNA, if they displayed the same expression trend among two cell lines. We considered as "discordant" a circRNA and the correspondent mRNA showing a different or opposite expression trend among two cell lines.

Our interest was mainly focused on "discordant" couples, as the different expression trend between the circRNA and the mRNA could suggest a circRNA-specific regulation and function, independently from its linear counterpart. Even if also circRNAs showing a "concordant" expression trend with their linear counterparts could have specific molecular

roles, the focus on "discordant" couples could make the discovery of functional circRNAs easier.

Therefore, we started our analysis by selecting "discordant" circRNA-mRNA couples. Then, for each comparison (RD *vs* RH4; RD *vs* myoblasts; RH4 *vs* myoblasts) we applied a filter on the significance of the circRNA's and mRNA's differential expression. Subsequently, we filtered for circRNA $\log_2$ Fold Change, and then for circRNA expression level, as summarised in ***Fig. 21A***. In the end, we selected 34 candidate circRNAs for experimental validation.

To confirm the covalently closed structure of these circRNAs, we performed RT-PCRs using divergent primers in order to selectively amplify the back-splicing junction, and then an RNase R (a 3' exoribonuclease degrading only linear RNAs) resistance assay (***Fig. 21B***) [14].

The RT-PCR-based screening detected nearly all the selected circRNAs. Indeed, we obtained amplicons of the expected size for all of them but one, circZNF124 (***Fig. 21C***).

We then performed the RNase R resistance assay on the 24 most expressed circRNAs, excluding circZNF124 and other 9 circRNAs that were sub-optimally amplified by RT-PCR (***Fig. 21C, right***). The 24 circRNAs were all resistant to RNase R treatment, confirming their covalently closed structure (***Fig. 21D***).

We then selected 3 candidates for further analysis. We shortlisted the most expressed circRNAs, preferring the ones harbouring a potential ORF to possibly investigate the functions of circRNA-derived proteins. The chosen candidates were circAFF1, circHIPK3 and circVAMP3. While the first two circRNAs harbour an ORF spanning their back-splicing junction, circVAMP3 ORF stops upstream its back-splicing junction and therefore its protein-coding potential was not further investigated (***Fig. 22A***).

The differential expression of these three circRNAs among myoblasts, RD and RH4 cells was confirmed by qRT-PCR (***Fig. 22B***).

CircAFF1 was significantly upregulated in RMS cell lines compared to myoblasts, while its mRNA counterpart showed no comparable changes.

CircHIPK3 displayed a slight upregulation in RH4 cells. This circRNA is also exceptionally abundant and has been widely studied for its role in governing tumorigenesis in a variety of malignancies [40].

CircVAMP3 was upregulated selectively in RH4 cells in two biological replicates out of three, while its mRNA only showed a slight downregulation between myoblasts and RMS cells.

Subsequently, the subcellular localisation of these circRNAs was evaluated thanks to a cytoplasmic-nuclear

fractionation. All of them were prevalently cytoplasmic (***Fig. 22C***). Only circVAMP3 showed about a 20% of nuclear localisation (***Fig. 22C***). This circRNA is composed of two exons and it is possible that a circVAMP3-isoform could include the 799-bp intron between its exons, being retained in the nucleus.

For circAFF1 and circHIPK3 which harbour a predicted ORF spanning their back-splicing junction, we investigated their association to polysomes by performing a sucrose gradient fractionation of the cytoplasmic cell lysate. We compared their polysome-association profile with the ones of circZNF609 (positive control) and circPMS1 (negative control). However, neither circAFF1 nor circHIPK3 were enriched in polysome fractions, therefore suggesting their ORFs are not functional at least in our system (***Fig. 22D***).

Fig. 21

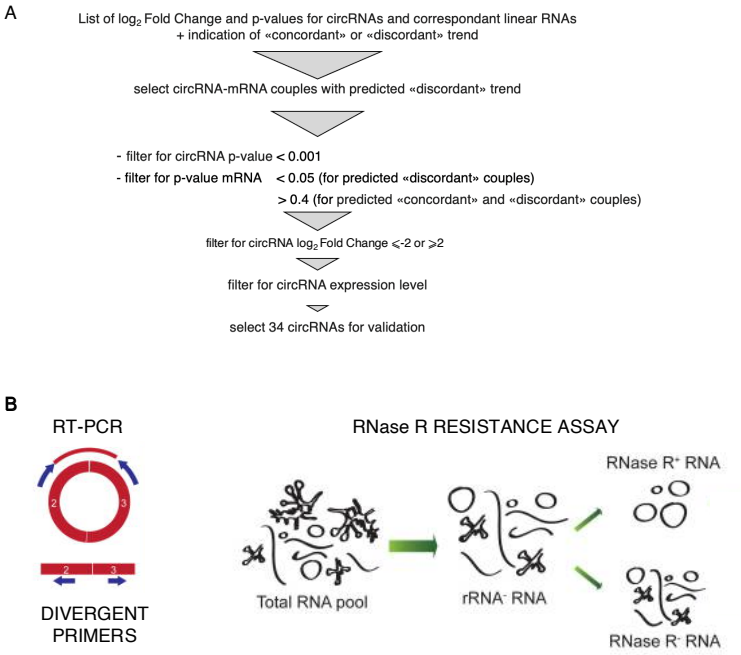
A
List of log2 Fold Change and p-values for circRNAs and correspondant linear RNAs
+ indication of «concordant» or «discordant» trend
select circRNA-mRNA couples with predicted «discordant» trend
- filter for circRNA p-value < 0.001
- filter for p-value mRNA < 0.05 (for predicted «discordant» couples)
> 0.4 (for predicted «concordant» and «discordant» couples)
filter for circRNA log2 Fold Change ⩽-2 or ⩾2
filter for circRNA expression level
select 34 circRNAs for validation
B
RT-PCR
DIVERGENT
PRIMERS
RNase R RESISTANCE ASSAY
Total RNA pool
rRNA- RNA
RNase R+ RNA
RNase R- RNA

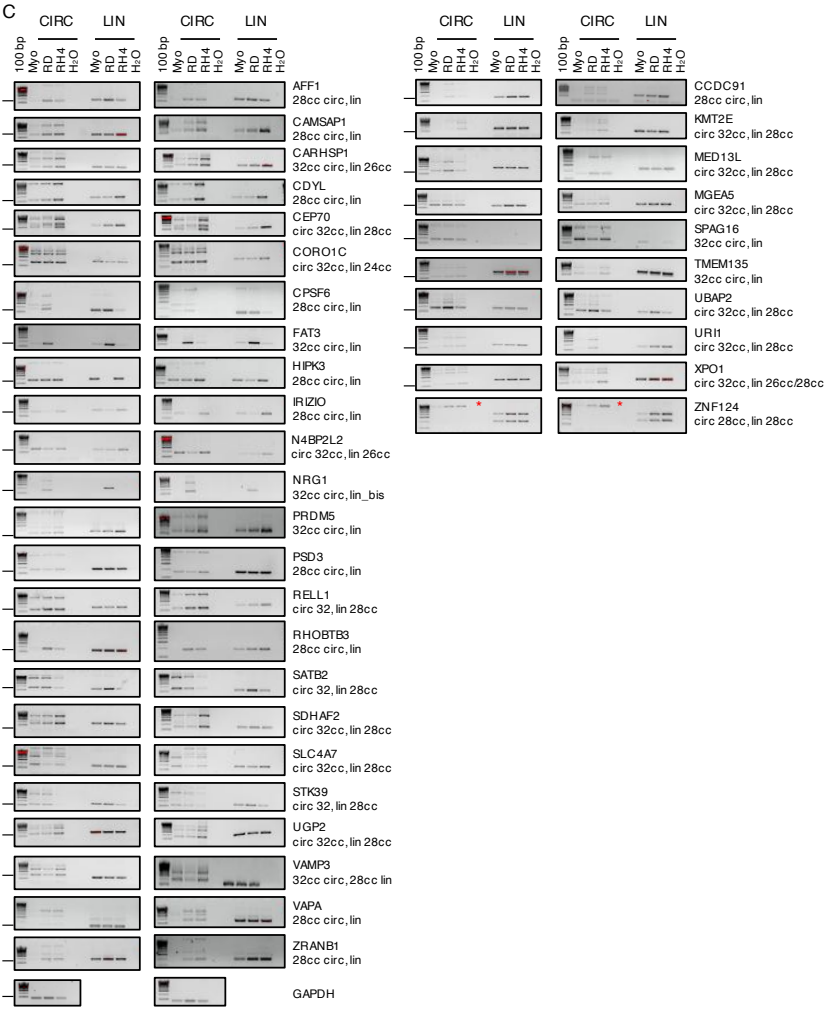
C
CIRC
LIN
100 bp
Myo
RD
RH4
H2O
AFF1
28cc circ, lin
CAMSAP1
28cc circ, lin
CARHSP1
32cc circ, lin 26cc
CDYL
28cc circ, lin
CEP70
circ 32cc, lin 28cc
CORO1C
circ 32cc, lin 24cc
CPSF6
28cc circ, lin
FAT3
32cc circ, lin
HIPK3
28cc circ, lin
IRIZIO
28cc circ, lin
N4BP2L2
circ 32cc, lin 26cc
NRG1
32cc circ, lin_bis
PRDM5
32cc circ, lin
PSD3
28cc circ, lin
RELL1
circ 32, lin 28cc
RHOBTB3
28cc circ, lin
SATB2
circ 32, lin 28cc
SDHAF2
circ 32cc, lin 28cc
SLC4A7
circ 32cc, lin 28cc
STK39
circ 32, lin 28cc
UGP2
circ 32cc, lin 28cc
VAMP3
32cc circ, 28cc lin
VAPA
28cc circ, lin
ZRANB1
28cc circ, lin
GAPDH
CCDC91
28cc circ, lin
KMT2E
circ 32cc, lin 28cc
MED13L
circ 32cc, lin 28cc
MGEA5
circ 32cc, lin 28cc
SPAG16
32cc circ, lin
TMEM135
32cc circ, lin
UBAP2
circ 32cc, lin 28cc
URI1
circ 32cc, lin 28cc
XPO1
circ 32cc, lin 26cc/28cc
ZNF124
circ 28cc, lin 28cc

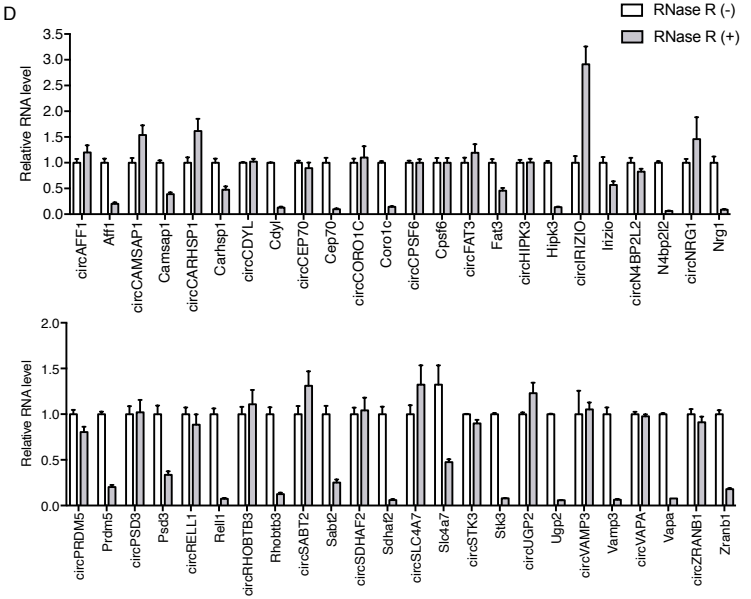

Fig. 21 Schematic representation of the filters applied during the bioinformatic selection of circRNAs differentially expressed among myoblasts, RD and RH4 cells (A). Schematic representation of two experimental methods for validating the covalently closed structure of circRNAs, adapted from Jeck and Sharpless, 2014. Two biological replicates of RT-PCR experiment amplifying the selected circRNAs (CIRC) and cognate mRNAs (LIN) differentially expressed among myoblasts (Myo), RD and RH4 cells; Gapdh mRNA amplification was used as loading control; PCR cycles (cc) loaded on the agarose gel are indicated on the right of the images, both for circRNAs (circ) and mRNAs (lin); horizontal bars on the left of the images indicate the expected amplicon size; N=2 (C). Representative qRT-PCR experiment showing circRNA and cognate mRNA levels in RD cells in control conditions (RNase R (-)) and upon RNase R treatment (RNase R (+)); N=2; relative RNA levels are shown as means of Fold Changes ± standard error of technical triplicates (D).

Fig. 22

A

CircRNA	Predicted protein molecular weight
circHIPK3	43 KDa
circAFF1	32 KDa
circVAMP3	-

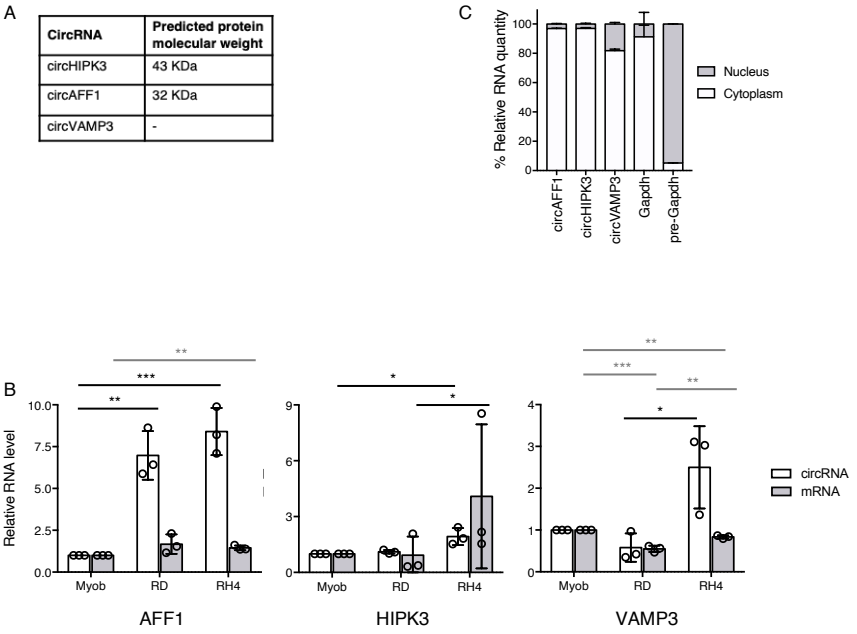

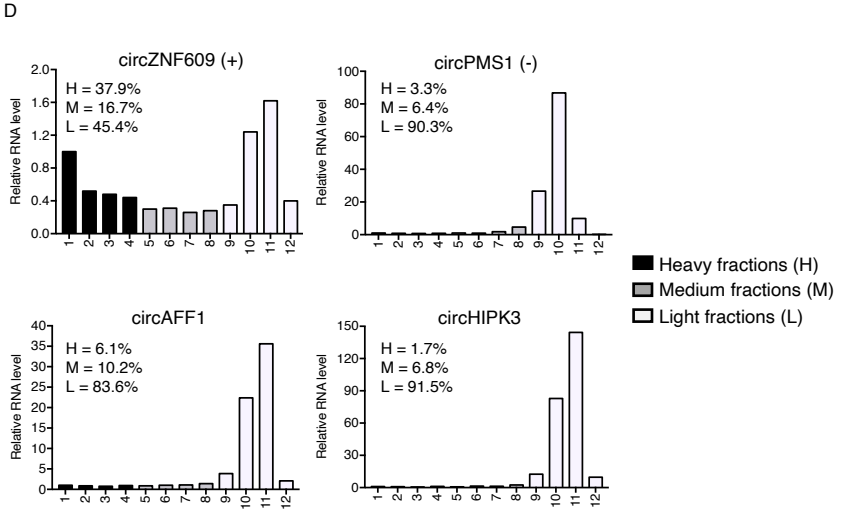

Fig. 22 Molecular weights of the proteins encoded by the predicted ORFs found in the selected circRNAs (A). qRT-PCR experiments representing the differential expression of the selected circRNAs and linear counterparts among myoblasts, RD and RH4 cells; black asterisks refer to circRNA confrontations, while grey asterisks refer to mRNA confrontations; N=3 (B). qRT-PCR data representing the subcellular localisation of the selected circRNAs; Gapdh and pre-Gapdh were used as positive controls for cytoplasmic and nuclear RNAs, respectively; N=2 (C). Representative qRT-PCR experiment showing the distribution of the selected ORF-containing circRNAs among the heavy, medium and light fractions of a sucrose gradient, in RD cells; N=2 (D).

In panel B, relative RNA levels are represented as mean of the Fold Changes ± standard deviation of biological replicates, and dots represent individual data points. Panel C represents the means of the nuclear and cytoplasmic RNA quantity calculated as $2^{-\Delta Ct}$ and then converted into percentages + standard deviation of biological replicates. Where statistical analysis was performed, the ratio of each sample *versus* its experimental control was tested by two-tailed unpaired Student's t test. p-value: *: p-value < 0.05, **: p-value < 0.01, ***: p-value < 0.001, ****: p-value < 0.0001.

CircHIPK3 knock-down enhances YAP/TAZ transcriptional activity in RH4 cells

To elucidate the molecular role of circAFF1, circVAMP3 and circHIPK3, we knocked down each of them separately in RH4 cells and performed an RNA-sequencing analysis. Now I will briefly describe the results regarding circHIPK3 depletion in RH4 cells.

After a differential expression analysis, we performed a GO BP term enrichment analysis on downregulated and upregulated genes upon circHIPK3 knock-down.

Only one category was found to be enriched among the downregulated genes, “ensheathment of neurons” (***Fig. 23A***).

On the other hand, many categories related to cell movement and cell-substrate adhesion were enriched among the upregulated genes (e.g. “integrin-mediated signalling pathway”, “actin filament-based movement”, “cell-substrate adhesion”), indicating that circHIPK3 could be involved in the regulation of these processes (***Fig. 23A***).

Interestingly, among the upregulated genes enriched in cell adhesion-related GO terms, we found Ccn1 (Cyr61), Ccn2 (Ctgf) and Ankrd1. These are well known direct targets of YAP and TAZ transcriptional activators [126].

YAP and TAZ are nucleocytoplasmic shuttling proteins, which accumulate in the nucleus in response to a variety of signals (e.g. activated Hippo pathway). In the

nucleus, they induce a gene expression programme generally promoting cell proliferation. YAP/TAZ are hyper-activated in many cancers, therefore being considered potent oncogenes [127].

Subsequently, we validated the differential expression of some YAP/TAZ pathway-related genes and some integrins involved in cell adhesion.

We observed a significant upregulation of Taz mRNA, while Yap showed no changes. Ankrd1, Ccn1, Ccn2 (downstream YAP/TAZ targets), as well as Fmn1 (an upstream YAP/TAZ activator), were significantly upregulated. On the other hand, we found Gsn and Stk3, two YAP/TAZ inhibitors, to be downregulated (***Fig. 23B***), suggesting that there could be a specific activation of the YAP/TAZ pathway.

Regarding integrins, we found ItgA3, ItgA6 and ItgB6 to be significantly upregulated following circHIPK3 depletion (***Fig. 23B***).

The deregulation of these genes was specifically due to circHIPK3 knock-down, as the depletion of Hipk3 mRNA had no relevant effects on most of them (***Fig. 23C***). For some of these genes, however, HIPK3 knock-down induced an opposite effect compared to circHIPK3 depletion, such as in the case of Ccn2, Fmn1, Stk3 and ItgA6. This will lead us to

further investigate the role of the linear Hipk3 mRNA in the YAP/TAZ pathway activation.

Since we observed an upregulation of YAP/TAZ target genes, we investigated whether YAP/TAZ transcriptional activity was enhanced upon circHIPK3 knock-down.

Therefore, we exploited a YAP/TAZ activity reporter vector (8xGTIIC-luciferase), kindly provided by Prof. Stefano Piccolo's lab [128]. The vector carries a YAP/TAZ-responsive synthetic promoter driving luciferase expression. This promoter contains eight tandem binding sites for TEAD, a partner of YAP and TAZ which mediates their transcriptional activity (***Fig. 23D, top***).

The depletion of either YAP or TAZ decreased the luciferase signal as expected. On the other hand, circHIPK3 knock-down increased luciferase signal compared to control condition (***Fig. 23D, bottom***). This suggests that circHIPK3 knock-down could enhance YAP/TAZ transcriptional activity, with the consequent upregulation of their target genes Ankrd1, Ccn1 and Ccn2.

We then checked YAP/TAZ protein subcellular localisation upon circHIPK3 knock-down. Preliminary data revealed an increased TAZ protein level both in the cytoplasm and in the nucleus (***Fig. 23E***), strengthening the hypothesis that its transcriptional activity could be enhanced following circHIPK3 depletion.

Fig. 23

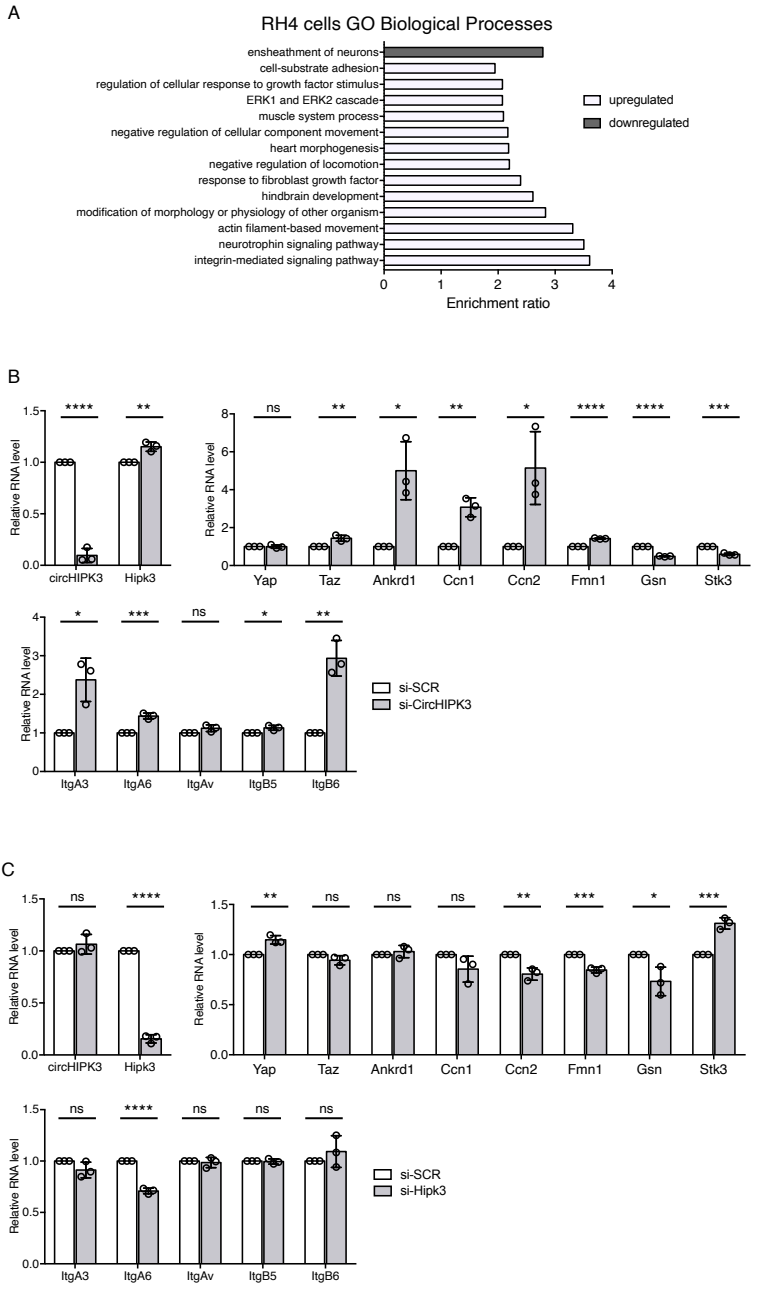
A
RH4 cells GO Biological Processes
ensheathment of neurons
cell-substrate adhesion
regulation of cellular response to growth factor stimulus
ERK1 and ERK2 cascade
muscle system process
negative regulation of cellular component movement
heart morphogenesis
negative regulation of locomotion
response to fibroblast growth factor
hindbrain development
modification of morphology or physiology of other organism
actin filament-based movement
neurotrophin signaling pathway
integrin-mediated signaling pathway
upregulated
downregulated
Enrichment ratio
B
Relative RNA level
circHIPK3
Hipk3
Yap
Taz
Ankrd1
Ccn1
Ccn2
Fmn1
Gsn
Stk3
ItgA3
ItgA6
ItgAv
ItgB5
ItgB6
si-SCR
si-CircHIPK3
C
si-SCR
si-Hipk3

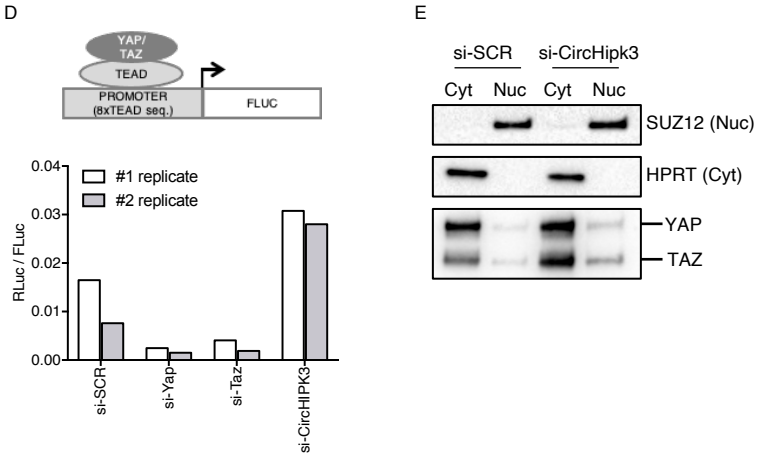

Fig. 23 Gene Ontology (GO) Biological Process term enrichment analysis on genes downregulated (grey) and upregulated (white) upon circHIPK3 knock-down in RH4 cells (A). Relative RNA levels of circHIPK3, Hipk3 mRNA and transcripts encoding factors related to YAP/TAZ and cell-adhesion pathways in control conditions (si-SCR) and upon circHIPK3 knock-down (si-CircHIPK3); N=3 (B). Relative RNA levels of circHIPK3, Hipk3 mRNA and transcripts encoding factors related to YAP/TAZ and cell-adhesion pathways in control conditions (si-SCR) and upon HIPK3 knock-down (si-HIPK3); N=3 (C). Luciferase assay using a YAP/TAZ-sensitive reporter vector (top) in RH4 cells, in control conditions (si-SCR), upon YAP or TAZ depletion (si-Yap, si-Taz: positive controls) and upon circHIPK3 knock-down (si-CircHIPK3); 2 individual biological replicates are shown separately (D). Representative Western blot of a nucleocytoplasmic subcellular fractionation in RH4 cells in control conditions (si-SCR) and upon circHIPK3 knock-down (si-CircHIPK3), showing YAP/TAZ localisation; SUZ12 and HPRT were used as nuclear (Nuc) and cytoplasmic (Cyt) controls, respectively; N=2 (E).

Relative RNA levels are represented as mean of the Fold Changes ± standard deviation of biological replicates, and dots represent individual data points. The ratio of each sample *versus* its experimental control was tested by two-tailed unpaired Student's t test. p-value: *: p-value < 0.05, **: p-value < 0.01, ***: p-value < 0.001, ****: p-value < 0.0001.

Discussion and conclusions

CircRNAs are a class of covalently closed RNAs, ubiquitously expressed among eukaryotes and often conserved among different species. CircRNA conservation, tissue-specificity and abundance suggest they could be important regulators of many biological processes.

In my work, I focused on a particular circRNA, circZNF609, and on its molecular function in modulating cell proliferation in RMS.

We previously observed that circZNF609 knock-down induced a block of cell proliferation in human primary myoblasts [28]. By performing a RNA-sequencing analysis on circZNF609-depleted myoblasts, we observed that a large group of proliferation-related genes was significantly downregulated [84].

To better investigate circZNF609 role in regulating cell proliferation, we explored its expression and function in a muscle-related tumour, RMS. We found the circRNA to be overexpressed in both ERMS and ARMS subtypes with respect to myoblasts, coherently with its putative role in safeguarding cell proliferation by preventing DNA damage accumulation and sustaining a correct mitotic progression.

Thanks to a flow cytometric analysis of cell cycle, we found that circZNF609 depletion induced a slow-down of the G1-S transition in ERMS, promoting an accumulation of cells

in G1 phase and reduction of cells in S phase. Therefore, we investigated whether known factors controlling G1-S checkpoint were deregulated following circZNF609 knock-down, and we observed an impaired RB protein phosphorylation and an increased p-AKT degradation by the proteasome.

Subsequently, we performed an RNA-sequencing analysis on RD (ERMS) and RH4 (ARMS) cells depleted of circZNF609.

In RD cells, the knock-down of the circRNA inhibited pathways related to both G1-S transition (e.g. it downregulated genes targeted by RB through E2F1 regulation) and mitotic progression. Among the master regulators of cell proliferation which are downregulated upon circZNF609 depletion, we found TCF19, MCM7, CENPU and ZWINT. These factors are not only key regulators of the G1-S transition, but also have a fundamental role in chromosome segregation, highlighting the importance of circZNF609-mediated control of the mitotic checkpoint.

On the other hand, circZNF609-depleted RH4 cells (ARMS) showed no alteration in cell cycle progression and in proliferation-related pathways, although we found the levels of p-RB and p-AKT proteins to be downregulated in a similar manner as in RD cells.

We hypothesised that the different behaviour of ARMS and ERMS cells in response to circZNF609 depletion could be due to a significant downregulation of p53 expression in RH4 with respect to RD cells. We also found a significant upregulation of p53-target cell cycle-related genes in RH4 compared to RD cells. The alteration of many cell cycle-related pathways (including the p53 pathway) in ARMS cells could explain why the effects of circZNF609 depletion alone are not sufficient for significantly reducing the proliferation of these tumour cells.

Interestingly, p53 is a fundamental guardian of the G1-S checkpoint, and cells in which a functional p53 is lost cannot arrest at the G1-S transition in response to specific signals, e.g. unrepaired DNA damage, bypassing the checkpoint [129].

This first part of my work about circZNF609 effects on cell cycle progression in RMS cells was the subject of a first-author peer-reviewed publication [84].

Subsequently, in order to unveil circZNF609 mechanism of action, we looked for its molecular interactors to understand the direct partners mediating its effect on cell cycle progression.

CircZNF609 has already been reported to interact with different miRNAs, acting as a competing endogenous RNA to regulate cell proliferation, migration and differentiation [130–132]. Based on our analysis, it is not likely that circZNF609

could sequester many of the miRNAs described in the literature, at least in our system. Nevertheless, we tested whether circZNF609 could act as a sponge for miR-150-5p, regulating the expression of the miRNA-target Akt3 as described in [133]. However, we found neither Akt3 RNA/protein nor miR-150-5p to be altered upon circZNF609 depletion (data not shown), suggesting that the circRNA is not acting as a sponge for this miRNA in RMS cells [84].

While we are still optimising an experimental strategy to identify putative circRNA-bound proteins, an efficient pulldown protocol to identify circRNA-interacting transcripts has been set up in our lab.

Therefore, we pulled down circZNF609 following psoralen-mediated crosslinking, as we were specifically interested in direct circRNA-mRNA interactions. An RNA-sequencing analysis was then performed on the recovered RNA fraction, revealing that circZNF609 interacts with Ckap5 mRNA, a transcript encoding a microtubule polymerase which regulates microtubule dynamics and mitotic spindle assembly.

CircZNF609 knock-down slightly reduced Ckap5 mRNA stability and significantly downregulated its protein levels. By analysing the predicted interaction region between the circRNA and the mRNA, we found that it includes three tandem binding sites for HUR, an RBP which enhances mRNA stability and translation.

The fact that Ckap5 mRNA can interact with HUR protein and their binding is reduced upon circZNF609 depletion, raised the hypothesis that circZNF609-Ckap5 RNA-RNA interaction could increase Ckap5 transcript stability and protein levels by promoting HUR binding on Ckap5 mRNA.

So far, there are still some important details to be clarified about the circZNF609/Ckap5 mRNA/HUR protein circuit, in order to understand its molecular mechanism.

To confirm that the interaction between circZNF609 and Ckap5 mRNA involves the predicted sequences, we designed an antisense LNA (Locked Nucleic Acid) oligonucleotide which pairs to circZNF609 and blocks its interaction with Ckap5 mRNA in the predicted region. This would allow us to demonstrate that the interaction between the two RNAs occurs in this specific region.

Following the LNA transfection, we will analyse Ckap5 RNA stability and protein levels to elucidate whether the downregulation of CKAP5 observed upon circZNF609 knock-down is directly mediated by the interaction of its mRNA with the circRNA. We will also analyse the phenotype of the LNA-treated cells, in order to elucidate whether the impaired cell cycle progression observed upon circZNF609 knock-down could be reproduced by the disruption of the circZNF609-Ckap5 mRNA interaction.

Finally, we will need to clarify how circZNF609 could promote the binding of HUR protein on Ckap5 mRNA. It is reported that HUR can mainly bind single stranded RNAs [134], thus so far we hypothesise that HUR binds circZNF609 and then, thanks to the circZNF609-Ckap5 interaction, HUR could be released on the mRNA.

Besides Ckap5 mRNA, HUR can bind a large group of transcripts involved in microtubule dynamics and mitosis as Ckap5. These transcripts were also downregulated upon circZNF609 knock-down, and include AurkA, Tacc1, Tacc3, Ndc80, Cyclins B1 and B2. However, unlike Ckap5, these transcripts did not interact with circZNF609 as they were not pulled down with it (data not shown). Therefore, we hypothesised that circZNF609 depletion could have an indirect effect on these targets, maybe mediated by CKAP5 itself, as all these factors are part of a CKAP5-centric network of genetic interactions required for the formation of a correct bipolar spindle [135].

Since CKAP5 regulates microtubule cytoskeleton organisation and mitotic spindle assembly, we reasoned about the fact that the defects in mitosis-related pathways and factors, highlighted by the Gene Ontology and msVIPER analyses, could depend on the circRNA-mediated regulation of CKAP5 levels. Intriguingly, preliminary data indicated that circZNF609-depleted cells displayed significant defects in

microtubule dynamics and chromosome segregation leading to aneuploidy, that could be ascribed to CKAP5 alteration.

As aneuploidy due to aberrant chromosome segregation could alter gene expression, often impairing fundamental cellular processes such as DNA repair, we investigated whether circZNF609 knock-down could increase DNA damage in RMS cells. Through COMET assay we detected an increase of the damaged DNA content, as confirmed also by the upregulation of γH2AX histone variant following circZNF609 depletion.

To confirm the hypothesis that the accumulation of DNA damage is due to the mitotic aberrations caused by the circZNF609-mediated decrease in CKAP5 protein levels, we will repeat these experiments comparing circZNF609-depleted cells with cells transfected with the antisense oligonucleotide which blocks circZNF609-Ckap5 mRNA interaction.

Cells can sense damaged DNA, inducing the activation of specific mechanisms to prevent its replication, including the p53-dependent checkpoint. It has been reported that chromosome mis-segregation-induced DNA damage and cellular stress associated with aneuploidy can activate the p53 checkpoint, producing a G1-S arrest upon an aberrant mitosis [136].

Therefore, we hypothesise that circZNF609 directly induces CKAP5-mediated mitotic aberrations, such as

chromosome mis-segregation, with subsequent accumulation of DNA damage. This could be responsible for the activation of the p53-dependent G1-S checkpoint, which will prevent cells with damaged DNA from entering the S phase at the following cycle.

In support of this hypothesis, we observed that CKAP5 knock-down could recapitulate some of the circZNF609-induced effects on RNAs and proteins involved in the G1-S transition, e.g. downregulation of E2f1, Tcf19, Mcm7, Cenpu mRNAs, and decreased levels of p-RB protein.

These data, together with the fact that Ckap5 mRNA and circZNF609 interact directly with each other, could suggest that the effects of circZNF609 depletion on G1-S-regulating factors can be mediated by CKAP5 downregulation. However, the effects of circZNF609 depletion and CKAP5 knock-down are not completely overlapping, maybe because CKAP5 knock-down strongly reduces CKAP5 protein levels, while circZNF609 depletion only reduces CKAP5 protein levels down to about 50%. This could explain why CKAP5 depletion has a more dramatic effect on cell cycle progression than circZNF609 depletion. Moreover, other signalling pathways and feedback regulations could intervene upon CKAP5 knock-down. Further investigations in this direction will allow us to better understand the phenotypic differences in CKAP5- and circZNF609-depleted cells, not only at the

level of microtubule dynamics and mitotic progression, but also at the molecular level (e.g. the insensitivity of p-AKT protein and transcripts encoding for cyclins to CKAP5 knock-down).

Another interesting point is that in circZNF609-depleted RD cells we only observe a G1-S slow-down of cell cycle progression with no apoptosis occurring, contrary to what would be expected upon the activation of p53 checkpoint. However, these cells accumulate a low amount of chromosome alterations, carry a p53 gain-of-function mutation and are malignant cells probably adapted to a certain amount of damaged DNA content and aneuploidy. All these aspects could converge in order to allow circZNF609-depleted RD cells to escape the apoptosis and continue to proliferate, despite a G1-S transition slow-down.

The activation of the p53-dependent pathway in response to DNA damage accumulation could reinforce our previously mentioned hypothesis that circZNF609-depleted RH4 cells do not show any defect in cell cycle progression because of a strong downregulation of p53 expression compared to RD cells. Therefore, in RH4 cells, circZNF609 knock-down-induced errors in chromosome segregation and subsequent DNA damage accumulation might not be counteracted by the activation of the p53 checkpoint. Thus, RH4 cells can keep proliferating, adapting to chromosome

instability and DNA damage spread in the limited timeframe in which we analysed them. However, this is just one of the possible mechanisms that could explain why RH4 cells are resistant to cell proliferation slow-down, and other pathways could allow them to adapt to the presence of damaged DNA and aberrant karyotype.

In conclusion, this work elucidated a novel molecular circuit in which circZNF609 regulates the stability of Ckap5 mRNA and its protein levels. So far, little is known about circRNA-mRNA base-pairing-mediated interactions. By characterising circZNF609 binding to Ckap5 transcript and its direct effects on CKAP5-dependent processes, we contributed to the understanding of a circRNA-mRNA axis regulating RMS cancer cell proliferation, for the first time.

This could represent a significant advance in the understanding of RMS cell cycle control pathways and could inspire new therapeutic strategies based on circZNF609 knock-down or on the blocking of its interaction with Ckap5.

Interestingly, circZNF609 depletion can alter microtubule polymerisation and mitotic spindle assembly. Indeed, microtubule-targeting drugs as Vincristine are used in first-line chemotherapy to treat RMS. Thus, in the next future, we are going to investigate whether circZNF609 depletion could make RMS cells more sensitive to these drugs, paving the way to improved targeted therapies for treating this cancer.

The last part of my work investigated the deregulation of other circRNA molecules among myoblasts and RMS subtypes, in order to gain a deeper insight into the role of circRNAs in this tumour.

We identified several circRNAs differentially expressed among myoblasts, ERMS and ARMS cells and, after a multi-step filtering process, we selected 3 candidates for further analyses: circHIPK3, circAFF1 and circVAMP3.

I started by analysing circHIPK3 role in regulating ARMS cell biology. Thanks to an RNA-sequencing analysis of circHIPK3-depleted RH4 cells, we observed that circHIPK3 knock-down upregulates several genes involved in cell-substrate adhesion and actin-based cell movement.

Among the pathways altered by circHIPK3 depletion, there is the YAP/TAZ signalling pathway which sustains cell proliferation and is often deregulated in cancer. Indeed, we discovered that circHIPK3 knock-down can enhance YAP/TAZ transcriptional activity, as demonstrated by the upregulation of Ankrd1, Ccn1 and Ccn2 which are known transcriptional targets of the YAP/TAZ factors.

The characterisation of circHIPK3 molecular mechanism of action in activating the YAP/TAZ pathway is still at its beginning.

As circHIPK3 has been shown to be an efficient miRNA-sponge in many cancers [40], we investigated whether

among the circHIPK3-bound miRNAs there were some targeting transcripts involved in the YAP/TAZ pathway.

By consulting databases of miRNA-target interactions such as PITA [137] and miRanda [138], we found that circHIPK3 has 2 binding sites for miR-550a-5p, a miRNA targeting Taz mRNA (according to miRWalk 3.0 database [139]). Since Taz is upregulated upon circHIPK3 knock-down, we are currently investigating whether circHIPK3 could directly regulate TAZ by stabilising miR-550a-5p.

Another intriguing circuit we are studying is the one linking actin-cytoskeleton remodelling to YAP/TAZ activation. It is known that YAP/TAZ can both sense and mediate mechanical stimuli [128]. Since upon circHIPK3 depletion we observed a significant alteration of actin filament-based movement and cell adhesion-related genes, we will investigate whether this could contribute to the YAP/TAZ pathway activation.

Indeed, upon circHIPK3 depletion, we observed an upregulation of Fmn1 and a downregulation of Gsn RNA levels. Formin (FMN1) promotes the polymerisation of linear actin cables, while Gelsolin (GSN) is an actin-depolymerising factor. Interestingly, it has been reported that YAP/TAZ nuclear translocation and transcriptional activity are sustained by an increased tension in the actin cytoskeleton (e.g. FMN1-dependent actin polymerisation), while are inhibited by a

reduced tension (e.g. GSN-dependent actin depolymerisation) [140].

Moreover, by consulting PITA and miRanda databases, we found that circHIPK3 hosts 3 binding sites for miR-103a-3p, in addition to the 2 binding sites for miR-550a-5p previously mentioned. Both miR-103a-3p and miR-550a-5p can target Fmn1 transcript (according to miRWalk 3.0 database). We are currently investigating whether circHIPK3 can directly control actin cytoskeleton mechanics by stabilising Fmn1-targeting miRNAs, therefore contributing to the YAP/TAZ pathway activation.

If verified, this circHIPK3/miRNAs/mRNAs axis could represent the first example of circHIPK3 acting not as a canonical miRNA sponge but as a miRNA stabiliser [40]. circHIPK3 is a very abundant circRNA and it hosts five binding sites for these miRNAs overall (3 for miR-103a-3p and 2 for miR-550a-5p). Moreover, Fmn1 can be targeted by both the miRNAs. These characteristics and the cooperative action of the two involved miRNAs on the same target could make this circuit very strong. Indeed, cooperative circuits involving either more than one circRNA and the same miRNAs, or one circRNA sponging different miRNAs with the same targets, can reinforce circRNA activity in modulating miRNA-targets' expression, especially when the circRNA hosts only a few binding sites for a specific miRNA.

In conclusion, our research laid the groundwork for the comprehension of the molecular function of some circRNAs in RMS biology. Our future efforts will aim to further elucidate the roles of circHIPK3 and other circRNAs in RMS tumorigenesis both *in vitro*, and *in vivo* using xenograft mouse models.

We are also interested in better characterising how circRNAs can be involved in other aspects of RMS biology, such as cancer heterogeneity. As many other solid and blood tumours, also RMS includes a subpopulation of cancer stem cells (CSCs) with capacity to self-renew, extensively proliferate *in vivo* and resist to pharmacological therapies [141].

Thus, by isolating CSCs from mixed RMS cell populations we could investigate whether circRNAs are differentially expressed between CSCs and non-CSCs, and whether the knock-down of circRNAs overexpressed in CSCs can have a specific impact on their *in vivo* proliferation, aggressiveness and insensitivity to chemotherapy.

Finally, we would also like to investigate the expression of circRNAs in tumour biopsies and in patient-derived extracellular fluids, to explore the possibility to use them as RMS biomarkers. Many circRNAs are expressed in human serum exosomes, and ARMS and ERMS cells can produce exosomes with a specific miRNA content [142]. It

would be very interesting to elucidate whether circRNAs could load specific miRNA-cargoes into exosomes. This would allow us to study paracrine signalling mediated by exosome-contained circRNAs and its role in RMS tumorigenesis.

Materials and methods

Cell cultures and transfections

Wild-type human primary myoblasts (Telethon Biobank) were obtained from a skeletal muscle biopsy from a 2-year-old male child. They were cultured in a growth medium made of DMEM (Sigma-Aldrich), 10% FBS (Sigma-Aldrich), L-glutamine (Sigma-Aldrich) 2 mM, insulin (Sigma-Aldrich) 50 mg/ml, FGFb (Millipore - Merck) 25 ng/ml, EGF (Corning) 1 ng/ml, penicillin-streptomycin 1X (Sigma-Aldrich). Human ERMS RD cells and ARMS RH4 cells were kindly provided by Prof. C. Dominici's lab. RD and RH4 cells were cultured in DMEM high-glucose supplemented with 10% FBS, 2 mM L-glutamine and penicillin-streptomycin. All cell lines were tested for mycoplasma contamination.

To transfect cells with siRNAs, 3 pmol siRNA (Dharmacon) and 0.15 µl Dharmafect-1 Transfection Reagent (Dharmacon) in 150 µl DMEM were added to each 100 µl of culture medium in the plate. For HUR knock-down, 60 pmol siRNA were used for each 100 µl of culture medium. The transfection mixture was briefly vortexed, left at RT for 20 min and then seeded in the plate. Medium was replaced 24 h after the transfection and cells were harvested after another 24 h, unless differently specified.

Patient biopsies

Tumour samples from 11 primary RMS tumours, 5 ARMSs and 6 ERMSs, were obtained at diagnosis before any treatment from children admitted to the Department of Oncology at Alder Hey Children's NHS Foundation Trust, Liverpool, United Kingdom. Control RNA was extracted from normal skeletal muscle biopsies obtained from 3 children undergoing surgery for non-oncological conditions. Institutional written informed consent was obtained from the patient's parents or legal guardians. The study underwent ethical review and approval according to the local institutional guidelines (Alder Hey Children's NHS Foundation Trust Ethics Committee, approval number 09/H1002/88).

Flow cytometric analysis of cell cycle

Cells were pelleted and 100 µl PBS (Sigma-Aldrich) and 10 µl RNase A (Sigma-Aldrich) were added to the pellet (1 mg/ml). Cells were incubated at 37°C for 30 min. Then propidium iodide (Sigma-Aldrich) was added (1 mg/ml) and cells were incubated at room temperature, in the dark, for 5 min. Samples were processed using a BD FACSCalibur Flow Cytometer (BD Biosciences, Franklin Lakes, NJ, USA) machine and Cell Quest Pro (BD Biosciences) software. Results were analyzed using ModFit 3.1 software (BD

Biosciences). Three independent biological replicates of FACS analysis were performed, unless differently specified.

Proteasome inhibition

Cells in 10 cm plates were transfected with either si-SCR or si-Circ (Dharmacon) as previously described. 24 h after transfection, si-Circ-transfected cells were split into three 60 mm plates and the si-SCR-transfected cells were sub-cultured as well. After additional 24 h, si-SCR-transfected cells and one plate of si-Circ-transfected cells were harvested; fresh medium supplemented either with MG132 (10 μM, dissolved in DMSO, Sigma-Aldrich) or with an equal volume of 100% DMSO (Sigma-Aldrich) was added to the other two si-Circ-transfected plates. DMSO- and MG132-treated cells were harvested after 5 h of treatment. Two independent biological replicates of this experiment were performed.

Actinomycin D treatment

Cells in 6 cm plates were transfected with either si-SCR or si-Circ (Dharmacon) as previously described. 24 h after transfection, si-SCR- and si-Circ-transfected cells were split into five 35 mm plates. 48 h after transfection, one plate si-SCR and one plate si-Circ were harvested (0 h). For both si-SCR and si-Circ, fresh medium was replaced to the remaining plates, and supplemented with either Actinomycin D (three

plates, final concentration = 5μg/ml in DMSO) or an equal volume of 100% DMSO (one plate). Actinomycin D-treated cells were harvested after 2.5 h, 5 h and 7.5 h of treatment, while DMSO-treated cells were harvested after 7.5 h of treatment. An equal quantity of RNA was used for the reverse transcription reaction. Graphs represent ΔCts normalised with respect to the reference sample (0h) which was set as 1. The experiment was performed in 3 biological replicates.

COMET assay

COMET assay was performed according to the protocol described in [143]. Cell lysis and electrophoresis were performed in alkaline conditions. DNA was stained with 20 μl of a 10 mg/ml Ethidium Bromide solution (Thermo-Fisher) in 10 ml of distilled water for 20 min at RT, then slides were rinsed with distilled water to remove excess stain. Slides were imaged on a Zeiss AXIO Observer A1 microscope. Comet tail moment was measured using the ImageJ Macro "Comet Assay" by Robert Bagnell available at https:// www.med.unc.edu/ microscopy/ resources/ imagej-plugins-and-macros/ comet-assay/. Three independent biological replicates of this experiment were performed, two of them 48 h after transfection and one of them 72 h after transfection. Since the results were comparable, the data from the three experiments are shown altogether in *Fig. 19B*.

Fluorescent *in situ* hybridisation (FISH) and immunofluorescence

Cells were cultured on pre-coated glass coverslips (0,4 mg/ml Collagen Rat Tail, Corning), and then fixed in 4% paraformaldehyde (Electron Microscopy Sciences) in PBS for 20 min at 4°C. After dehydration steps with ice-cold ethanol series (50%, 70%, 100%), cells were stored at -20°C in absolute ethanol until use. Detection of circZNF609 was performed using RNAscope assay (Advanced Cell Diagnostics, Bio-Techne) according to manufacturer's instructions, with a little modification. Briefly, fixed cells were permeabilized with Protease III (diluted 1:15) before hybridization with BA-HS-ZNF609circRNA-1ZZ-Exon1 probe (ref. 708461), designed by ACD and ordered as a single-plex probe to detect the back-splicing junction of the circRNA. A probe specific for the exon 2-exon 3 junction of ZNF609 mRNA (BA-HS-ZNF609linearRNA-1ZZ- Exon2-3 probe, ref. 798471) and for the bacterial RNA dapB, were used as positive and negative controls, respectively. The cells were incubated with probe solution (45 ul for each coverslip) at 40°C for 2 h in the EZ Hybridization oven using the humidity control tray and slide rack (ACD Instruments). Amplification and detection steps were performed using Basescope detection reagents – RED (ref. 322910) and SIGMA-FAST™ Fast Red TR/Naphthol AS-MX Tablets (Sigma-Aldrich) for fluorescent

signal development. The washings after each amplification step were performed three times for 5 min with 2 ml of 1X wash buffer (ADC ref. 310091) at RT.

When FISH staining was combined to immunofluorescence, the samples were washed twice for 5 min with 2 ml of ddH_2O after SIGMA-FAST™ incubation and then blocked with 1% goat serum/PBS for 15 min at RT. Primary antibodies were diluted 1:100 in 1% goat serum/PBS and incubated overnight at 4°C. Anti-KDEL, anti-GM130 antibodies were kindly provided by Dr De Jaco's lab. Anti-Tubulin and anti-Pericentrin were kindly provided by Dr Giulia Guarguaglini's lab. Anti-γH2AX (Ser 139) antibody was purchased from Santa Cruz Biotechnology (sc-517348). Fluorescent secondary antibodies were diluted 1:200 in 1% goat serum/PBS and incubated for 45 min at RT. After extensive washings with PBS, cells were incubated with DAPI solution (Sigma, D9542; 1ug/ml/PBS) for 5 min at RT and then mounted using ProLong Diamond Antifade Mountant (ThermoFischer Scientific, P-36961).

Samples were imaged on confocal microscopes (Spinning disk Olympus IX73 and laser scanning FluoViewFV10i Olympus) equipped with 60X NA1.35 oil (UPLANSApo) and water (UPLSAP) objectives respectively. The Z-stacks (200 and 300 nm Z-spacing) were collected with MetaMorph or Fluoview software and merged with maximum

intensity projection (MIP) method. All images were processed only in intensity threshold, contrast and brightness. Post-acquisition processing was applied using MetaMorph (Molecular Devices) and FIJI software to the entire image.

Microtubule de-/re-polymerisation assay and analysis of mitotic phenotypes

These experiments were performed in collaboration with Dr P. Lavia's lab. The protocols used for microtubule de-/re-polymerization assays and immunostainings were previously described in [144,145].

Western Blot

Cells were harvested with a suitable volume of Protein Extraction Buffer (100 mM Tris pH 7.5, EDTA 1 mM, SDS 2%, PIC 1X (Complete-EDTA free, Roche–Merck), incubated 5 min on ice, then incubated on a wheel for 30 min at 4°C, and centrifuged at 13000 rpm for 10 min at 4°C. Proteins (25-30 μg) were loaded on 4%–12% bis-tris-acrylamide gel (Thermo Fisher Scientific-Life Technologies) and transferred to a nitrocellulose membrane. The membrane was blocked in 5% milk and hybridized with the following antibodies: anti-GAPDH (6C5, sc-32233, Santa Cruz Biotechnology), anti-RB (G3-245, 554136, BD Biosciences), anti-phospho-RB Ser780 (D59B7, 8180, Cell Signaling Technology), anti-AKT (9272,

Cell Signaling Technology), anti-phospho-AKT Ser473 (9271, Cell Signaling Technology), anti-$p27^{Kip1}$ (C-19, sc-528, Santa Cruz Biotechnology), anti-β ACTIN (A3854, Sigma-Aldrich), anti-HUR (sc-5261, Santa Cruz Biotechnology), anti-phospho-H2AX Ser139 (sc-517348, Santa Cruz Biotechnology), anti-CKAP5 (A301-971A, Bethyl), anti-DDX27 (17087-1-AP, Proteintech), anti-PES1 (A300-903A, Bethyl), anti-YAP/TAZ (63.7, sc-101199, Santa Cruz Biotechnology, kindly provided by Prof S. Piccolo's lab). Images were acquired using a ChemiDoc MP Imager (Bio-Rad) and analysed using Image Lab 5.2.1 software (Bio-Rad). Whole images were adjusted in contrast and brightness when necessary. In some cases, protein samples were run twice, to allow multiple hybridizations for proteins with the same molecular weight. Anti-GAPDH hybridization was performed for each running, but only one anti-GAPDH hybridization is shown. However, for protein quantification each specific signal was compared with the corresponding anti-GAPDH hybridization. Each experiment was performed on three independent biological replicates, unless differently specified.

RNA isolation and treatments

Total RNA was extracted with Qiazol reagent (Qiagen) and Direct-zol RNA Miniprep kit (Zymo Research), according to the manufacturer's protocol. 15-minute DNase-I treatment

was performed during routine RNA extractions according to the manufacturer's protocol.

Reverse transcription reaction for routine experiments was performed using PrimeScript RT Reagent Kit (Takara Bio) on an appropriate amount of RNA (usually between 100 ng and 500 ng). cDNA was diluted to 1 ng/µl with ddH_2O and used for the qRT-PCR reaction or RT-PCR reaction. Reverse transcription of RNA derived from RNase R treatment, pulldown experiments and RIP assays was performed using the SuperScript VILO Master Mix (Thermo-Fisher), according to the manufacturer's protocol.

RT-PCR was performed using MyTaq-HS DNA Polymerase (Bioline) and usually 20 ng of cDNA, according to the manufacturer's protocol. DNA amplification was performed with 2720 Thermal Cycler (Applied Biosystem) following the manufacturer's protocol. PCR products were analysed by a 2%-agarose-gel electrophoresis. Images were acquired on a Gel Doc EZ Imager (Biorad).

qRT-PCR was performed as follows: 6 µl cDNA (usually 1 ng/µl) were added to 7,5 µl PowerUp SYBR Green Master Mix (Thermo Fisher Scientific) and 1.5 µl of a 5 µM primers mix. DNA amplification was achieved following the manufacturer's protocol. An ABI 7500 Fast qPCR (Thermo Fisher Scientific) instrument was used for amplification and data analysis. RNA levels are relative to Gapdh mRNA in

routine experiments. Each experiment was performed on three biological replicates, unless differently indicated. Relative RNA quantity was calculated as the Fold Change ($2^{-\Delta\Delta Ct}$) with respect to the control sample set as 1, unless differently specified.

RNase R treatment

RNase R treatment was performed as described in [28]. Briefly, 1 µg of total RNA was diluted in 20 µl of ddH_2O with 4U RNase R and 2 µl of 10X enzyme buffer (Epicentre). The reaction was incubated 15 min at 37°C, and then 20 min at 65°C with the addition of 1mM EDTA. As a negative control (RNase R (-)) total RNA was incubated with the same reaction mixture devoid of the enzyme. 1 pg of a DNA spike-in, produced from the multiple cloning site of pcDNA3.1(-) (Life Technologies), was added to each reaction for qRT-PCR normalization. Treated RNA was purified with RNA Clean & Concentrator-5 kit (Zymo Research), following manufacturer's instructions. 500 ng of RNase R (-) and an equal volume of RNase-treated (RNase R (+)) RNA were reverse-transcribed and then analysed by qRT-PCR.

Nucleus-cytoplasm subcellular fractionation

For RNA analysis, nucleus-cytoplasm subcellular fractionation was performed using the Paris Kit (Thermo-

Fisher), according to the manufacturer's instruction. RNA was extracted as previously described. For the reverse transcription reaction, 500 ng of RNA from the cytoplasmic fraction and an equal volume from the nuclear fraction were used. For qRT-PCR data representation, ΔCts were calculated (average nuclear Ct – average cytoplasmic Ct); nuclear RNA quantity was calculated as $2^{-\Delta Ct}$ and then converted into percentage.

For protein analysis, the subcellular fractionation protocol was adapted from [146]. Briefly, cells were lysed with Cytoplasmic Lysis Buffer (10 mM Hepes buffer pH=7.9, 0.34 M sucrose, 3 mM $CaCl_2$, 2 mM MgAc, 0.1 mM EDTA, 1 mM DTT, 0.5% NP-40, Protease Inhibitor Cocktail). Nuclear pellet was isolated by centrifugation at 2600 xg for 15 min. Supernatant containing cytoplasmic fraction was kept, and nuclei were then washed with Cytoplasmic Lysis Buffer without NP-40. Nuclear lysis was performed in Nuclear Lysis Buffer (20 mM Hepes buffer pH =7.9, 3 mM EDTA, 10% glycerol, 150 mM KAc, 1.5 mM $MgCl_2$, 1 mM DTT, 0.1% NP-40, Protease Inhibitor Cocktail). To digest DNA in the nuclear fraction, DNase I digestion (New England Biolabs) was performed according to the manufacturer's protocol.

Polysome fractionation

To analyse circRNA association to polysomes, cytoplasm fractionations on sucrose gradients were performed

as described in [28]. Briefly, $5x10^6$ cells were scraped in 450 mL of TNM lysis buffer (10mM Tris-HCl pH=7.5, 10mM NaCl, 10mM $MgCl_2$) supplemented with 0.1 mg/ml cycloheximide, 1X PIC (Complete EDTA-free, Roche) and 60U of RiboLock RNase Inhibitor (Thermo Scientific). Lysates were incubated 10 min on ice, and then centrifuged at 13000 rpm for 5 min at 4°C to pellet nuclei. Supernatants (cytoplasmic fraction) were recovered and centrifuged on 9.8 mL 15%–50% sucrose gradient at 37,000 rpm in a polyallomer centrifuge tube with a SW41 rotor (Beckman) for 1.5 h, at 4°C. 12 sucrose gradient fractions were collected with a Bio-logic LP instrument (Biorad). To each fraction, 1 pg of a spike-in DNA, 10 μg of glycogen and 100 μg of Proteinase K (Roche) were added. Samples were incubated 1 hr at 37°C. RNA was isolated from each fraction following a Trizol phenol-chloroform extraction protocol.

Luciferase assay

Cells in a 24-well plate were transfected with either si-SCR (Dharmacon) si-circHIPK3 (Dharmacon), si-YAP or si-TAZ (Invitrogen, kindly provided by Prof. S. Piccolo's lab) as previously described. 24 h after transfection, cells were transfected with 25 ng of 8xGTIIC-luciferase vector (expressing Renilla luciferase; kindly provided by Prof. S. Piccolo's lab) and 25 ng of pRL-TK luciferase vector

(expressing Firefly luciferase used to normalise Renilla luciferase signal; from Promega). 24 h after the second transfection, cells were harvested. For the luciferase assay, Dual-Luciferase Reporter Assay Kit (Promega) was used according to the manufacturer's instructions. Cells were washed twice in PBS and lysed using an appropriate amount of 1X PLB. Lysed cells were harvested and centrifuged for few seconds to allow debris precipitation. 10 µl of lysate were used for each reaction, and each sample was measured in technical triplicate. Firefly luciferase signal was measured by adding Luciferase Assay Reagent II (LAR II). Then the reaction was quenched, and Renilla luciferase signal was measured by adding Stop&Glo reagent. For the measurements, a Glomax-Multi+ Detection System (Promega) machine was used. The experiment was performed on two independent biological replicates.

RNA-pulldown

The psoralen-crosslinked RNA-pulldown protocol was adapted from [104]. Briefly, $1x10^7$ RD cells for each biological replicate were pelleted, resuspended in 1 ml of ice-cold complete PBS supplemented with 0.5 mg/ml of 4'-aminomethyl-4,5',8-trimethylpsoralen (AMT, Cayman Chemical), and crosslinked at 365 nm for five 2-minute cycles. 1 volume of Guanidinium Hydrochloride 6M and 1 volume of

AMT were added. The lysate was subdivided into eight 250-µl aliquots. To each aliquot, 25 ul of a 20 mg/mL solution of Proteinase K (Ambion) and 6.5 µL of 20% SDS were added. Then the samples were incubated at 65°C for 1 h. RNA was precipitated through phenol/chloroform extraction. 10% of the total RNA was kept as Input, then 50 µg of RNA for each pulldown (*odd*, *even*, LacZ) were incubated at 95°C for 3 min and 500 pmol of probe mix were added. 500 ul of 2x Binding Buffer (20 mM Tris-HCl pH=7.5, 1 M NaCl, 2 mM EDTA, 0.1% SDS) were added to each pulldown sample, then they were all incubated at 65°C for 5 min. Samples were put on a rotor and incubated for 4 h, at RT. Magnetic beads (Promega) were washed 3 times with 1x Binding Buffer, then 100 µl of beads were added to each sample and incubated on a rotor at 4°C, over-night. Beads were washed twice with 400 µl of 1x Binding Buffer and twice with 400 µl of 1x Wash Buffer (10 mM Tris-HCl pH=7.5, 200 mM NaCl, 1 mM EDTA, 0.05% SDS). Then RNA was purified through phenol/chloroform extraction. Reverse crosslinking was performed by UV-irradiating RNA samples at 254 nm for 10 min.

For the native pulldown, cells were lysed with an appropriate volume of Lysis Buffer (10 mM Hepes, 20 mM KCl, 1.5 mM $MgCl_2$, 0.5 mM EDTA, 1% NP40, 1 mM DTT, supplemented with Protein Inhibitor Cocktail and RNase inhibitor). Lysates were kept in ice for 10 min and then

centrifuged at 4000 rcf at 4°C for 5 min. Supernatants were collected. 1 mg of lysate was used for each pulldown sample, while 100 μg (10%) was kept as Input. The rest of the protocol is very similar to the one described above. The Hybridisation Buffer used for probe hybridisation contained 300 mM NaCl, 100 mM Tris-HCl pH=7.5, 0.2% SDS, 10 mM EDTA, 15% Formamide, 1% NP40, 1 mM DTT, and was supplemented with Protein Inhibitor Cocktail and RNase inhibitor.

RIP assay

The RNA-immunoprecipitation (RIP) assay for HUR protein was performed in RD cells according to the protocol described in [147]. Anti-HUR primary antibody was purchased by Santa Cruz Biotechnology (sc-5261).

RNA-sequencing experiments and bioinformatic analyses

For total RNA-sequencing (mRNA differential expression analysis) in myoblasts, RD and RH4 cells, total RNA was extracted and treated with DNase I (New England Biolabs) as described before. Two biological replicates for each condition (human primary myoblasts, RD cells and RH4 cells) were performed. Total RNA was sequenced on an Illumina Hiseq 2500 Sequencing system using TruSeq Stranded Total RNA Library Prep Kit with Ribo-Zero treatment at the Institute of Applied Genomics (IGA; Udine,

Italy). An average of about 13 million and 30 million 125-nucleotide long paired-end reads were produced for myoblast and RMS samples, respectively. Adapter sequences and poor-quality ends were removed using the Trimmomatic software [148]; reads with length < 20 nt after trimming were filtered out. Reads were mapped to human GRCh38 genome and Ensembl 90 transcriptome [149] using STAR software [150], with parameters --outSAMstrandField intronMotif --outFilterType BySJout --outFilterMultimapNmax 20 --alignSJoverhangMin 8 --alignSJDBoverhangMin 1 --outFilterMismatchNmax 999 --outFilterMismatchNoverLmax 0.04 --outFilterIntronMotifs RemoveNoncanonical. Number of reads and mapping statistics are reported in [84]. Htseq-count software [151] was used to count reads mapping to Ensembl 90 human genes; the overlap resolution mode was set to intersection-strict. Differential gene expression was performed using edgeR R package [152] after filtering out genes with a CPM (Count Per Million) value less than 1 in at least two samples. edgeR software is particularly suited for experiments with few replicates [153]. TMM normalization was applied independently for myoblast and RMS samples. Pearson correlation-based sample hierarchical clustering, as well as gene expression heatmaps were drawn based on log_2-transformed RPKM values, calculated using the edgeR rpkm

function. Model fitting and testing were performed using glmFIT and glmLRT functions. FDR cutoff for selecting significant differentially expressed genes was set to 0.05 and absolute $\log_2$ Fold Change was set to > 0.5. Gene Ontology (GO) terms [154] and Reactome pathways [155] enrichment analyses were performed using WebGestalt web server [156] and all genes tested for differential expression as a background; an adjusted p-value cutoff of 0.05 was used to select enriched categories. EnrichmentBrowser R package [157] was employed to perform KEGG pathways [90] based Gene Graph Enrichment analysis [89], using an absolute $\log_2$ Fold Change significance level equal to 0.5 and a statistical significance level equal to 0.05. Transcriptional regulator activity analysis was performed through msviper function included in the Viper R package [91] using RPKMs as expression values; the ARACNe-AP-inferred [158] human sarcoma [92] regulon used in the analysis was taken from the aracne.networks R package, available at https://bioconductor.org/packages/release/data/experiment/html/aracne.networks.html. A p-value cutoff of 0.05 was used to filter results, which were then ranked based on p-value; the top 30 transcriptional regulators were used to draw the msVIPER analysis plot.

CircRNA identification in myoblasts, RD and RH4 cells, and their differential expression have been performed as

described in [18]. Briefly, Trimmomatic [148] and Cutadapt [159] were used to remove adaptor sequences; minimum read length after trimming was set to 20. Reads were then aligned to the human reference genome (GRCh38) using BWA-MEM [160] with -T 19 option. circRNA detection in each sample was then carried out using CIRI2 software [161], which is able to identify circRNAs by searching for reads which map to back-splicing junctions. To identify circRNA host genes, the programme was provided with Ensembl 90 gene annotation [149]. For each back-splicing event found, CIRI2 reports the number of reads mapping to the back-splicing junction and on the corresponding linear splicing junctions, calculated summing all the reads mapping linearly on both the splice junctions involved in back-splicing; the latter are not reported if no read is assigned to the back-splicing junction, even if the circular RNA is detected in other samples. In order to count the reads mapping to linear splicing sites in samples in which no reads where mapped to corresponding back-splicing junctions detected in other samples, alignment files from each sample were modified by adding reads mapping to circRNAs found only in other samples and CIRI2 was rerun on these files. Putative back-splicing events that were spanning two non-overlapping genes, which were likely to be due to mapping errors, were excluded from further analysis. Reads mapping to back-splicing junctions and to their cognate linear

splicing junctions were converted to Count Per Million (CPM) values using edgeR R package [152] and used for circRNA and linear RNA quantification. To evaluate the differential expression of circRNAs between cell lines, we provided the edgeR software with the read counts of both the back-splicing events and their cognate linear splicing events. Events not having 2 or more counts in at least two samples were not tested for differential expression. Model fitting and testing was performed using the glmFIT and glmLRT functions. We set a threshold on the FDR for circRNA and linear counterparts' differential expression (FDR <0.001 and FDR <0.05, respectively).

For the RNA-sequencing of the circZNF609-pulldown, Ovation RNA v2 followed by Ovation Ultralow v2 kit was used to prepare cDNA libraries. The sequencing reactions, performed on an Illumina NovaSeq6000 Sequencing system at the Institute of Applied Genomics (IGA; Udine, Italy), produced an average of 43.5 million 150 nucleotide long paired-end reads per sample. Reads were pre-processed using Trimmomatic software [148]. Alignment to human GRCh38 genome and Ensembl 90 transcriptome [149] was performed using STAR aligner [150]. Alignment file was further pre-processed by filtering out reads mapping to rRNAs and tRNAs, removing PCR duplicates using Picard Mark

Duplicates (available at http://broadinstitute.github.io/picard) and discarding the multi-mapped reads using bamtools [162]. Properly paired reads were extracted using SAMtools [163]. GRCh38 genome was binned into 170 bp long non-overlapping reads using BEDtools window tool [164]. Properly paired fragments falling in each bin were counted using BEDtools intersect tool; this way, sample-specific count files were created. Such files were given as input to Piranha tool [165] to call peaks for *odd* and *even* circRNA pulldown samples and LacZ pulldown sample, using Input sample counts as a covariate. *Odd* peaks overlapping *even* peaks were identified using BEDtools intersect tool. Normalized coverage was calculated for such overlapping peaks in each sample, by dividing fragment counts by the total number of mapping fragments. Peaks where both *odd* and *even* coverages were at least four-fold higher than both Input and LacZ coverages were selected as circZNF609 pulldown enriched regions. BEDtools intersect tool was used to annotate such regions based on their overlap with Ensembl 90 exons and to filter out transcripts hosting LacZ peaks.

Data availability

RNA-sequencing raw data generated in human primary myoblasts, RD and RH4 cells described in [84] have been deposited at Gene Expression Omnibus (GSE117609).

Oligonucleotides, siRNAs and probes used in this study

Oligonucleotides

circZNF609	FW	AAACCGGAGCCAGAGGAAGG
	RV	CAGCTATGTTCTCAGACCTGC
Znf609	FW	GCACGGCTATTCCTACAGTC
	RV	TTCACCACCTGAGACCTTGC
Rb	FW	GACCTAGATGAGATGTCGTTC
	RV	GCATTATCAACTTTGGTACTGG
Tcf19	FW	CAGGAAGAAACTCCGTGTAGAC
	RV	CAGCAACAAGGAGCTGCACAG
Cenpu	FW	TCCTCCTTTACATAGCACAGC
	RV	CGATTTCACTTGCTTCATTTCC
Zwint	FW	ATGGAGGCAGCGGAGACAGA
	RV	TCCGCTACCTGAAGCTGGCTG
Mcm7	FW	CTGTCATACATTGATCGACTGG
	RV	CTCTAAGGTCAGTTCTCCACTC
Gapdh	FW	CCAAAATCAAGTGGGGCGATG
	RV	GGCAGAGATGATGACCCTTT
b-Actin	FW	CGTACCACTGGCATCGTGAT
	RV	GTAGTCAGTCAGGTCCCGGC
Ddx27	FW	GCAGCCACTACATTAGATGAGA
	RV	GTCTTCCTGCTCCTTTGGTTC
Pes1	FW	ATGGGAAGAGCGAGTGGAAC
	RV	GGGAAGGTGGAAAACAGGAAG
Ckap5	FW	GGACACAAAGGACATTTCTGCAC
	RV	TTGGTTCCAGTATTCCCTGCG
E2f1	FW	GCTGGACCACCTGATGAATATC
	RV	CAATGCTACGAAGGTCCTGAC
Cdk1	FW	CAGGTCAAGTGGTAGCCATG
	RV	GGAATCCTGCATAAGCACATC
Cyclin A2	FW	CTGAGAATGGAGCATCTAGTTTTG
	RV	GAGGTATGGGTCAGCATCTATC

Cyclin B1	FW	CTGTGTCAGGCTTTCTCTGATG
	RV	CGACCCAGTAGGTATTTTGG
Cyclin B2	FW	CTCTGCAGTGACTACGTTAAG
	RV	GTCTCCTGCAGAAGCCTAAAC
cicrPMS1	FW	GATCTCCTCATGAGCTTTGGTATCC
	RV	CTTGAAAGGAGTCGAACTGTTGCC
Yap	FW	CCTGATGATGTACCTCTGCCA
	RV	CCTGCCATGTTGTTGTCTGAT
Taz	FW	TATCATTCGAGGGAGCAGAGCA
	RV	TGTTGGGGATTGATGTTCATGG
Ankrd1	FW	AGTAGAGGAACTGGTCACTGG
	RV	TGGGCTAGAAGTGTCTTCAGAT
Ccn1	FW	CCTTGTGGACAGCCAGTGTA
	RV	ACTTGGGCCGGTATTTCTTC
Ccn2	FW	AGGAGTGGGTGTGTGACGAG
	RV	CCAGGCAGTTGGCTCTAATC
Fmn1	FW	CTCCAAAGACACAACTCAACAGA
	RV	TTCCCACAGTTTGAGATCGTT
Gsn	FW	GGGAGAGCTTCAACAATGGC
	RV	GGCCTTCAGTCTTTCATACCG
Stk3	FW	AAGACATGAGGAACAGCAACG
	RV	CCCACACTCTCCACACTAGTC
ItgA3	FW	ATGTGGCTTGGAGTGACTGTG
	RV	AGTCCAGCTCTAGGTCATTGC
ItgA6	FW	ATTCCTACCCTGATGTTGCTGT
	RV	GTTTTCTGGCGGAGGTCAATTC
ItgAv	FW	AGGTCCTCAAATGTGACTGGT
	RV	CTCACAGATGCTCCAAACCAC
ItgB5	FW	AGAATGTCTGCTAATCCACCCA
	RV	TATCTCACCTCCACAGCCATTT
ItgB6	FW	CGCAAAACTTATTCCTGGAGCT
	RV	TACTTCCAGTTCCACCTCAGAC
Aff1	FW	GACTATCGACAGCAGACCTTTG
	RV1	GGTTGCGTCTTTCCTTCTCTC

	RV2	CTAGGCGTATGTATTGCTGTC
Camsap1	FW	TCAGTGCCTCGAAAGAACTTCC
	RV1	GGACAGGAGAAGCTTGATAAC
	FW_lin	CAACGTTCAGTGCCTCGAAA
	RV_lin	CGGACCTTTTGATGAGCTGG
Carhsp1	FW	AGGAGTCTGCAAATGCTTCTGC
	RV1	AGCCCGACTGAAGCTTGATG
	RV2	ATTCTTGGGTGGGATGGAGCA
Ccdc91	FW	GAGGCCATTTCTTTTCAAGATAG
	RV1	GACTCACAATGCTATTTGCTGC
	RV2	GTTGCTTAACTGAAGACTGCAG
Cdyl	FW	ATACACCCACTAGTGCCTCAG
	RV1	TCCTCGCTGTCATAGCCTTTC
	RV2	TCCTTTTGCTGGCAGTCACTC
Cep70	FW	CGAGCAGCCAATCAAGAACA
	RV1	CCCATTCTGCTTCTTCCTGC
	RV2	GACAATGCGATCTTCTTCCTCC
Coro1c	FW	CCTCAACACATTCAGCAGCA
	RV1	CATCTTGGAAAAGGTCAGACTTC
	FW_lin	TGCCCACATAACGATCAGGTC
	RV_lin	GCCTTCCAAAATCACCACAGG
Cpsf6	FW	AAGCAGAGAACGAGAGAGGC
	RV1	TAATCTCGGTCTTCTGGGGC
	FW_lin	CAGAGAGAGAAGCAGAGAACG
	RV_lin	GAAGCAAACTGCTGGACAAGC
Fat3	FW	GAGAGATCCAGTACTCCATCAG
	RV1	GCTTGAAAAGCAGGAGGATGAG
	RV2	ACCTCAATGGTGGAGTAGAGTG
Hipk3	FW	CGGCCAGTCATGTATCAAAG
	RV1	CCTGGAATACACAACTGCTTGG
	RV2	CTGATCATACTCCAAGGCTC
Irizio	FW	AGCATGCCGCTCCTGAAGAT
	RV1	TTCTTCCCAGCCTTTGCGTTC
	RV2	AGCTGCTATCCTCTTCCTCAC

Kmt2e	FW	TCGAATTTACCAGAGGCGAACG
	RV1	GTCTGGTAAATCTGAGGTCCAAG
	RV2	AACTGGTGGGGATAACTGTTGG
Med13l	FW	TGATACCATTTTGCAGCAGC
	RV1	GAATTGGATCATCTTGGGCTGG
	FW_lin	CCAGCCCAAGATGATCCAATTC
	RV_lin	CAGATTGTGGATCGCTTTGAAG
N4bp2L2	FW	CAGACAGGTTTGTGAACCAGC
	RV1	CGTGGCTCACTCGTTACTTCTT
	RV2	CATCAGTGCTGAACACAATGCC
Nrg1	FW	CTAGGTTCTGGTTCCTCTTGTG
	RV1	CTATTCAAGCATAGTGGCTGTCC
	FW_lin	CAGCAGCATGGGGAAAGGA
	RV_lin	CCGATTCCTGGCTTTTCATCTC
Prdm5	FW	CCCTATCAATGTCCTTACTGTG
	RV1	CCTGTAGGCTTGATGCTGAAG
	FW_lin	AGCGTCCCTATCAATGTCCT
	RV_lin	TCCTCTTGTGCTCATCCAGG
Psd3	FW	AGTCCATTGCCTTACCTGTGC
	RV1	TTCCACATTGCTGCTGGTACC
	RV2	CAGCAGATCCTTGGAGAAATC
Rell1	FW	TGTCTGTTAGTGGGGCTGAAAC
	RV1	GGATCATACAGGCTGTTATCTGC
	FW_lin	ACCTGTGAAGAGAGAACGCA
	RV_lin	TTTTATCCACGTGCCTGCTG
Rhobtb3	FW	GATTCTGGGGATGTTTCAAATG
	RV1	TTGGGGTTGTAAAATACCACG
	RV2	TTCGAAGACAACATCGGCAAG
Satb2	FW	TGCCAATGTGTCAGCAACCAAG
	RV1	TTTCCGCACCAGGACAAACTC
	RV2	TGGTAAATGCATTGGACGCTGG
Sdhaf2	FW	GCTAAAGAACATCTGCAGCAC
	RV1	TGTCACACTGAGCAAAGGAGAC
	RV2	TTAGCAAAGTCTCTCAGCAGG

Slc4a7	FW	ATTCCCCATGATCTCTTCACGG
	RV1	TTCTCCGGTGGTGATGTTTGTG
	RV2	AGACTGTGCAAAGAGAGAGTTG
Spag16	FW	ATGCACCAGAAGGTCCTACTC
	RV1	CAAGAGTTCTGGTCATTCCCA
	RV2	TCAGGTTTGGATTTGGTTGC
Stk39	FW	GCCCACCCAATGCTAATGAA
	RV1	CTTGGCTTTCTGGAAGAATTTGC
	RV2	AGAGAAGAGCTCCTGAGATAC
Tmem135	FW	GCTCACAATTTATATGGCCAAC
	RV1	CATATACAAGGCCCCATTAGC
	RV2	TTGCATATGCTGCCTCTGGT
Ubap2	FW	GACAAACCTTCAGATCGTGG
	RV1	CACTTGTTTCTGTGGTTGCG
	RV2	AGCAGCTTCCCAAACTACTAG
Ugp2	FW	GACCTGGATGGATTTCGGAAG
	RV1	TTCTAGCTCTTGCCGAATGAC
	RV2	CACCATTGAGTTTCACCACCAC
Uri1	FW	GTCACTGTTTTACTGGGGGAC
	RV1	CTGAGTCTTTCTCGAAGGGCA
	RV2	CTTCTGTGAATTCAACTCTGGA
Vamp3	FW	ATGTGGGCAATCGGGATTAC
	RV1	GCACGGTCGTCTAACTCAGA
	RV2	GCAGGTTCTAAGTCAAAAGTC
Vapa	FW	GGAAAGAGGCAAAACCTGATG
	RV1	GGTGCTGTAGTCTTCACTTTG
	RV2	TTGGCATAGGTCCATCTTGC
Xpo1	FW	TGTCAACAAGTTAGGGGGAC
	RV1	ACCAATCATGTACCCCACAG
	RV2	GTGTAGGTGGAATAGCAAGG
Znf124	FW	CAGTCGTTCCAGTCACCTTCG
	RV1	CTGCATCACGTCTCTATAGAG
	FW_lin	GACCAGAGCATTGAAGATCAG
	RV_lin	CCACATTGCTTACATTCATAGCG

Zranb1	FW	CTGTGGGAAGCAAGGAGGAA
	RV1	CGTACTTCATCTGCGGTGAG
	FW_lin	CTGTGGGAAGCAAGGAGGAA
	RV_lin	CGTACTTCATCTGCGGTGAG

Regarding circRNA-mRNA couples, the oligonucleotides FW+RV1 were used for circRNA amplification. The oligonucleotides FW+RV2 or FW_lin+RV_lin were used for mRNA amplification.

Custom siRNAs

si-Circ	AGUCAAGUCUGAAAAGCAAUU	Dharmacon
si-Circ+Lin	CACACTACCAGACAACATCAAGUUU	Dharmacon
si-CircHIPK3	GGUACUACAGGUAUGGCCUUU	Dharmacon
si-YAP	CUGGUCAGAGAUACUUCUU	Invitrogen
	GACAUCUUCUGGUCAGAGA	Invitrogen
si-TAZ	AGGUACUUCCUCAAUCACA	Invitrogen
	ACGUUGACUUAGGAACUUU	Invitrogen

Commercial siRNAs

si-SCR	Cat.# D-001810-10-05	Dharmacon
si-Lin	Cat.# J-022257-20	Dharmacon
si-HUR	Cat.# J-003773-08	Dharmacon
si-CKAP5	Cat.# J-006847-05-0002	Dharmacon
si-HIPK3	Cat.# J-004810-09-0002	Dharmacon

Custom biotinylated probes for circZNF609 pulldown (Sigma)

<u>*Odd* set:</u>

Probe 1	CCAGTGGACAACATCATTGC
Probe 3	AAGATTCAAGGCTCTTCCTT
Probe 5	TCACTTGGAGTGAACAGGGA
Probe 7	AGCAGGCGACACTCATTCTC

Even set:

Probe 2	TGCCACATTGGTCAGTACAT
Probe 4	CATCTTAGAGTCAACGTCCC
Probe 6	ATCCTTTTCTGAACAAGTCC

Biotinylated probes for LacZ control pulldown (Sigma)

Probe 1	AATGTGAGCGAGTAACAACC
Probe 2	TTAAGTTGGGTAACGCCAG
Probe 3	AATAATTCGCGTCTGGCCTT
Probe 4	AATTCAGACGGCAAACGCT
Probe 5	ATCTTCCAGATAACTGCCGT

Table 1

GGEA ranking in RD and RH4 cells depleted of circZNF609

RD cells

Gene set	***Nr rels***	***Raw score***	***Norm score***	***P-val***
Hsa03030_dna_replication	5	4,52	0,904	0,000999
Hsa03410_base_excision_repair	5	4,52	0,904	0,000999
Hsa03420_nucleotide_excision_repair	5	4,52	0,904	0,000999
Hsa04610_complement_and_coagulation_cascades	5	4,31	0,862	0,000999
Hsa05410_hypertrophic_cardiomyopathy_(hcm)	17	14,4	0,845	0,000999
Hsa05412_arrhythmogenic_right_ventricular_cardiomyopathy_(arvc)	20	15,7	0,783	0,000999
Hsa04612_antigen_processing_and_presentation	18	12,2	0,679	0,000999
Hsa04512_ecm-receptor_interaction	327	221	0,676	0,000999
Hsa04145_phagosome	26	17,4	0,668	0,000999
Hsa05414_dilated_cardiomyopathy_(dcm)	35	23,1	0,659	0,000999
Hsa04330_notch_signaling_pathway	68	43,2	0,635	0,000999
Hsa04510_focal_adhesion	654	394	0,602	0,000999
Hsa04110_cell_cycle	243	143	0,589	0,000999
Hsa05206_micrornas_in_cancer	162	95,2	0,587	0,000999
Hsa05165_human_papillomavirus_infection	767	446	0,582	0,000999
Hsa04151_pi3k-akt_signaling_pathway	1040	584	0,563	0,000999
Hsa03320_ppar_signaling_pathway	78	47,4	0,607	0,002
Hsa05222_small_cell_lung_cancer	174	99,6	0,573	0,003
Hsa05144_malaria	6	4,49	0,748	0,00699
Hsa04710_circadian_rhythm	39	23,8	0,611	0,00699
Hsa05217_basal_cell_carcinoma	82	47,6	0,58	0,00699
Hsa05150_staphylococcus_aureus_infection	3	2,31	0,77	0,018
Hsa04215_apoptosis	35	20,8	0,594	0,021

Hsa04114_oocyte_meiosis	227	126	0,555	0,025
Hsa04115_p53_signaling_pathway	40	23,2	0,581	0,044
Hsa04015_rap1_signaling_pathway	572	311	0,544	0,046
Hsa05120_epithelial_cell_signaling_in_helicobacter_pylori_infection	48	27,7	0,578	0,049

RH4 cells

Gene set	***Nr rels***	***Raw score***	***Norm score***	***P-val***
Hsa04512_ecm-receptor_interaction	268	154	0,574	0,000999
Hsa04350_tgf-beta_signaling_pathway	73	41,1	0,563	0,002
Hsa04390_hippo_signaling_pathway	191	103	0,54	0,003
Hsa04510_focal_adhesion	569	298	0,523	0,00599
Hsa04151_pi3k-akt_signaling_pathway	921	475	0,516	0,00599
Hsa05010_alzheimer's_disease	27	15,8	0,587	0,011
Hsa04924_renin_secretion	45	25,6	0,569	0,011
Hsa04010_mapk_signaling_pathway	710	368	0,518	0,012
Hsa04727_gabaergic_synapse	167	89,4	0,535	0,013
Hsa05410_hypertrophic_cardiomyopathy_(hcm)	10	6,34	0,634	0,018
Hsa04022_cgmp-pkg_signaling_pathway	180	95,3	0,529	0,028
Hsa05412_arrhythmogenic_right_ventricular_cardiomyopathy_(arvc)	12	7,15	0,596	0,038
Hsa04270_vascular_smooth_muscle_contraction	160	84,4	0,527	0,043
Hsa04971_gastric_acid_secretion	109	58,2	0,534	0,045

Table 2

List of all the mRNAs enriched in circZNF609 pulldown identified by the RNA-sequencing analysis

Gene name	*P-value*	*Read Odd*	*Read Even*	*Read Input*	*Read LacZ*
Des	0,0000	1720,36	1478,89	33,05	0,00
	0,0001	364,03	289,16	14,69	0,00
Os9	0,0001	873,66	301,30	58,76	4,03
Srek1	0,0002	649,85	2858,45	38,56	96,65
Anp32b	0,0019	818,39	10470,33	99,15	199,33
	0,0022	635,02	10847,78	82,63	64,43
Slc4a1ap	0,0019	327,62	218,52	7,34	0,00
Ddx27	**0,0020**	**613,45**	**3244,73**	**51,41**	**66,44**
	0,0030	**199,54**	**396,21**	**22,03**	**2,01**
Anp32a	0,0036	382,90	362,00	64,26	50,34
Mdn1	0,0040	155,05	179,90	11,02	0,00
Znf609	0,0040	1042,19	1229,47	1,84	0,00
Ppig	0,0044	422,00	795,73	62,43	74,50
Pes1	**0,0048**	**315,49**	**208,59**	**29,38**	**0,00**
Tnnt1	0,0054	146,96	128,02	12,85	30,20
Knop1	0,0059	187,41	273,71	29,38	30,20
Ckap5	**0,0066**	**138,87**	**239,49**	**12,85**	**0,00**
	0,0038	**161,79**	**250,53**	**12,85**	**0,00**
Pnisr	0,0073	126,74	134,65	9,18	10,07
Nucks1	0,0079	246,73	391,80	51,41	6,04
Huwe1	0,0084	107,86	128,02	1,84	16,11
Hmgn5	0,0099	105,16	433,73	3,67	10,07

References

1. Hsu MT, Coca-Prados M (1979) Electron microscopic evidence for the circular form of RNA in the cytoplasm of eukaryotic cells. *Nature* **280**: 339–340.
2. Nigro JM, Cho KR, Fearon ER, Kern SE, Ruppert JM, Oliner JD, Kinzler KW, Vogelstein B (1991) Scrambled exons. *Cell* **64**: 607–613.
3. Cocquerelle C, Mascrez B, Hétuin D, Bailleul B (1993) Mis-splicing yields circular RNA molecules. *FASEB J* **7**: 155–160.
4. Wang PL, Bao Y, Yee MC, Barrett SP, Hogan GJ, Olsen MN, Dinneny JR, Brown PO, Salzman J (2014) Circular RNA is expressed across the eukaryotic tree of life. *PLoS One* **9**: e90859.
5. Sanger HL, Klotz G, Riesner D, Gross HJ, Kleinschmidt AK (1976) Viroids are single stranded covalently closed circular RNA molecules existing as highly base paired rod like structures. *Proc Natl Acad Sci U S A* **73**: 3852–3856.
6. Danan M, Schwartz S, Edelheit S, Sorek R (2012) Transcriptome-wide discovery of circular RNAs in Archaea. *Nucleic Acids Res* **40**: 3131–3142.
7. Memczak S, Jens M, Elefsinioti A, Torti F, Krueger J, Rybak A, Maier L, Mackowiak SD, Gregersen LH, Munschauer M, et al. (2013) Circular RNAs are a large class of animal RNAs with regulatory potency. *Nature* **495**: 333–338.
8. Starke S, Jost I, Hung L-H, Correspondence AB, Rossbach O, Schneider T, Schreiner S, Bindereif A (2015) Exon Circularization Requires Canonical Splice Signals. *Cell Rep* **10**: 103–111.
9. Ashwal-Fluss R, Meyer M, Pamudurti NR, Ivanov A, Bartok O, Hanan M, Evantal N, Memczak S, Rajewsky N, Kadener S (2014) CircRNA Biogenesis Competes with Pre-mRNA Splicing. *Mol Cell* **56**: 55–66.
10. Jeck WR, Sorrentino JA, Wang K, Slevin MK, Burd CE, Liu J, Marzluff WF, Sharpless NE (2013) Circular RNAs are abundant, conserved, and associated with ALU repeats. *RNA* **19**: 141–157.
11. Liang D, Wilusz JE (2014) Short intronic repeat sequences facilitate circular RNA production. *Genes Dev* **28**: 2233–2247.
12. Ivanov A, Memczak S, Wyler E, Torti F, Porath HT, Orejuela MR, Piechotta M, Levanon EY, Landthaler M, Dieterich C, et al. (2015) Analysis of intron sequences reveals hallmarks of circular RNA biogenesis in animals. *Cell Rep* **10**: 170–177.
13. Rybak-Wolf A, Stottmeister C, Glažar P, Jens M, Pino N, Hanan M, Behm M, Bartok O, Ashwal-Fluss R, Herzog M, et al. (2014) Circular RNAs in the Mammalian Brain Are Highly Abundant,

Conserved, and Dynamically Expressed. *Mol Cell* **58**: 870–885.
14. Jeck WR, Sharpless NE (2014) Detecting and characterizing circular RNAs. *Nat Biotechnol* **32**: 453–461.
15. Kramer MC, Liang D, Tatomer DC, Gold B, March ZM, Cherry S, Wilusz JE (2015) Combinatorial control of Drosophila circular RNA expression by intronic repeats, hnRNPs, and SR proteins. *Genes Dev* **29**: 2168–2182.
16. Conn SJ, Pillman KA, Toubia J, Conn VM, Salmanidis M, Phillips CA, Roslan S, Schreiber AW, Gregory PA, Goodall GJ (2015) The RNA binding protein quaking regulates formation of circRNAs. *Cell* **160**: 1125–1134.
17. Errichelli L, Dini Modigliani S, Laneve P, Colantoni A, Legnini I, Capauto D, Rosa A, De Santis R, Scarfò R, Peruzzi G, et al. (2017) FUS affects circular RNA expression in murine embryonic stem cell-derived motor neurons. *Nat Commun* **8**: 14741.
18. Di Timoteo G, Dattilo D, Centrón-Broco A, Colantoni A, Guarnacci M, Rossi F, Incarnato D, Oliviero S, Fatica A, Morlando M, et al. (2020) Modulation of circRNA Metabolism by m6A Modification. *Cell Rep* **31**: 107641.
19. Salzman J, Gawad C, Wang PL, Lacayo N, Brown PO (2012) Circular RNAs Are the Predominant Transcript Isoform from Hundreds of Human Genes in Diverse Cell Types. *PLoS One* **7**: e30733.
20. Guo JU, Agarwal V, Guo H, Bartel DP (2014) Expanded identification and characterization of mammalian circular RNAs. *Genome Biol* **15**: 409.
21. Hansen TB, Jensen TI, Clausen BH, Bramsen JB, Finsen B, Damgaard CK, Kjems J (2013) Natural RNA circles function as efficient microRNA sponges. *Nature* **495**: 384–388.
22. Piwecka M, Glažar P, Hernandez-Miranda LR, Memczak S, Wolf SA, Rybak-Wolf A, Filipchyk A, Klironomos F, Cerda Jara CA, Fenske P, et al. (2017) Loss of a mammalian circular RNA locus causes miRNA deregulation and affects brain function. *Science (80-)* **357**: eaam8526.
23. Capel B, Swain A, Nicolis S, Hacker A, Walter M, Koopman P, Goodfellow P, Lovell-Badge R (1993) Circular transcripts of the testis-determining gene Sry in adult mouse testis. *Cell* **73**: 1019–1030.
24. Panda AC (2018) Circular RNAs act as miRNA sponges. *Adv Exp Med Biol* **1087**: 67–79.
25. Di Timoteo G, Rossi F, Bozzoni I (2020) Circular RNAs in cell differentiation and development. *Development* **147**: dev182725.
26. Holdt LM, Stahringer A, Sass K, Pichler G, Kulak NA, Wilfert W,

Kohlmaier A, Herbst A, Northoff BH, Nicolaou A, et al. (2016) Circular non-coding RNA ANRIL modulates ribosomal RNA maturation and atherosclerosis in humans. *Nat Commun* **7**: 12429.

27. Du WW, Yang W, Liu E, Yang Z, Dhaliwal P, Yang BB (2016) Foxo3 circular RNA retards cell cycle progression via forming ternary complexes with p21 and CDK2. *Nucleic Acids Res* **44**: 2846–2858.
28. Legnini I, Di Timoteo G, Rossi F, Morlando M, Briganti F, Sthandier O, Fatica A, Santini T, Andronache A, Wade M, et al. (2017) Circ-ZNF609 Is a Circular RNA that Can Be Translated and Functions in Myogenesis. *Mol Cell* **66**: 22-37.e9.
29. Pamudurti NR, Bartok O, Jens M, Ashwal-Fluss R, Stottmeister C, Ruhe L, Hanan M, Wyler E, Perez-Hernandez D, Ramberger E, et al. (2017) Translation of CircRNAs. *Mol Cell* **66**: 9-21.e7.
30. Begum S, Yiu A, Stebbing J, Castellano L (2018) Novel tumour suppressive protein encoded by circular RNA, circ-SHPRH, in glioblastomas. *Oncogene* **37**: 4055–4057.
31. Zhang M, Zhao K, Xu X, Yang Y, Yan S, Wei P, Liu H, Xu J, Xiao F, Zhou H, et al. (2018) A peptide encoded by circular form of LINC-PINT suppresses oncogenic transcriptional elongation in glioblastoma. *Nat Commun* **9**: 4475.
32. Xia X, Li X, Li F, Wu X, Zhang M, Zhou H, Huang N, Yang X, Xiao F, Liu D, et al. (2019) A novel tumor suppressor protein encoded by circular AKT3 RNA inhibits glioblastoma tumorigenicity by competing with active phosphoinositide-dependent Kinase-1. *Mol Cancer* **18**: 131.
33. Liang W-C, Wong C-W, Liang P-P, Shi M, Cao Y, Rao S-T, Tsui SK-W, Waye MM-Y, Zhang Q, Fu W-M, et al. (2019) Translation of the circular RNA circβ-catenin promotes liver cancer cell growth through activation of the Wnt pathway. *Genome Biol* **20**: 84.
34. Li Z, Huang C, Bao C, Chen L, Lin M, Wang X, Zhong G, Yu B, Hu W, Dai L, et al. (2015) Exon-intron circular RNAs regulate transcription in the nucleus. *Nat Struct Mol Biol* **22**: 256–264.
35. Bach DH, Lee SK, Sood AK (2019) Circular RNAs in Cancer. *Mol Ther - Nucleic Acids* **16**: 118–129.
36. Yu T, Wang Y, Fan Y, Fang N, Wang T, Xu T, Shu Y (2019) CircRNAs in cancer metabolism: A review. *J Hematol Oncol* **12**: 90.
37. Zheng Q, Bao C, Guo W, Li S, Chen J, Chen B, Luo Y, Lyu D, Li Y, Shi G, et al. (2016) Circular RNA profiling reveals an abundant circHIPK3 that regulates cell growth by sponging multiple miRNAs. *Nat Commun* **7**: 11215.

38. Liu N, Zhang J, Zhang LY, Wang L (2018) CircHIPK3 is upregulated and predicts a poor prognosis in epithelial ovarian cancer. *Eur Rev Med Pharmacol Sci* **22**: 3713–3718.
39. Yu H, Chen Y, Jiang P (2018) Circular RNA HIPK3 exerts oncogenic properties through suppression of miR-124 in lung cancer. *Biochem Biophys Res Commun* **506**: 455–462.
40. Xie Y, Yuan X, Zhou W, Kosiba AA, Shi H, Gu J, Qin Z (2020) The circular RNA HIPK3 (circHIPK3) and its regulation in cancer progression: Review. *Life Sci* **254**: 117252.
41. Su M, Xiao Y, Ma J, Tang Y, Tian B, Zhang Y, Li X, Wu Z, Yang D, Zhou Y, et al. (2019) Circular RNAs in Cancer: Emerging functions in hallmarks, stemness, resistance and roles as potential biomarkers. *Mol Cancer* **18**:.
42. Shang Q, Yang Z, Jia R, Ge S (2019) The novel roles of circRNAs in human cancer. *Mol Cancer* **18**: 6.
43. Hanniford D, Ulloa-Morales A, Karz A, Berzoti-Coelho MG, Moubarak RS, Sánchez-Sendra B, Kloetgen A, Davalos V, Imig J, Wu P, et al. (2020) Epigenetic Silencing of CDR1as Drives IGF2BP3-Mediated Melanoma Invasion and Metastasis. *Cancer Cell* **37**: 55–70.
44. Zhang M, Huang N, Yang X, Luo J, Yan S, Xiao F, Chen W, Gao X, Zhao K, Zhou H, et al. (2018) A novel protein encoded by the circular form of the SHPRH gene suppresses glioma tumorigenesis. *Oncogene* **37**: 1805–1814.
45. Guarnerio J, Bezzi M, Jeong JC, Paffenholz SV, Berry K, Naldini MM, Lo-Coco F, Tay Y, Beck AH, Pandolfi PP (2016) Oncogenic Role of Fusion-circRNAs Derived from Cancer-Associated Chromosomal Translocations. *Cell* **165**: 289–302.
46. Zhao Z, Li X, Jian D, Hao P, Rao L, Li M (2017) Hsa_circ_0054633 in peripheral blood can be used as a diagnostic biomarker of pre-diabetes and type 2 diabetes mellitus. *Acta Diabetol* **54**: 237–245.
47. Zhao Z, Li X, Gao C, Jian D, Hao P, Rao L, Li M (2017) Peripheral blood circular RNA hsa-circ-0124644 can be used as a diagnostic biomarker of coronary artery disease. *Sci Rep* **7**: 39918.
48. Zhang YG, Yang HL, Long Y, Li WL (2016) Circular RNA in blood corpuscles combined with plasma protein factor for early prediction of pre-eclampsia. *BJOG An Int J Obstet Gynaecol* **123**: 2113–2118.
49. Meng S, Zhou H, Feng Z, Xu Z, Tang Y, Li P, Wu M (2017) CircRNA: Functions and properties of a novel potential biomarker for cancer. *Mol Cancer* **16**: 94.
50. Łabno A, Tomecki R, Dziembowski A (2016) Cytoplasmic RNA

decay pathways - Enzymes and mechanisms. *Biochim Biophys Acta - Mol Cell Res* **1863**: 3125–3147.
51. Enuka Y, Lauriola M, Feldman ME, Sas-Chen A, Ulitsky I, Yarden Y (2016) Circular RNAs are long-lived and display only minimal early alterations in response to a growth factor. *Nucleic Acids Res* **44**: 1370–1383.
52. Chen S, Li T, Zhao Q, Xiao B, Guo J (2017) Using circular RNA hsa_circ_0000190 as a new biomarker in the diagnosis of gastric cancer. *Clin Chim Acta* **466**: 167–171.
53. Xuan L, Qu L, Zhou H, Wang P, Yu H, Wu T, Wang X, Li Q, Tian L, Liu M, et al. (2016) Circular RNA: A novel biomarker for progressive laryngeal cancer. *Am J Transl Res* **8**: 932–939.
54. Bahn JH, Zhang Q, Li F, Chan T-M, Lin X, Kim Y, Wong DTW, Xiao X (2015) The Landscape of MicroRNA, Piwi-Interacting RNA, and Circular RNA in Human Saliva. *Clin Chem* **61**: 221–230.
55. Memczak S, Papavasileiou P, Peters O, Rajewsky N (2015) Identification and Characterization of Circular RNAs As a New Class of Putative Biomarkers in Human Blood. *PLoS One* **10**: e0141214.
56. Li Y, Zheng Q, Bao C, Li S, Guo W, Zhao J, Chen D, Gu J, He X, Huang S (2015) Circular RNA is enriched and stable in exosomes: a promising biomarker for cancer diagnosis. *Cell Res* **25**: 981–984.
57. Dou Y, Cha DJ, Franklin JL, Higginbotham JN, Jeppesen DK, Weaver AM, Prasad N, Levy S, Coffey RJ, Patton JG, et al. (2016) Circular RNAs are down-regulated in KRAS mutant colon cancer cells and can be transferred to exosomes. *Sci Rep* **6**: 37982.
58. Egas-Bejar D, Huh WW (2014) Rhabdomyosarcoma in adolescent and young adult patients: current perspectives. *Adolesc Health Med Ther* **5**: 115–125.
59. Ognjanovic S, Linabery AM, Charbonneau B, Ross JA (2009) Trends in childhood rhabdomyosarcoma incidence and survival in the United States, 1975-2005. *Cancer* **115**: 4218–4226.
60. Hartley AL, Birch JM, Marsden HB, Harris M, Blair V (1988) Neurofibromatosis in children with soft tissue sarcoma. *Pediatr Hematol Oncol* **5**: 7–16.
61. Li FP, Fraumeni JF (1969) Soft-tissue sarcomas, breast cancer, and other neoplasms. A familial syndrome? *Ann Intern Med* **71**: 747–752.
62. Birch JM, Hartley AL, Marsden HB, Harris M, Swindell R (1984) Excess risk of breast cancer in the mothers of children with soft tissue sarcomas. *Br J Cancer* **49**: 325–331.
63. Horn RC, Enterline HT (1958) Rhabdomyosarcoma: A

clinicopathological study and classification of 39 cases. *Cancer* **11**: 181–199.

64. Kashi VP, Hatley ME, Galindo RL (2015) Probing for a deeper understanding of rhabdomyosarcoma: Insights from complementary model systems. *Nat Rev Cancer* **15**: 426–439.
65. Breneman JC, Lyden E, Pappo AS, Link MP, Anderson JR, Parham DM, Qualman SJ, Wharam MD, Donaldson SS, Maurer HM, et al. (2003) Prognostic factors and clinical outcomes in children and adolescents with metastatic rhabdomyosarcoma-a report from the intergroup rhabdomyosarcoma study IV. *J Clin Oncol* **21**: 78–84.
66. Noujaim J, Thway K, Jones RL, Miah A, Khabra K, Langer R, Kasper B, Judson I, Benson C, Kollàr A (2015) Adult pleomorphic rhabdomyosarcoma: A multicentre retrospective study. *Anticancer Res* **35**: 6213–6217.
67. Neha B, Manjunath AP, Girija S, Pratap K (2015) Botryoid rhabdomyosarcoma of the cervix: Case report with review of the literature. *Sultan Qaboos Univ Med J* **15**: e433–e437.
68. Sun X, Guo W, Shen JK, Mankin HJ, Hornicek FJ, Duan Z (2015) Rhabdomyosarcoma: Advances in Molecular and Cellular Biology. *Sarcoma* **2015**: 1–14.
69. Xia SJ, Pressey JG, Barr FG (2002) Molecular pathogenesis of rhabdomyosarcoma. *Cancer Biol Ther* **1**: 97–104.
70. Seale P, Sabourin LA, Girgis-Gabardo A, Mansouri A, Gruss P, Rudnicki MA (2000) Pax7 is required for the specification of myogenic satellite cells. *Cell* **102**: 777–786.
71. Bajard L, Relaix F, Lagha M, Rocancourt D, Daubas P, Buckingham ME (2006) A novel genetic hierarchy functions during hypaxial myogenesis: Pax3 directly activates Myf5 in muscle progenitor cells in the limb. *Genes Dev* **20**: 2450–2464.
72. O-Sullivan I, Zhang W, Wasserman DH, Liew CW, Liu J, Paik J, Depinho RA, Stolz DB, Kahn CR, Schwartz MW, et al. (2015) FoxO1 integrates direct and indirect effects of insulin on hepatic glucose production and glucose utilization. *Nat Commun* **6**: 7079.
73. Barr FG (2001) Gene fusions involving PAX and FOX family members in alveolar rhabdomyosarcoma. *Oncogene* **20**: 5736–5746.
74. Dias P, Parham DM, Shapiro DN, Webber BL, Houghton PJ (1990) Myogenic regulatory protein (MyoD1) expression in childhood solid tumors: Diagnostic utility in rhabdomyosarcoma. *Am J Pathol* **137**: 1283–1291.
75. Kumar S, Perlman E, Harris CA, Raffeld M, Tsokos M (2000) Myogenin is a specific marker for rhabdomyosarcoma: An

immunohistochemical study in paraffin-embedded tissues. *Mod Pathol* **13**: 988–993.
76. Zhang M, Linardic CM, Kirsch DG (2013) RAS and ROS in Rhabdomyosarcoma. *Cancer Cell* **24**: 689–691.
77. Zhu B, Davie JK (2015) New insights into signalling-pathway alterations in rhabdomyosarcoma. *Br J Cancer* **112**: 227–231.
78. Panda SP, Chinnaswamy G, Vora T, Prasad M, Bansal D, Kapoor G, Radhakrishnan V, Agarwala S, Laskar S, Arora B, et al. (2017) Diagnosis and Management of Rhabdomyosarcoma in Children and Adolescents: ICMR Consensus Document. *Indian J Pediatr* **84**: 393–402.
79. Jordan MA (2002) Mechanism of action of antitumor drugs that interact with microtubules and tubulin. *Curr Med Chem - Anti-Cancer Agents* **2**: 1–17.
80. Mukhtar E, Adhami VM, Mukhtar H (2014) Targeting microtubules by natural agents for cancer therapy. *Mol Cancer Ther* **13**: 275–284.
81. Van Erp AEM, Versleijen-Jonkers YMH, Van Der Graaf WTA, Fleuren EDG (2018) Targeted therapy-based combination treatment in rhabdomyosarcoma. *Mol Cancer Ther* **17**: 1365–1380.
82. Reed NP, Henderson MA, Oltz EM, Aune TM (2013) Reciprocal regulation of Rag expression in thymocytes by the zinc-finger proteins, Zfp608 and Zfp609. *Genes Immun* **14**: 7–12.
83. van den Berg DLC, Azzarelli R, Oishi K, Martynoga B, Urbán N, Dekkers DHW, Demmers JA, Guillemot F (2017) Nipbl Interacts with Zfp609 and the Integrator Complex to Regulate Cortical Neuron Migration. *Neuron* **93**: 348–361.
84. Rossi F, Legnini I, Megiorni F, Colantoni A, Santini T, Morlando M, Di Timoteo G, Dattilo D, Dominici C, Bozzoni I (2019) Circ-ZNF609 regulates G1-S progression in rhabdomyosarcoma. *Oncogene* **38**: 3843–3854.
85. Dyson N (1998) The regulation of E2F by pRB-family proteins. *Genes Dev* **12**: 2245–2262.
86. Laplante M, Sabatini DM (2012) mTOR signaling in growth control and disease. *Cell* **149**: 274–293.
87. Nitulescu GM, Van De Venter M, Nitulescu G, Ungurianu A, Juzenas P, Peng Q, Olaru OT, Grădinaru D, Tsatsakis A, Tsoukalas D, et al. (2018) The Akt pathway in oncology therapy and beyond (Review). *Int J Oncol* **53**: 2319–2331.
88. Besson A, Gurian-west M, Chen X, Kelly-spratt KS, Kemp CJ, Roberts JM (2006) A pathway in quiescent cells that controls p27 Kip1 stability, subcellular localization, and tumor suppression. *Genes Dev* **20**: 47–64.

89. Geistlinger L, Csaba G, Küffner R, Mulder N, Zimmer R (2011) From sets to graphs: Towards a realistic enrichment analysis of transcriptomic systems. *Bioinformatics* **27**: 366–373.
90. Ogata H, Goto S, Sato K, Fujibuchi W, Bono H, Kanehisa M (1999) KEGG: Kyoto encyclopedia of genes and genomes. *Nucleic Acids Res* **27**: 29–34.
91. Alvarez MJ, Shen Y, Giorgi FM, Lachmann A, Ding BB, Ye BH, Califano A (2016) Network-based inference of protein activity helps functionalize the genetic landscape of cancer. *Nat Genet* **48**: 838–847.
92. Weinstein JN, Collisson EA, Mills GB, Shaw KM, Brad A, Ellrott K, Shmulevich I, Sander C, Stuart JM (2013) The cancer genome atlas pan-cancer analysis project. *Nat Genet* **45**: 1113–1120.
93. Krautkramer KA, Linnemann AK, Fontaine DA, Whillock AL, Harris TW, Schleis GJ, Truchan NA, Marty-Santos L, Lavine JA, Cleaver O, et al. (2013) Tcf19 is a novel islet factor necessary for proliferation and survival in the INS-1 β-cell line. *Am J Physiol Endocrinol Metab* **305**: E600-10.
94. Qu K, Wang Z, Fan H, Li J, Liu J, Li P, Liang Z, An H, Jiang Y, Lin Q, et al. (2017) MCM7 promotes cancer progression through cyclin D1-dependent signaling and serves as a prognostic marker for patients with hepatocellular carcinoma. *Cell Death Dis* **8**: e2603–e2603.
95. Wang S, Liu B, Zhang J, Sun W, Dai C, Sun W, Li Q (2017) Centromere protein U is a potential target for gene therapy of human bladder cancer. *Oncol Rep* **38**: 735–744.
96. Endo H, Ikeda K, Urano T, Horie-Inoue K, Inoue S (2012) Terf/TRIM17 stimulates degradation of kinetochore protein ZWINT and regulates cell proliferation. *J Biochem* **151**: 139–144.
97. Ying H, Xu Z, Chen M, Zhou S, Liang X, Cai X (2018) Overexpression of Zwint predicts poor prognosis and promotes the proliferation of hepatocellular carcinoma by regulating cell-cycle-related proteins. *Onco Targets Ther* **11**: 689–702.
98. Feng G, Zhang T, Liu J, Ma X, Li B, Yang L, Zhang Y, Xu Z, Qin T, Zhou J, et al. (2017) MLF1IP promotes normal erythroid proliferation and is involved in the pathogenesis of polycythemia vera. *FEBS Lett* **591**: 760–773.
99. Liu P, Slater DM, Lenburg M, Nevis K, Cook JG, Vaziri C (2009) Replication licensing promotes cyclin D1 expression and G 1 progression in untransformed human cells. *Cell Cycle* **8**: 125–136.
100. Mio C, Lavarone E, Conzatti K, Baldan F, Toffoletto B, Puppin C, Filetti S, Durante C, Russo D, Orlacchio A, et al. (2016) MCM5 as a target of BET inhibitors in thyroid cancer cells. *Endocr Relat*

Cancer **23**: 335–347.
101. Felix CA, Kappel CC, Mitsudomi T, Nau MM, Tsokos M, Crouch GD, Nisen PD, Winick NJ, Helman LJ (1992) Frequency and Diversity of p53 Mutations in Childhood Rhabdomyosarcoma. *Cancer Res* **6**: 2243–2247.
102. Miyachi M, Kakazu N, Yagyu S, Katsumi Y, Tsubai-shimizu S, Kikuchi K, Tsuchiya K, Iehara T, Hosoi H (2009) Restoration of p53 Pathway by Nutlin-3 Induces Cell Cycle Arrest and Apoptosis in Human Rhabdomyosarcoma Cells. *Clin Cancer Res* **15**: 4077–4085.
103. Taylor AC, Shu L, Danks MK, Poquette CA, Shetty S, Thayer MJ, Houghton PJ, Harris LC (2000) P53 mutation and MDM2 amplification frequency in pediatric rhabdomyosarcoma tumors and cell lines. *Med Pediatr Oncol* **35**: 96–103.
104. Martone J, Mariani D, Santini T, Setti A, Shamloo S, Colantoni A, Capparelli F, Paiardini A, Dimartino D, Morlando M, et al. (2020) SMaRT lncRNA controls translation of a G-quadruplex-containing mRNA antagonizing the DHX36 helicase. *EMBO Rep* **21**: e49942.
105. Cassimeris L, Morabito J (2004) TOGp, the Human Homolog of XMAP215/Dis1, Is Required for Centrosome Integrity, Spindle Pole Organization, and Bipolar Spindle Assembly. *Mol Biol Cell* **15**: 1580–1590.
106. Brouhard GJ, Stear JH, Noetzel TL, Al-Bassam J, Kinoshita K, Harrison SC, Howard J, Hyman AA (2008) XMAP215 Is a Processive Microtubule Polymerase. *Cell* **132**: 79–88.
107. Miller MP, Asbury CL, Biggins S (2016) A TOG Protein Confers Tension Sensitivity to Kinetochore-Microtubule Attachments. *Cell* **165**: 1428–1439.
108. Milunovic-Jevtic A, Jevtic P, Levy DL, Gatlin JC (2018) In vivo mitotic spindle scaling can be modulated by changing the levels of a single protein: the microtubule polymerase XMAP215. *Mol Biol Cell* **29**: 1311–1317.
109. Grimm T, Hölzel M, Rohrmoser M, Harasim T, Malamoussi A, Gruber-Eber A, Kremmer E, Eick D (2006) Dominant-negative Pes1 mutants inhibit ribosomal RNA processing and cell proliferation via incorporation into the PeBoW-complex. *Nucleic Acids Res* **34**: 3030–3043.
110. Kellner M, Rohrmoser M, Forné I, Voss K, Burger K, Mühl B, Gruber-Eber A, Kremmer E, Imhof A, Eick D (2015) DEAD-box helicase DDX27 regulates 3′ end formation of ribosomal 47S RNA and stably associates with the PeBoW-complex. *Exp Cell Res* **334**: 146–159.
111. Mann M, Wright PR, Backofen R (2017) IntaRNA 2.0: Enhanced

and customizable prediction of RNA-RNA interactions. *Nucleic Acids Res* **45**: W435–W439.
112. Fan XC, Steitz JA (1998) Overexpression of HuR, a nuclear-cytoplasmic shuttling protein, increases the in vivo stability of ARE-containing mRNAs. *EMBO J* **17**: 3448–3460.
113. Brennan CM, Steitz JA (2001) HuR and mRNA stability. *Cell Mol Life Sci* **58**: 266–277.
114. Mazan-Mamczarz K, Galbán S, De Silanes IL, Martindale JL, Atasoy U, Keene JD, Gorospe M (2003) RNA-binding protein HuR enhances p53 translation in response to ultraviolet light irradiation. *Proc Natl Acad Sci U S A* **100**: 8354–8359.
115. Galbán S, Kuwano Y, Pullmann R, Martindale JL, Kim HH, Lal A, Abdelmohsen K, Yang X, Dang Y, Liu JO, et al. (2008) RNA-Binding Proteins HuR and PTB Promote the Translation of Hypoxia-Inducible Factor 1α. *Mol Cell Biol* **28**: 93–107.
116. Mazan-Mamczarz K, Hagner PR, Corl S, Srikantan S, Wood WH, Becker KG, Gorospe M, Keene JD, Levenson AS, Gartenhaus RB (2008) Post-transcriptional gene regulation by HuR promotes a more tumorigenic phenotype. *Oncogene* **27**: 6151–6163.
117. Yeap BB, Voon DC, Vivian JP, McCulloch RK, Thomson AM, Giles KM, Czyzyk-Krzeska MF, Furneaux H, Wilce MCJ, Wilce JA, et al. (2002) Novel binding of HuR and poly(C)-binding protein to a conserved UC-rich motif within the 3′-untranslated region of the androgen receptor messenger RNA. *J Biol Chem* **277**: 27183–27192.
118. Wein G, Rössler M, Klug R, Herget T (2003) The 3′-UTR of the mRNA coding for the major protein kinase C substrate MARCKS contains a novel CU-rich element interacting with the mRNA stabilizing factors HuD and HuR. *Eur J Biochem* **270**: 350–365.
119. Lebedeva S, Jens M, Theil K, Schwanhäusser B, Selbach M, Landthaler M, Rajewsky N (2011) Transcriptome-wide Analysis of Regulatory Interactions of the RNA-Binding Protein HuR. *Mol Cell* **43**: 340–352.
120. Kishore S, Jaskiewicz L, Burger L, Hausser J, Khorshid M, Zavolan M (2011) A quantitative analysis of CLIP methods for identifying binding sites of RNA-binding proteins. *Nat Methods* **8**: 559–564.
121. Dudekula DB, Panda AC, Grammatikakis I, De S, Abdelmohsen K, Gorospe M (2016) Circinteractome: A web tool for exploring circular RNAs and their interacting proteins and microRNAs. *RNA Biol* **13**: 34–42.
122. Ganem NJ, Pellman D (2012) Linking abnormal mitosis to the acquisition of DNA damage. *J Cell Biol* **199**: 871–881.

123. Williams BR, Prabhu VR, Hunter KE, Glazier CM, Whittaker CA, Housman DE, Amon A (2008) Aneuploidy affects proliferation and spontaneous immortalization in mammalian cells. *Science (80-)* **322**: 703–709.
124. Stingele S, Stoehr G, Peplowska K, Cox J, Mann M, Storchova Z (2012) Global analysis of genome, transcriptome and proteome reveals the response to aneuploidy in human cells. *Mol Syst Biol* **8**: 608.
125. Hartwell LH, Weinert TA (1989) Checkpoints: Controls that ensure the order of cell cycle events. *Science (80-)* **246**: 629–634.
126. Piccolo S, Dupont S, Cordenonsi M (2014) The biology of YAP/TAZ: Hippo signaling and beyond. *Physiol Rev* **94**: 1287–1312.
127. Pocaterra A, Romani P, Dupont S (2020) YAP/TAZ functions and their regulation at a glance. *J Cell Sci* **133**: jcs230425.
128. Dupont S, Morsut L, Aragona M, Enzo E, Giulitti S, Cordenonsi M, Zanconato F, Le Digabel J, Forcato M, Bicciato S, et al. (2011) Role of YAP/TAZ in mechanotransduction. *Nature* **474**: 179–183.
129. Vaziri C, Saxena S, Jeon Y, Lee C, Murata K, Machida Y, Wagle N, Hwang DS, Dutta A (2003) A p53-dependent checkpoint pathway prevents rereplication. *Mol Cell* **11**: 997–1008.
130. Jin C, Zhao W, Zhang Z, Liu W (2019) Silencing circular RNA circZNF609 restrains growth, migration and invasion by up-regulating microRNA-186-5p in prostate cancer. *Artif Cells, Nanomedicine Biotechnol* **47**: 3350–3358.
131. Tong H, Zhao K, Wang J, Xu H, Xiao J (2020) CircZNF609/miR-134-5p/BTG-2 axis regulates proliferation and migration of glioma cell. *J Pharm Pharmacol* **72**: 68–75.
132. Wu L, Xia J, Yang J, Shi Y, Xia H, Xiang X, Yu X (2018) Circ-ZNF609 promotes migration of colorectal cancer by inhibiting Gli1 expression via microRNA-150. *J BUON* **23**: 1343–1349.
133. Peng L, Chen G, Zhu Z, Shen Z, Du C, Zang R, Su Y, Xie H, Li H, Xu X, et al. (2017) Circular RNA ZNF609 functions as a competitive endogenous RNA to regulate AKT3 expression by sponging miR-150-5p in Hirschsprung's disease. *Oncotarget* **8**: 808–818.
134. López De Silanes I, Zhan M, Lal A, Yang X, Gorospe M (2004) Identification of a target RNA motif for RNA-binding protein HuR. *Proc Natl Acad Sci U S A* **101**: 2987–2992.
135. Barr AR, Bakal C (2015) A sensitised RNAi screen reveals a ch-TOG genetic interaction network required for spindle assembly. *Sci Rep* **5**: 10564.
136. Santaguida S, Richardson A, Iyer DR, M'Saad O, Zasadil L,

Knouse KA, Wong YL, Rhind N, Desai A, Amon A (2017) Chromosome Mis-segregation Generates Cell-Cycle-Arrested Cells with Complex Karyotypes that Are Eliminated by the Immune System. *Dev Cell* **41**: 638–651.

137. Kertesz M, Iovino N, Unnerstall U, Gaul U, Segal E (2007) The role of site accessibility in microRNA target recognition. *Nat Genet* **39**: 1278–1284.
138. Enright AJ, John B, Gaul U, Tuschl T, Sander C, Marks DS (2003) MicroRNA targets in Drosophila. *Genome Biol* **5**: R1.
139. Sticht C, De La Torre C, Parveen A, Gretz N (2018) Mirwalk: An online resource for prediction of microrna binding sites. *PLoS One* **13**: e0206239.
140. Aragona M, Panciera T, Manfrin A, Giulitti S, Michielin F, Elvassore N, Dupont S, Piccolo S (2013) A mechanical checkpoint controls multicellular growth through YAP/TAZ regulation by actin-processing factors. *Cell* **154**: 1047–1059.
141. Walter D, Satheesha S, Albrecht P, Bornhauser BC, D'Alessandro V, Oesch SM, Rehrauer H, Leuschner I, Koscielniak E, Gengler C, et al. (2011) CD133 positive embryonal rhabdomyosarcoma stem-like cell population is enriched in rhabdospheres. *PLoS One* **6**: e19506.
142. Ghayad SE, Rammal G, Ghamloush F, Basma H, Nasr R, Diab-Assaf M, Chelala C, Saab R (2016) Exosomes derived from embryonal and alveolar rhabdomyosarcoma carry differential miRNA cargo and promote invasion of recipient fibroblasts. *Sci Rep* **6**: 37088.
143. Olive PL, Banáth JP (2006) The comet assay: A method to measure DNA damage in individual cells. *Nat Protoc* **1**: 23–29.
144. Torosantucci L, De Luca M, Guarguaglini G, Lavia P, Degrassi F (2008) Localized RanGTP accumulation promotes microtubule nucleation at kinetochores in somatic mammalian cells. *Mol Biol Cell* **19**: 1873–1882.
145. Verrico A, Rovella P, Di Francesco L, Damizia M, Staid DS, Le Pera L, Schininà ME, Lavia P (2020) Importin-β/karyopherin-β1 modulates mitotic microtubule function and taxane sensitivity in cancer cells via its nucleoporin-binding region. *Oncogene* **39**: 454–468.
146. Masuda Y, Takahashi H, Sato S, Tomomori-Sato C, Saraf A, Washburn MP, Florens L, Conaway RC, Conaway JW, Hatakeyama S (2015) TRIM29 regulates the assembly of DNA repair proteins into damaged chromatin. *Nat Commun* **6**: 7299.
147. Keene JD, Komisarow JM, Friedersdorf MB (2006) RIP-Chip: The isolation and identification of mRNAs, microRNAs and protein

components of ribonucleoprotein complexes from cell extracts. *Nat Protoc* **1**: 302–307.
148. Bolger AM, Lohse M, Usadel B (2014) Trimmomatic: A flexible trimmer for Illumina sequence data. *Bioinformatics* **30**: 2114–2120.
149. Zerbino DR, Achuthan P, Akanni W, Amode MR, Barrell D, Bhai J, Billis K, Cummins C, Gall A, Girón CG, et al. (2018) Ensembl 2018. *Nucleic Acids Res* **46**: D754–D761.
150. Dobin A, Davis CA, Schlesinger F, Drenkow J, Zaleski C, Jha S, Batut P, Chaisson M, Gingeras TR (2013) STAR: Ultrafast universal RNA-seq aligner. *Bioinformatics* **29**: 15–21.
151. Anders S, Pyl PT, Huber W (2015) HTSeq-A Python framework to work with high-throughput sequencing data. *Bioinformatics* **31**: 166–169.
152. Robinson MD, McCarthy DJ, Smyth GK (2009) edgeR: A Bioconductor package for differential expression analysis of digital gene expression data. *Bioinformatics* **26**: 139–140.
153. Schurch NJ, Schofield P, Gierliński M, Cole C, Sherstnev A, Singh V, Wrobel N, Gharbi K, Simpson GG, Owen-Hughes T, et al. (2016) How many biological replicates are needed in an RNA-seq experiment and which differential expression tool should you use? *RNA* **22**: 839–851.
154. Carbon S, Dietze H, Lewis SE, Mungall CJ, Munoz-Torres MC, Basu S, Chisholm RL, Dodson RJ, Fey P, Thomas PD, et al. (2017) Expansion of the gene ontology knowledgebase and resources: The gene ontology consortium. *Nucleic Acids Res* **45**: D331–D338.
155. Fabregat A, Jupe S, Matthews L, Sidiropoulos K, Gillespie M, Garapati P, Haw R, Jassal B, Korninger F, May B, et al. (2018) The Reactome Pathway Knowledgebase. *Nucleic Acids Res* **46**: D649–D655.
156. Zhang B, Kirov S, Snoddy J (2005) WebGestalt: An integrated system for exploring gene sets in various biological contexts. *Nucleic Acids Res* **33**: 741–748.
157. Geistlinger L, Csaba G, Zimmer R (2016) Bioconductor's EnrichmentBrowser: Seamless navigation through combined results of set- & network-based enrichment analysis. *BMC Bioinformatics* **17**: 1–11.
158. Lachmann A, Giorgi FM, Lopez G, Califano A (2016) ARACNe-AP: Gene network reverse engineering through adaptive partitioning inference of mutual information. *Bioinformatics* **32**: 2233–2235.
159. Martin M (2011) Cutadapt removes adapter sequences from high-throughput sequencing reads. *EMBnet.journal* **17**: 10–12.

160. Li H (2013) Aligning sequence reads, clone sequences and assembly contigs with BWA-MEM. *arXiv.org* **00**: 1–3.
161. Gao Y, Zhang J, Zhao F (2018) Circular RNA identification based on multiple seed matching. *Brief Bioinform* **19**: 803–810.
162. Barnett DW, Garrison EK, Quinlan AR, Stŕmberg MP, Marth GT (2011) Bamtools: A C++ API and toolkit for analyzing and managing BAM files. *Bioinformatics* **27**: 1691–1692.
163. Li H, Handsaker B, Wysoker A, Fennell T, Ruan J, Homer N, Marth G, Abecasis G, Durbin R (2009) The Sequence Alignment/Map format and SAMtools. *Bioinformatics* **25**: 2078–2079.
164. Quinlan AR, Hall IM (2010) BEDTools: A flexible suite of utilities for comparing genomic features. *Bioinformatics* **26**: 841–842.
165. Uren PJ, Bahrami-Samani E, Burns SC, Qiao M, Karginov F V., Hodges E, Hannon GJ, Sanford JR, Penalva LOF, Smith AD (2012) Site identification in high-throughput RNA-protein interaction data. *Bioinformatics* **28**: 3013–3020.

List of publications

Research articles in peer-reviewed scientific journals

1. Di Timoteo G*, Dattilo D*, Centrón-Broco A, Colantoni A, Guarnacci M, **Rossi F**, Incarnato D, Oliviero S, Fatica A, Morlando M, Bozzoni I. (2020) Modulation of circRNA metabolism by m^6A modification. *Cell Rep*. 31(6):107641. (**contributed equally to this work*)

2. **Rossi F**, Legnini I, Megiorni F, Colantoni A, Santini T, Morlando M, Di Timoteo G, Dattilo D, Dominici C, Bozzoni I. (2019) Circ-ZNF609 regulates G1-S progression in rhabdomyosarcoma. *Oncogene*. 38(20):3843–3854.

3. Legnini I, Di Timoteo G, **Rossi F**, Morlando M, Briganti F, Sthandier O, Fatica A, Santini T, Andronache A, Wade M, Laneve P, Rajewsky N, Bozzoni I. (2017) Circ-ZNF609 is a circular RNA that can be translated and functions in myogenesis. *Mol Cell*. 66(1):22–37.e9.

4. Espinosa-Medina I*, Saha O*, Boismoreau F, Chettouh Z, **Rossi F**, Richardson WD, Brunet JF. (2016) The sacral autonomic outflow is sympathetic. *Science*. 354(6314):893–897. (**contributed equally to this work*)

Review articles in peer-reviewed scientific journals

1. Di Timoteo G*, **Rossi F***, Bozzoni I. (2020) Circular RNAs in cell differentiation and development. *Development*. 147(16):dev182725. (**contributed equally to this work*)

Acknowledgements

I would like to thank Prof. Irene Bozzoni for having accepted me in her research group and for having taught me that curiosity, interest and hard work are the first rules for good Science.

I would like to thank Dr Manolo Beltran Nebot, for the unvaluable help and suggestions he gave me regarding the circZNF609/Ckap5/HuR story, and all his precious and kind advice at the bench.

A very special thank goes to my other lab colleagues, Dr Gaia di Timoteo, Dario Dattilo and Alvaro Centron Broco, for supporting me in every-day lab life with enthusiasm, kindness and great professionalism.

I would like to thank Marco Guarnacci and Chiara Grelloni, respectively past and present Master's students of the lab, who helped me in my experimental work with passion and dedication.

Another special thank goes to the Bioinformatics Lab members, Dr Alessio Colantoni, Alvaro Centron Broco and Adriano Setti, who put their time and skills at the disposal of this project.

Thanks to all the past and present members of the Bozzoni Lab, particularly Prof Mariangela Morlando, Dr Julie Martone, Prof Alessandro Fatica, Dr Ivano Legnini and Dr

Olga Sthandier, for the very useful discussions we had together. I would also like to thank Dr Davide Mariani for his precious help with the psoralen-crosslinked pulldown protocol which he previously optimised.

I thank Dr Tiziana Santini, for having taught me how to perform FISH and immunofluorescence experiments and for the confocal microscopy analyses she made for this work.

I would like to thank our collaborators, particularly Dr Francesca Megiorni and Prof. Carlo Dominici's Lab at Policlinico Umberto I (Rome) for their precious help with FACS analyses and for kindly providing us with RMS cell lines and biopsies. Thanks to Dr Patrizia Lavia's Lab and Michela Damizia in particular (CNR, Rome), for their great help with the analysis of microtubule dynamics and mitosis which I described in this work.

I also thank Prof. Stefano Piccolo for the enlightening discussion we had about the YAP/TAZ pathway regulation and for kindly providing us with YAP/TAZ siRNAs, antibodies and reporter construct.

Finally, I would like to thank my family, for supporting and trusting me in every occasion with great love, and all my friends, particularly Virginia, Chiara, Emanuele and Pietro, for their enormous kindness and affection.